MODELING SEED DISPERSAL AND POPULATION MIGRATION GIVEN A DISTRIBUTION OF SEED HANDLING TIMES AND VARIABLE DISPERSAL MOTILITY: CASE STUDY FOR PINYON AND JUNIPER IN UTAH

by

Ram C. Neupane

A dissertation submitted in partial fulfilment
of the requirements for the degree

of

DOCTOR OF PHILOSOPHY

in

Mathematics

Approved:

_____	_____
Dr. James Powell Major Professor	Dr. Brynja Kohler Committee Member
_____	_____
Dr. Richard Cutler Committee Member	Dr. Nghiem Nguyen Committee Member
_____	_____
Dr. Thomas Edwards Committee Member	Dr. Mark McLellan Vice President for Research and Dean of the School of Graduate Studies

UTAH STATE UNIVERSITY
Logan, Utah

2015

ABSTRACT

Modeling Seed Dispersal and Population Migration

Given a Distribution of Seed Handling Times

and Variable Dispersal Motility:

Case Study for Pinyon and

Juniper in Utah.

by

Ram C. Neupane, Doctor of Philosophy

Utah State University, 2015

Major Professor: Dr. James A. Powell

Department: Mathematics and Statistics

The distribution of fruiting tree species is strongly determined by the behavior and range of vertebrate dispersers, particularly birds. Birds either consume and digest seeds or carry and cache them at some distance from the source tree. These carried seeds are described by a dispersal kernel, which captures the probability that the seed will move a certain distance by the end of the process. Initially, we model active seed dispersal of this nature, introducing seed handling time probabilities into the dispersal model to generate a seed digestion kernel (SDK) which is used to estimate the speed at which juniper and pinyon forest boundaries move. Our finding suggests that pinyon may be able to migrate up to two orders of magnitude more rapidly.

In the core of this dissertation, we add ecological diffusion to the dispersal model and approximate SDKs in highly variable landscapes. Spatial variability in habitat directly affects the movement of dispersers and leads to anisotropic dispersal kernels. We introduce multiple scales and apply homogenization method to determine leading order solutions for the SDK. Returning to the integrodifference equation model for adult trees, we investigate the rate of forest migration in variable landscapes. We show that speeds calculated using the harmonic average motility and mean seed handling time accurately predict rates of invasion for the spatially variable system.

Regional scale forest distribution models are frequently used to project tree migration based on climate and geographic variables such as elevation, latitude and 'trained' using landscape and regional presence-absence data. How seeds are distributed in these models, however, is far more problematic since it is difficult to accurately parameterize dispersal models using large-scale presence-absence data, particularly for actively dispersed tree species. In the final section, we implement the HSDKs to find dispersal probabilities on the large scales, linking small-pixel environmental variables to large-scale migration.

(136 pages)

PUBLIC ABSTRACT

Modeling Seed Dispersal and Population Migration

Given a Distribution of Seed Handling Times

and Variable Dispersal Motility:

Case Study for Pinyon and

Juniper in Utah.

by

Ram C. Neupane, Doctor of Philosophy

Utah State University, 2015

Major Professor: Dr. James A. Powell

Department: Mathematics and Statistics

The spread of fruiting tree species is strongly determined by the behavior and range of fruit-eating animals, particularly birds. Birds either consume and digest seeds or carry and cache them at some distance from the source tree. These carried and settled seeds provide some form of distribution which generates tree spread to the new location. Firstly, we modal seed dispersal by birds and introduce it in a dispersal model to estimate seed distribution. Using this distribution, we create a population model to estimate the speed at which juniper and pinyon forest boundaries move.

Secondly, we introduce a fact that bird movement occurs based on local habitat type to receive modified dispersal model. Birds can easily move many kilometers but habitat changes on the scale of tens of meters with rapidly varying. We develop a new technique to solve the modified dispersal model and approximate the form of transported

seed distributions in highly variable landscapes. Using a tree population model, we investigate the rate of forest migration in variable landscapes. We show that speeds calculated using average motility of animals and mean seed handling times accurately predict the migration rate of trees.

Regional scale forest distribution models are frequently used to project tree migration based on climate and geographic variables such as elevation, and regional presence-absence data. It is difficult to accurately use dispersal models based on large-scale presence-absence data, particularly for tree species dispersed by birds. The challenge is that variables associated with seed dispersal by birds are represented only few meters while the smallest pixel size for the distribution models begins with few kilometers. Transported seed distribution estimated in the variable landscape offers a tool to make use of this scale separation. Finally, we develop a scenarios that allows us to find large scale dispersal probabilities based on small scale environmental variables.

ACKNOWLEDGMENTS

I would like to express my deepest gratitude to my advisor, Dr. James A. Powell, for his guidance and insight during my program of study here in USU. I am grateful forever to him for inspiring me to reach this accomplishment.

I would also like to thank Dr. Brynja Kohler, Dr. Richard Cutler, Dr. Nghiem Nguyen and Dr. Thomas Edwards Jr. for serving as a committee members and giving suggestions for this completion. I appreciate helpful feedback from Dr. Martha Garlick and USU's MathBio group. This research was funded by Utah State University graduate student stipend and PhD completion fellowship.

Finally, I would also like to thank to my wife, Sarala Sharma, for her continuous, moral and emotional support throughout my studies.

Ram C. Neupane

CONTENTS

Page

LIST OF TABLES

LIST OF FIGURES

CHAPTER 1

INTRODUCTION

The diffusion equation represents a fundamental framework for determining the spatial spread of organisms (Hengeveld 1988, Okubo and Levin 1989, Shigesada et al., 1995, Skalski and Gilliam 2003, Morales and Carlo 2006). Fisher (1937) studied asymptotic rates of invasion of mutant genes and his ideas were extended by Skellam (1951) to ecological problems (the spread of animal and plant populations on landscape scales). Later on, diffusion equations were used to describe the spread of the cereal leaf beetle, muskrat, small cabbage white butterfly (Andow et al., 1990) and dispersal of cholla (Allen et al., 1991).

At population and landscape scales movement is often modeled by Fickian diffusion (Reeve et al., 2008), in which population redistribution is driven by population gradients. This means that the movement of individuals tends from higher concentrations to lower concentrations, and changes in local habitat only alter the movement rate down the gradient (Okubo 2001). However, animal responses to spatial heterogeneity are not likely to be Fickian. When deer bed down at or inside a treeline they do not randomly diffuse past the forest edge, and when American robins forage for juniper berries they exhibit high fidelity to the location of the trees and simply avoid the surrounding steppe, unless they are choosing to move between patches of juniper. In both of these cases the animals are making movement choices based on the patch of habitat in which they currently reside, not perceptions of population gradients. A more appropriate way to describe animal movement in which organisms make random steps based on current habitat types is "ecological diffusion" (Turchin 1998). In this approach differences in population

dispersion are driven by residence times in differing habitat types. Where residence times are high (in juniper for robins) populations accumulate, and where residence times are low (in sagebrush) the population density is low. An ecological diffusion model supports discontinuous solutions at boundaries, consequently, deer can accumulate inside of a forest patch without diffusing out into the adjacent meadow against their will. Turchin (1998) observed that residence time and motility (the analog of diffusivity) are inversely proportional. Thus, if the motility is low in a patch (residence time is high) then individuals don't choose to leave the patch very frequently and the population density increases.

Diffusion models usually assume that animal movement properties are constant in space and time, but in fact animals move differently in different habitats. Movement occurs while animals search for food, water, breeding sites, mates and shelter. When animal motility is independent in space, Neubert et al., 1995 have discussed two limiting cases of seed spread. If every dispersal agent requires exactly the same amount of time to handle individual seeds, seed dispersal on the landscape is Gaussian. On the other hand, if these agents drop seeds at a constant rate in both time and space, seed spread in a Laplace distribution. Both extremes, however, are unlikely in real life scenarios. Neupane and Powell (2015) hypothesized that handling time is sampled from a distribution after seeds are picked. Using a time-dependent seed handling function they calculated seed digestion kernels (SDK). Neupane and Powell showed that the SDK accurately described seed dispersal for pinyon pine and Utah juniper, as reflected in historical migration rate of these species.

Birds play a major, but different, role for dispersing pinyon (*Pinus monophylla*) and juniper (*Juniperus osteosperma*). Junipers produce seeds which are available most of the winter, and consequently many birds (particularly American robins, *Turdus migratorius*, and cedar waxwings, *Bombycilla cedrorum*) consume juniper berries (Chambers et al., 1999). The berries are then digested and seeds deposited some time later by defecation. Digestion does not impede the seeds' ability to germinate, particularly in the case of robins (Chavez-Ramirez and Slack, 1994), and juniper is thus dispersed while robins forage over scores of meters.

By contrast, pinyon seed dispersal by Clark's nutcracker (*Nucifraga columbiana*) and pinyon jays (*Gymnorhinus cyanocephalus*) occurs primarily through seed caching in the summer and fall, when the cones mature. Some seeds are consumed immediately, but the majority are placed in a sublingual pouch and carried several kilometers to remote cache sites, where they are buried in small groups (Vanderwall and Balda 1977, Balda and Bateman 1971). Most of the cache sites are found during the winter, but a substantial percentage of caches are never revisited and the cached seeds are in an ideal situation for germination, which determines pinyon distribution.

Variation in climate also influences the expansion of pinyon-juniper (P-J) woodland via impacts on germination and survival rates. The abundance of summer rainfall and warming in the winter and spring have caused P-J boundaries to shift northwards (Neilson 1987, Miller and Wigand 1994). Juniper can sustain more severe drought than pinyon (Breshears et al., 2005), making pinyon more sensitive to climate than juniper (Mueller et al., 2005). Although juniper is more drought tolerant than pinyon, both species have

declined as their habitat shrinks in the southwestern United States because of accelerated global warming. Recent drought conditions in northern New Mexico, Arizona and southern Utah are more severe than any historic drought. Consequently, P-J habitat boundaries are shifting northwards (Breshears, et al., 1997, Allen and Breshears, 1998, Breshears, et al., 2005) rapidly.

Edith and Leathwick (2009) have defined species distribution models (SDMs) as "the models that relate species distribution data (occurrence or abundance at known locations) with information on the environmental and/or spatial characteristics of those locations. These models can be used to provide understanding and/or to predict species distribution across a landscape". To project future spread of plants and animals, the use of species distribution models has increased drastically (Guisan and Thuiller 2005, Lobo et al., 2010). These models mainly depend on species presence/absence data and environmental predictor variables (maximum summer temperature, minimum winter temperature, precipitation, land cover, distance of intermittent water, distance of perennial water, distance of agricultural zone and distance of human modified area). To estimate the future shifting pinyons and junipers (in Western US), Gibson et al., 2013 used climatic, topographic and presence-absence data existing in big grids (approximately 2400 ha. in area of each grid) for these species. Many ecologists use climate data, soil type data and landscape use data in species distribution models (Peters et al., 2013, Menke et al., 2009 and Luoto et al., 2007). Araujo and Guisan (2006) demonstrated that climate predictor can be used to project species distribution accurately. Barbet-Massin and Jetz (2014) observed that climate predictors can provide accurate results for bird distributions. However, Austin

and Van Niel (2011) concluded that climatic and non-climatic predictors are equally important and need to be tested at high resolution in order to achieve projection accuracy.

There is no consistency in spatial resolution grid size (from $1\ km^2$ to $2500\ km^2$) used in species distribution models (Gibson et al., 2013, Sanchez-Fernandez et al., 2011, Luoto et al., 2007, Austin and Van Niel 2011). Scales are often chosen due to database management, computational efficiency or data availability constraints as opposed to mechanistic or biological concerns, even though scale choice creates uncertainties in the resulting projected distribution. Data with fine resolution may not match with environmental factors appropriately. However, almost always the scale of distribution model grids is much larger than the resolution of habitat variability which influences vertebrate motion.

This makes the use of seed dispersal kernels, which describe the probability of seeds moving from one cell to another, very problematic in species distribution models. The migration of fruiting trees normally occurs when birds transport seeds from parent plants to new sites (Gosper et al., 2005, Renne et al., 2002, Glyphis et al., 1981). The scale of habitat patches is tens of meters but birds can easily fly kilometer every easily. This behavior generates spatial dependence on small scales with modulation on large scales. This multi-scale dependence is perfectly suited to the method of homogenization (Garlick et al., 2010). In principle, dispersal kernels generated via homogenization can accurately represent the large scale modulation of dispersal probabilities while incorporating small-scale habitat features.

In chapter 2, we numerically calculate the seed digestion kernel (SDK) based on probability density functions (PDFs) of seed handling times. Once the kernel is determined, we will use it in a generic IDE population model to estimate invasion speeds and compare with speeds generated from Gaussian and Laplace kernels, which are limiting cases. Surprisingly, in some parameter regimes the SDK yields more rapid invasion speeds than either Laplace or Gaussian kernels.

Predictions for juniper and pinyon migration rates will be generated using literature values for parameters. We find that pinyon has much higher potential to find and occupy new niches than juniper, consistent with observations of Holocene range expansion for the two species.

In chapter 3, we adapt the dispersal model from Neubert et al., 1995 by introducing ecological diffusion with highly variable motility and a modal distribution of seed handling times. We assume that motility varies on short scales and use multiple scales in space and time to apply the method of homogenization for solving the model. Using a solvability condition, we derive a simple constant diffusion equation on large scales and approximate the SDK. This kernel depends on the harmonic average of the motility. We then embed the kernel into an IDE population model for adult plants. The large scale diffusion equation depends on small-scale variability only through the harmonically averaged motility, which inflicts a large-scale isotropic structure on the dispersal kernel. We hypothesize that the harmonic average motility therefore predicts the invasion speed in spatially complex environments. Analytic and numerical simulation methods are used to compare predicted

and observed migration speeds. We conclude that observed speed converges asymptotically to the predicted constant speed.

In chapter 4, we modify the existing seed dispersal model to reflect animals' utilization of landscape and their space-dependent motility, using an ecological diffusion and variable seed handling time model. The homogenization technique will be used to solve this model assuming that habitat variability is reflected on 30m scales but dispersal is to be resolved on kilometer-scale grids. This generates a simple diffusion equation on large scales which describes large scale modulation of dispersal probabilities, depending on parameters that are defined only on the large grid. The actual solution is a dispersal kernel including both small scale variability with motility and utilization. Neupane and Powell (2015) estimated one dimensional continuous seed transport by frugivorous birds in a variable landscape. We extend the seed transport in two dimensions discretely on vary large grids based on underlying ecological diffusion model. We connect the kernel to discrete large-scale dispersal by integrating over large cells, estimating dispersal probabilities that depend on summed landscape cover fractions residence time spent in different cover types, and cover type utilization by frugivorous. Finally, explicit solutions in the constant and uniform handling time limits are derived and solution behavior explored on randomly generated landscapes.

REFERENCES

Allen, C.D and Breshears, D.D. (1998) Drought-induced shift of a forest-woodland ecotone: Rapid landscape response to climate variation. Ecology 95:14839-14842.

Allen, L.J.S., Allen, E.J., Kunst, C.R.G. and Sosebee, R.E., 1991. A diffusion model for dispersal of opuntia (Cholla) on rangeland. Journal of Ecology 79:1123-1135.

Andow, D.A., Kareiva, P.M., Levin, S.A. and A. Okubo, A., 1990. Spread of invading organisms. Landscape Ecology 4:177-188.

Araujo, M.B. and Guisan, A., 2006. Five (or so) challenges for species distribution modeling. *Journal of Biogeography* 33:1677-1688.

Austin, M.P. and Van Niel, K.P., 2011. Improving species distribution models for climate change studies: variable selection and scale. Journal of Biogeography 38:1-8.

Barbet-Massin, M. and Jetz, W., 2014. A 40-year, continent-wide, multispecies assessment of relevant climate predictors for species distribution modeling. A Journal of Conservation Biogeography 20:1285-1295.

Balda, R.P. and Bateman, G.C. (1971) Flocking and annual cycle of pinon jay, Gymnorhinus cyanocephalus. Cooper Ornithological Society 73:287-302.

Breshears, D.D., Cobb, N.S., Rich, P.M., Price, K.P., Allen, C.D., Balice, R.G., Romme, W.H., Kastens, J.H., Floyd, L.M., Belnap, J., Anderson, J.J., Myers, O.B. and Meyer, C.W. (2005) Regional vegetation die-off in response to global-change-type drought. Proceedings of the National Academy of Sciences 102:15144-15148.

Breshears, D.D., Myers, O.B., Johnson, S.R., Meyer, C.W. and Martens, S.N. (1997)

Differential use of spatially heterogeneous soil moisture by two semiarid woody species: Pinus edulis and Juniperus monosperma. Journal of Ecology 85:289-299.

Chambers, J.C., Vander Wall, S.B. and Schupp, E.W. (1999) Seed and seedling ecology of pinyon and juniper species in the pygmy woodland of western North America. Botanical review 65:1-38.

Chavez-Ramirez, F. and Slack, R.D. (1994) Effects of avian foraging and post-foraging behavior on seed dispersal patterns of Ashe juniper. Oikos 71:40-46.

Edith, J. and Leathwick, J.R., 2009. Species distribution models: ecological explanation and prediction across space and time. Annual Review Ecology, Evolution and Systematics 40:677-697.

Fisher, R.A., 1937. The wave of advance of advantageous genes. Annals of Eugenics 7:355-369.

Garlick, M.J., Powell, J.A., Hooten, M.B. and MacFarlane, L.R. (2010) Homogenization of large-scale movement methods in ecology. Bull. Math Biol. 73:2088-2108.

Gibson, J., Moisen, G., Frescino, T. and Edwards, Jr., T.C., 2013. Using publicly available forest inventory data climate-based models of tree species distribution: examining effects of true versus altered location coordinates. Ecosystems 17:43-53.

Gosper, C.R. Stansbury, C.D. and Vivian-Smith, G., 2005. Speed dispersal of fleshy fruited invasive plants by birds: contributing factors and management options. Diversity and Distributions 11:549-558.

Guisan, A. and Thuiller, W., 2005. Predicting species distribution: offering more than

simple habitat models. Ecology Letters 8:993-1009.

Hengeveld, R. 1988. Mechanisms of biological invasions. Journal of Biogeography 15:819-828.

Lobo, J.M., Jimenez-Valverde, A. and Hortal, J., 2010. The uncertain nature of absences and their Their importance in species distribution modeling. Ecography 33:103-114.

Luoto, M. Virkkala, R. and Heikkinen, R. K., 2007. The role of land cover in bioclimatic models depends on spatial resolution. Global Ecology and Biogeography 16:34-42.

Menke, S.B., Holway, D.A., Fisher, R.N. and Jetz, W., 2009. Characterizing and predicting species distributions across environments and scales: argentine ant occurrences in the eye of the beholder. Global ecology and Biogeography 18:50-63.

Miller, R.F. and P.E. Wigand, P.E. (1994) Holocene changes in semiarid pinyon-juniper woodlands. BioScience 44:465-474.

Morales, J.M. and Carlo, T.A., 2006. The effect of Plant distribution and frugivore density on the scale and shape of dispersal kernels. Ecology 87:1489-1496.

Mueller, R.C., Scudder, C.M., Porter, M.E., Trotter III, T.R., Gehring, C.A. and Whitham, T.G. (2005) Differential tree mortality in response to severe drought: evidence for ling-term vegetation shifts. Journal of Ecology 93:1085-1093.

Nelson, K.P. (1987) On the interface between current ecological studies and the

paleobotany of pinyon-juniper woodlands. In: Everett RL(ed) Proceedings of the Pinyon-Juniper Conference. General technical report INT-215. US Department of Agriculture, Forest Service, Intermountain Research Station, Reno, Nev., 93-98.

Neubert, M.G., Kot, M. and Lewis, M.A. (1995) Dispersal and pattern formation in a discrete-time predator-prey model. Theoretical Population Biology 48:7-43.

Neupane, R.C. and Powell, J.A., 2015. Mathematical model of active seed dispersal by frugivorous birds and migration potential of pinyon and juniper in Utah. *Applied Mathematics* 6:1506-1523.

Okubo, A. and Levin, S.A., 1989. A theoretical framework for data analysis of wind dispersal of seeds and pollen. Ecology 70:329-338.

Peters, M.P., Iverson, L.R., Prasad, A.M. and Matthews, S.N., 2013. Integrating fine scale soil data into species distribution models: preparing soil survey geographic (SSURGO) data from multiple counties. General technical report NRS-122, US Forest Service, Newtown square PA, http://www.nrs.fs.fed.us/.

Reeve, J.D., Cronin, J.T. and Haynes, K.J., 2008. Diffusion models for animals in complex landscapes: incorporating heterogeneity among substrates, individuals and edge behaviours. Journal of Animal Ecology 77:898-904.

Renne, Jr. I.J., Barrow, W.C., Randall Johnson, L.A. and Bridges, W.C., 2002. Generalized avian dispersal syndrome contributes to Chinese tallow tree (Sapium ebiferum, Euphorbiaceae) invasiveness. Diversity of Distributions 8(5):285-295.

Sanchez-Fernandez, D., Lobo, J.M. and Hernandez-Manrique, O.L., 2011. Species distribution models that do not incorporate global data misrepresent potential

distributions: a case study using Iberian diving beetles. Diversity and Distributions 17:163-171.

Shigesada, N., Kawasaki, K. and Takeda, Y., 1995. Modeling stratified diffusion in biological invasions. The American Naturalist 146:229-251.

Skalski, G.T. and Gilliam, J.F., 2003. A diffusion-based theory of organism dispersal in heterogeneous populations. The American Naturalist 161:441-458.

Skellam, J.G., 1951. Random dispersal in theoretical populations. Biometrika 38:196-218.

Turchin, P. (1998) Quantitative Analysis of Movement: Measuring and Modeling Population Redistribution on Animals and Plants. Sinauer Associates Inc., Sunderland, MA.

Vander Wall, S.B. and Balda, R.P. (1977) Coadaptations of the Clark's Nutcracker and the pinon pine for efficient seed harvest and dispersal. Ecology 47:89-111.

CHAPTER 2

MATHEMATICAL MODEL OF ACTIVE SEED DISPERSAL BY FRUGIVOROUS BIRDS AND MIGRATION POTENTIAL OF PINYON AND JUNIPER IN UTAH

Abstract

Seed dispersal of juniper and pinyon is a process in which frugivorous birds play an important role. Birds either consume and digest seeds or carry and cache them at some distance from the source tree. These transported and settled seeds can be described by a dispersal kernel, which captures the probability that the seed will move a certain distance by the end of the process. To model active seed dispersal of this nature, we introduce handling time probabilities into the dispersal model to generate a seed digestion kernel. In the limit of no variability in handling time the seed digestion kernel is Gaussian, whereas for uniform variability in handling time the kernel approaches a Laplace distribution. This allows us to standardize spatial movement (diffusion) and handling time (peak settling rate) parameters for all three distributions and compare. Analysis of the tails indicates that the seed digestion kernel decays at a rate intermediate between Gaussian and Laplace seed kernels. Using this seed digestion kernel, we create an invasion model to estimate the speed at which juniper and pinyon forest boundaries move. We find that the speed of seed invasion corresponding to the digestion kernel was faster than seeds resulting from Laplace and Gaussian kernels for more rapidly digested seeds. For longer handling times the speeds are bounded between the Laplace (faster) and Gaussian (slower) speeds. Using parameter

values from the literature we evaluate the migration potential of pinyon and juniper, finding that pinyon may be able to migrate up to two orders of magnitude more rapidly, consistent with observations of pine migration during the Holocene.

2.1 Introduction

Forest boundaries change over time, and in favorable climates can expand as tree seeds spread beyond the range of the forest and germinate into new trees. Seeds may spread in a variety of ways. Common seed dispersal agents include wind, transportation in water, and transportation via birds and animals (either through being consumed and digested or being carried and cached). Because the diet of birds and some animals is often made up of fleshy-fruited plants, the pattern of seed dispersal and activities of vertebrate dispersers are closely related (Corlett 1998, Wenny 2001). Birds in particular contribute heavily to the spread of some plant populations (Clark et al., 2001, Herrera 1995).

A case in point is seed dispersal and forest migration in two southwestern tree species: pinyon (*Pinus monophylla*) and juniper (*Juniperus osteosperma*). In both species birds play a major, but different, role. Junipers produce seeds which are available most of the winter, and consequently many birds (particularly American robins, *Turdus migratorius*, and cedar waxwings, *Bombycilla cedrorum*) consume juniper berries (Chambers et al., 1999). The berries are then digested and seeds deposited some time later by defecation. Digestion does not impede the seeds' ability to germinate, particularly in the case of robins (Chavez-Ramirez and Slack, 1994), and juniper is thus dispersed while robins forage over scores of meters.

By contrast, pinyon seed dispersal by Clark's nutcracker (*Nucifraga columbiana*) and pinyon jays (*Gymnorhinus cyanocephalus)* occurs primarily through seed caching in the summer and fall, when the cones mature. Some seeds are consumed immediately, but the majority are placed in a sublingual pouch and carried several kilometers to remote cache sites, where they are buried in small groups (Vanderwall and Balda 1977, Balda and Bateman 1971). Most of the cache sites are found during the winter, but a substantial percentage of caches are never revisited and the cached seeds are in an ideal situation for germination, which determines pinyon distribution.

Variation in climate also influences the expansion of pinyon-juniper (P-J) woodland via impacts on germination and survival rates. The abundance of summer rainfall and warming in the winter and spring have caused P-J boundaries to shift northwards (Neilson 1987, Miller and Wigand 1994). Juniper can sustain more severe drought than pinyon (Breshears et al., 2005, Weisberg et al., 2007), making pinyon more sensitive to climate than juniper (Mueller et al., 2005). Although juniper is more drought tolerant than pinyon, both species have declined as their habitat shrinks in the southwestern United States because of accelerated global warming. Recent drought conditions in northern New Mexico, Arizona and southern Utah are more severe than any historic drought. Consequently, P-J habitat boundaries are shifting northwards (Breshears, et al., 1997, Allen and Breshears, 1998, Breshears, et al., 2005) rapidly. On the other hand, climate change is creating new P-J habitat in central Nevada (Weisberg et al., 2007), the central Great Basin (Bradley and Fleishman, 2008), northeastern Utah (Gray et al., 2006) and southeastern Oregon (Miller and Rose, 1995). This begs the following research questions: (i) can either

pinyon or juniper disperse far enough northward to colonize the new habitat? (ii) How rapidly may we expect forest boundaries to move? We will contribute to answering these questions by developing a PDF (Probability Density Function) for seed distribution by active dispersers and using a population-level Integrodifference Equation (IDE) to evaluate the migration potential of these two species.

To model the spread of the seeds, we assume that seed cachers or frugivorous animals collect seeds (through consumption in the case of juniper berries or collection of pinyon seeds to cache at a distance) and then follow a random walk, using the modeling framework introduced by Neubert et al., 1995. However, unlike previously considered ``failure rates" or ``hazard functions" (rates at which seeds are deposited on the ground), we note that the distribution of settling times for seed dispersal by birds should be modeled as distributions in time. Seeds defecated or cached at times sampled from a seed handling PDF will be distributed on the ground in a spatial PDF, or seed digestion kernel (SDK), which is different from any previously-considered dispersal kernel. We will derive the SDK from first principles and find that the mean handling time plays a crucial role in determining its form. The different handling of juniper and pinyon seeds leads to very different dispersal behavior. We will compare the SDK with two limiting kernels discussed by Neubert et al., 1995, the Laplace and Gaussian kernels; the SDK behaves quite differently in the small handling time limit.

In this paper we numerically calculate the SDK based on PDFs of seed handling times. Once the kernel is determined, we will use it in a generic IDE population model to estimate invasion speeds and compare with speeds generated from Gaussian and Laplace

kernels, which are limiting cases. Surprisingly, in some parameter regimes the SDK yields more rapid invasion speeds than either Laplace or Gaussian kernels. Predictions for juniper and pinyon migration rates will be generated using literature values for parameters. We find that pinyon has much higher potential to find and occupy new niches than juniper, consistent with observations of Holocene range expansion for the two species.

2.2 Methods

2.2.1 Model for seed dispersal

We begin with a common model of dispersal and settling of propagules, (any material that is used for propagating an organism) introduced by Neubert et al., 1995

$$P_t = DP_{xx} - h(t)P, \quad P(x, t = 0) = \delta(x), \tag{2.1}$$

$$S_t = h(t)P, \quad S(x, t = 0) = 0. \tag{2.2}$$

In this model $P(x,t)$ represents the density of seeds during dispersal by frugivorous birds and animals, which are assumed to follow a random walk with diffusion rate *D*. The function $h(t)$ represents the hazard function or a failure rate of seeds (i.e. rate at which seeds are placed on the ground by either caching or defectation). The function $S(x,t)$ is the density of settled seeds (seeds on the ground) at time *t*. The Dirac delta function, $\delta(x)$, places seeds initially at the origin, with no seeds yet on the ground. Because the system conserves the integral of all seeds at all locations, the sum, *S(x,t) +P(x,t)*, is a PDF for seed location in space at time *t*. The SDK, *K(x)*, is the long time limit of this process,

$$K(x) = \lim_{t\to\infty} S(x,t).$$

An important modeling point is that, to be consistent with mechanisms of seed handling by vertebrates, the hazard function, *h(t)*, must be a PDF in time. For example, when researchers measure times required for seed digestion and defecation, results are communicated as skewed frequency distributions with a strong mode and tails which decline to zero (e.g. Holthuijzen and Adkisson 1984). This is in direct contrast to failure rates considered in Neubert et al., 1995, none of which are modal PDFs. Observed distributions of handling times are asymmetrical, with long tails, and consequently a minimal characterization of such PDFs requires three parameters (one controlling the shape to the left of the mode, one controlling the location of the mode, and one controlling the shape of the tail for large *t*). We therefore propose

$$h(t) = \frac{a\, t^{\alpha}}{b^{\beta}+t^{\beta}}\,,\ \beta > \alpha + 1 > 0. \tag{2.3}$$

In this distribution the constant *b* scales the mean digestion time of seeds while *a* is a normalization constant (not free, since it depends directly on the other three parameters so that *h(t)* integrates to one). The parameters α and β determine the shape of the tails of $h(t)$ (shown in Figure 2.1 and Figure 2.2); if $t << b$, $h(t) \sim t^{\alpha}$ while $h(t) \sim t^{\alpha-\beta}$ as $t \to \infty$. The rational form of this hazard function allows us to apply the method of steepest descents to analyze the asymptotic shape of seed digestion kernels below.

2.2.2 Solution Technique for Calculating SDK

We integrate the PDE directly and then approximate time integrals using the trapezoid rule. To begin, let

$$f(\tau) = \int_0^{\tau} \frac{at^{\alpha}}{b^{\beta}+t^{\beta}} dt\,. \tag{2.4}$$

Equation (2.1) becomes

$$P_t = DP_{xx} - f'(t)P. \tag{2.5}$$

An integrating factor of $e^{f(t)}$ can be used to give the solution

$$P(x,t) = \frac{e^{-f(t)}}{\sqrt{4\pi Dt}} e^{\frac{-x^2}{4Dt}} = \frac{e^{-\int_0^t h(\tau)d\tau}}{\sqrt{4\pi Dt}} e^{\frac{-x^2}{4Dt}}. \tag{2.6}$$

Using equation (2.6) in the model (2.2) then we get

$$K(x) = \lim_{t\to\infty} S(x,t) = \int_0^\infty \frac{h(t)}{\sqrt{4\pi Dt}} e^{-\int_0^t h(\tau)d\tau - \frac{x^2}{4Dt}} dt. \tag{2.7}$$

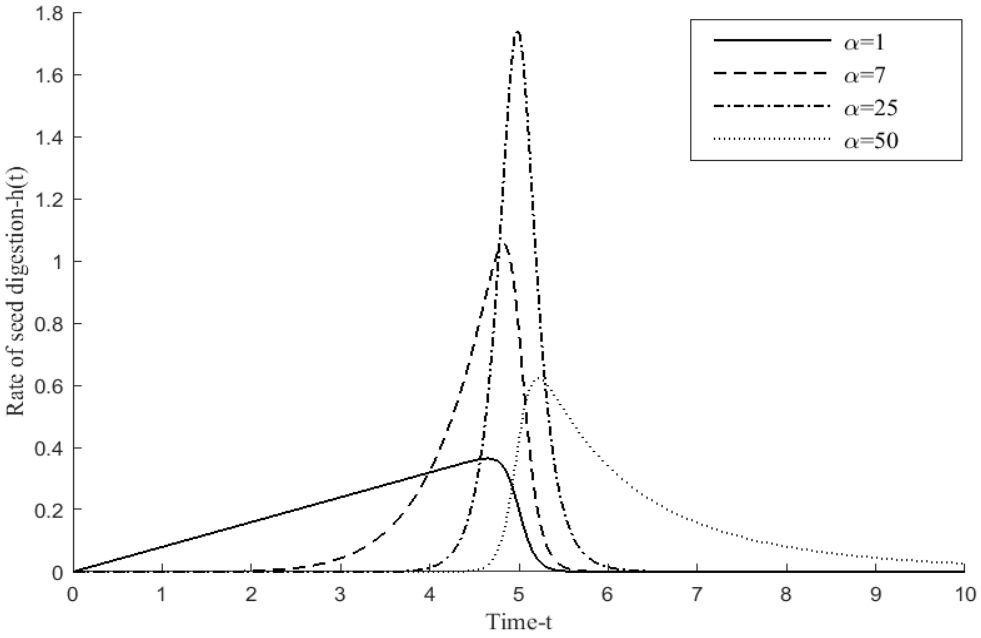

Figure 2.1 This plot demonstrates the shape of the seed settling rate, h(t), over time with $\beta = 55$ and various values of α. ($\alpha = 1$(-), $\alpha = 7$ (--), $\alpha = 25$ (-.) and $\alpha = 50$ (…)). In this plot, we see that the left tail of the distribution is shifting to the right as α increases.

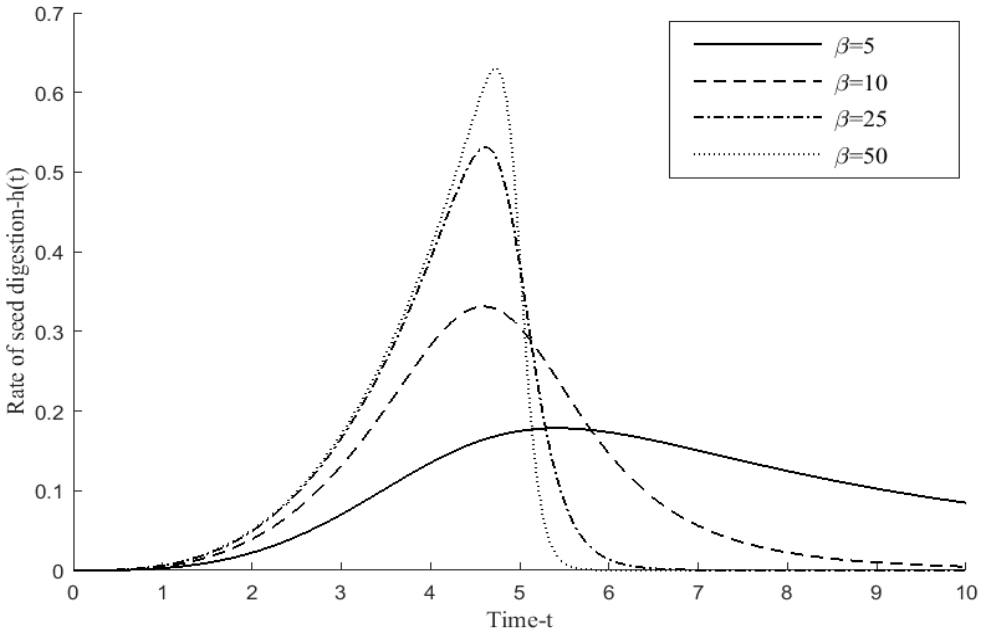

Figure 2.2 This plot demonstrates the shape of the seed settling rate, *h(t)*, over time with $\alpha = 3$ and various values of β (with $\beta = 5$ (-), $\beta = 10$ (--), $\beta = 25$ (-.), $\beta = 50$ (…)). As in Figure 2.1, we also see the right tail shifts to the right as β increases.

Numerical approximations are then calculated using the trapezoid rule for numerical integration. Solutions generated this way were cross-checked against the (much) more time-consuming finite difference solution of (2.1) and (2.2) (see Appendix A) to ensure accuracy. For the same size of time steps we found that direct quadrature of integrals in (2.7) was substantially more accurate (and rapid) than solution of the PDEs using finite differences.

2.2.3 Standardizing the three kernels for comparison

We wish to compare the SDK with the Gaussian and Laplace seed. The question is how to standardize the three kernels for comparison? Below we will show that the Laplace and Gaussian kernels arrive from different limiting choices for *h(t)*. We standardize by

choosing parameters so that peak seed drop rates occur at the same time for all three handling PDFs (see Figure 2.3). Since constant seed settling (which leads to the Laplace dispersal kernel) is not a PDF, we instead use a uniform distribution on a bounded interval with mean handling time precisely in the middle to coincide with the modes of the other two handling time distributions. Replacing a constant failure rate with a uniform PDF does not exactly generate the Laplace kernel; however, in Appendix B we show that the SDK generated by a uniform seed handling distribution is well-approximated by the Laplace distribution.

For convenience, we assume $\alpha = \beta - 2$ in equation (2.3) so that $\beta > \alpha + 1 > 0$ is always true. The function $h(t)$ is maximal at

$$t = \sqrt[\beta]{\frac{b^{\beta}(\beta-2)}{2}}\,. \tag{2.8}$$

We will call this time $\tilde{b}$. We wish to standardize the Gaussian and Laplace kernels so that their underlying seed processing PDFs have maxima at $t = \tilde{b}$. For the Gaussian, let

$$h(t) = \delta(t - \tilde{b})\,. \tag{2.9}$$

Then

$$G(x) = \int_0^{\infty} \frac{\delta(t-\tilde{b})}{\sqrt{4\pi D t}} e^{-\int_0^t \delta(\tau-\tilde{b})d\tau - \frac{x^2}{4Dt}} dt\,.$$

This gives

$$G(x) = \frac{1}{\sqrt{4\pi D\tilde{b}}} e^{\frac{-x^2}{4D\tilde{b}}}\,. \tag{2.10}$$

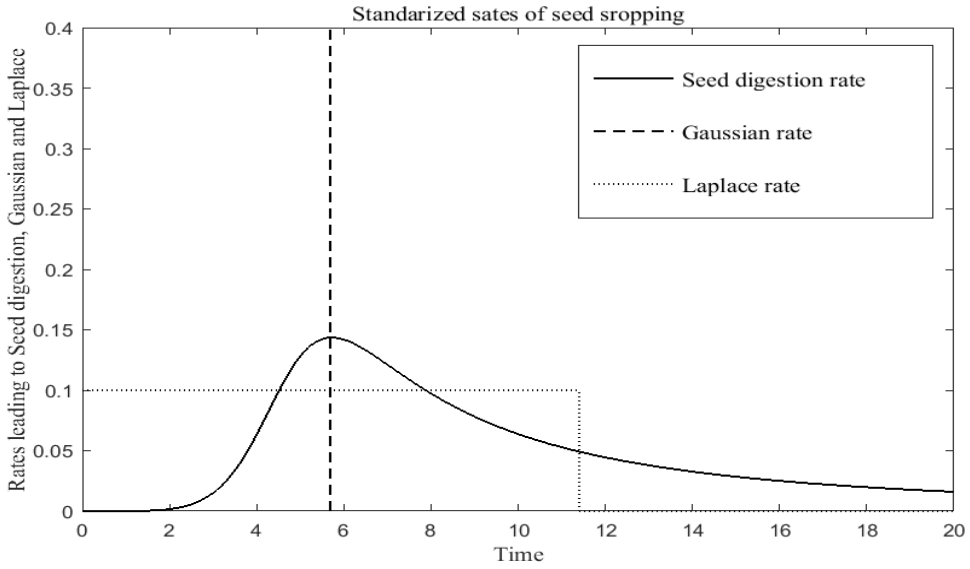

Figure 2.3 This plot provides an initial comparison of the three type of seed digestion rates, the PDF of seed digestion times (-) and the PDFs leading to the Gaussian kernel (---) and the Laplace kernel (…). For this comparison, we fixed $\beta = 7.5$, $\alpha = 5.5$ and $b = 5$. It can be seen that the three kernels share the same maximum to standardize the three kernels.

To generate a Laplace kernel we assume that the distribution of seed settling is a step function defined by

$$h(t) = \begin{cases} \dfrac{1}{2\tilde{b}}, & 0 < t \le 2\tilde{b}, \\ 0, & t > 2\tilde{b}. \end{cases} \tag{2.11}$$

As is shown in Appendix B, the solution to (2.1) and (2.2) with the step function defined in equation (2.11) is approximately the Laplace kernel

$$L(x) = \frac{1}{2\sqrt{2D\tilde{b}}} e^{\frac{-|x|}{\sqrt{2D\tilde{b}}}}. \tag{2.12}$$

After this standardization, the Gaussian kernel (2.10) and the Laplace kernel (2.12) are ready for comparison with the seed digestion kernel. Figure 2.4 illustrates the shape of seed distribution on the ground for the standardized kernels. Seeds seem to disperse to the

furthest for the Laplace (having fattest tail), $L(x)$, and least for the Gaussian (the thinnest tail) , $G(x)$. The pattern of seed dispersal under seed digestion kernel, $K(x)$, is bounded by the other two. This observation will be formalized using the method of steepest descents below.

2.2.4 Analyzing the tail of seed digestion kernels

Here, we approximate the tail of the SDK using the steepest descent method (Marsden and Hoffman, 1987) to compare tails with Gaussian and Laplace seed kernels. As in the previous section, we assume $\alpha = \beta - 2$ so that the rate of seed digestion equation

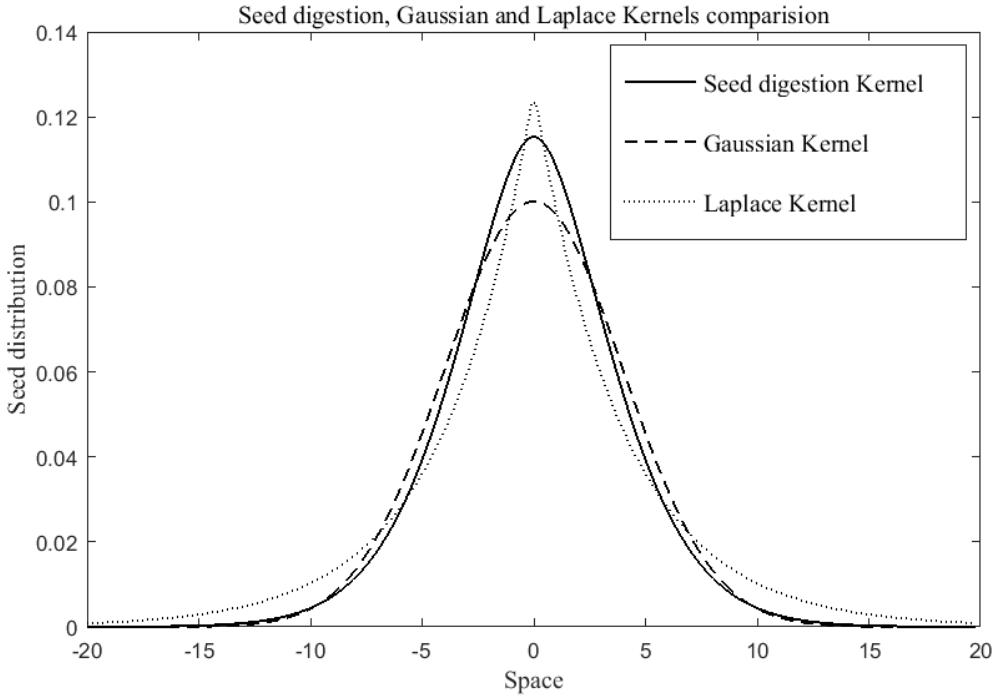

Figure 2.4 Comparison of the seed digestion kernel (-), Gaussian kernel (---) and Laplace kernel (…) with $b = 10, \alpha = 3$ and $\beta = 7$. The Gaussian tail decays more rapidly than tail of seed digestion and the seed digestion tail decays more slowly than Laplace (the fattest tail).

(2.3) becomes

$$h(t) = \frac{at^{\beta-2}}{b^{\beta} + t^{\beta}} . \tag{2.13}$$

Define the exponent in (2.7) as

$$H(t) = \int_0^t h(y)dy - \frac{x^2}{4Dt} . \tag{2.14}$$

The critical point of the function $H(t)$ is $t_0 = \left(\frac{x^2 b^{\beta}}{4aD - x^2} \right)^{\frac{1}{\beta}}$. Differentiating twice the equation (2.14) with respect to *t* and evaluating at $t = t_0$ we get

$$H''(t_0) = \frac{-\beta}{16aD^2 b^{\beta}} (4aD - x^2)^2 . \tag{2.15}$$

Let us suppose $g(t) = \frac{h(t)}{\sqrt{4\pi Dt}}$ in equation (2.7); then

$$g(t_0) = \frac{x^{\frac{2\beta-5}{\beta}} (4aD - x^2)^{\frac{5}{2\beta}}}{8b^2 D\sqrt{\pi bD}} . \tag{2.16}$$

Equations (2.15) and (2.16) can be used with the generalized steepest descent theorem to approximate (2.7), giving

$$K(x) \approx \frac{\sqrt{a} e^{H(t_0)}}{\sqrt{2\beta D} b^{(\frac{5-\beta}{2})} x^{(\frac{10-3\beta}{2\beta})} (4aD - x^2)^{(\frac{2\beta-5}{2\beta})}} . \tag{2.17}$$

Analyzing *K* as $x \to \infty$ gives the asymptotic behavior in the tail (see below).

2.2.5 Population Model for Evaluating Migration Potential

To determine how the shape of the SDK affects rates of invasion, the kernels must be imbedded in a population model. Below we present a simplification of the model used by Powell and Zimmermann (2004) to describe the general behavior of an invasion by perennial plants. For xeric-adapted species like pinyon and juniper dispersing into the new regions, competition for water and space occurs primarily among seedlings. We take

$$N_{t+1}(x) = T[K(x) * kN_t(x)] + (1-\omega)N_t(x), \tag{2.18}$$

where N_t represents the population density of adults in generation t. The function $K(x)$ is the SDK while ω is the mortality rate of adults per generation, k is the number of seeds produced per adult per generation, and

$$T = \frac{Mg\sigma N_t}{M + N_t}$$

is the Beverton-Holt model for seed survival and germination in competition with other seeds. Here M is the maximum number of surviving seeds, g is the germination rate, and σ is the seedling survival rate. The convolution in equation (2.18) is defined by

$$K(x) * kN_t(x) = \int_{-\infty}^{\infty} K(x-y)kN_t(y)dy = \int_{-\infty}^{\infty} K(y)kN_t(x-y)dy,$$

and the integral represents the total number seeds arriving at location x from all possible locations, y. Therefore, the first term on the right hand of the invasion model (2.18) predicts the distribution of new trees depending on the available sources and the second term provides the surviving number of old trees so that the total is the population of trees in the next generation.

2.2.6 Analysis of invasion speeds

To analyze invasion speeds for models like (2.18), we follow the analysis of Kot et al., 1996. Because the population density of a tree population approaches zero in advance of the invasion front, we can assume that as $x \to \infty$

$$N_t(x) \sim \varepsilon e^{-ux}, \tag{2.19}$$

with $\varepsilon << 1$. We assume that the spread of the tree population is a traveling wave with parameter u determining the shape of its leading edge. Introducing a constant, c, to represent the speed of invasion, the traveling wave of population density during an invasion satisfies

$$N_{t+1}(x) = N_t(x-c). \tag{2.20}$$

Combining equations (2.19) and (2.20)

$$N_{t+1}(x) = \varepsilon e^{-u(x-c)}. \tag{2.21}$$

Plugging this into equation (2.18),

$$\varepsilon e^{-u(x-c)} = T[\varepsilon k K(x) * e^{-ux}] + \varepsilon(1-\omega)e^{-ux}, \tag{2.22}$$

Taking only leading order terms,

$$e^{-u(x-c)} = R_0 K(x) * e^{-ux} + (1-\omega)e^{-ux}, \tag{2.23}$$

where $R_0 = kT'(0) = kg\sigma$ is the net reproductive rate.

Writing the convolution of equation (2.23) in terms of an integral, we have

$$e^{cu} = R_0 \int_{-\infty}^{\infty} K(v)e^{uv}dv + (1-\omega) = R_0 M(u) + (1-\omega), \tag{2.24}$$

where the moment generating function, *M(u)*, is defined by

$$M(u) = \int_{-\infty}^{\infty} K(v) e^{uv} dv . \tag{2.25}$$

Differentiating equation (2.24) with respect to u and setting to zero to find the extremal invasion speed gives

$$ce^{cu} = R_0 M'(u) . \tag{2.26}$$

Using equation (2.26) to eliminate c in (2.24) gives

$$F(u) = u \frac{R_0 M'(u)}{R_0 M(u) + (1-\omega)} - \log[R_0 M(u) + (1-\omega)] = 0 . \tag{2.27}$$

To find the invasion speed, $\tilde{c}$, we solve equation (2.27) numerically for u and then use (2.26). Both $M(u)$ and $M'(u)$ were approximated for specific u using the trapezoid rule; roots of $F(u)$ were found using fzero in MATLAB. Those roots are used in equation (2.24) to predict invasion speed.

2.3 Results

2.3.1 Shape of kernels based on mean digestion time scaling parameter

The mean digestion time scaling parameter b plays a major role in determining seed dispersal. Changing the value of b generates different shapes of solutions (see figure 2.5) with larger values of b corresponding to broader dispersal, as we expected. If digestion or caching takes longer, birds have more time to travel before depositing seeds, resulting in seeds traveling further from the source.

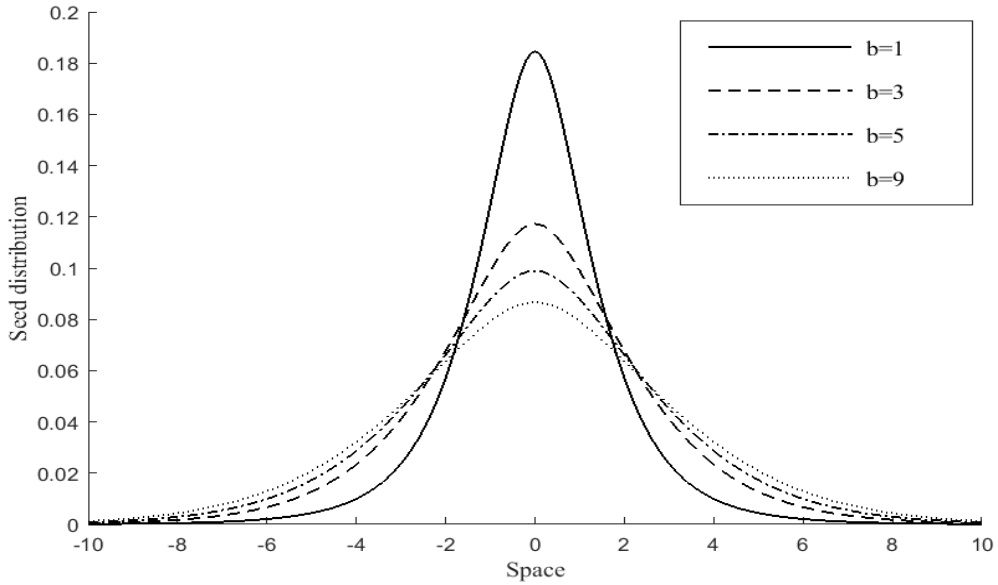

Figure 2.5 Comparison of seed digestion kernels for various mean seed handling times. In this figure, $b=1$(-), $b=3$(--), $b=5$(-.) and $b=9$(…), illustrating broader dispersal for larger mean digestion times.

2.3.2 Comparison of tails

We would like to characterize the shape of the tail of the SDK and place it in the context of the well-known Gaussian (2.10) and Laplace kernels (2.12). The exponents of the exponential functions for both kernels determine the shapes of the corresponding tails. To analyze the tails of these kernels, we consider large *x* and assume other parameter values are bounded. The dominant terms in the exponents of the Gaussian and Laplace kernels are $\frac{-x^2}{2^{\frac{7}{3}}bD}$ and $\frac{-x}{\sqrt{2^{\frac{2}{3}}bD}}$, respectively. It follows that the tail of the Gaussian kernel decays to zero much faster than the tail of the Laplace kernel when $x \gg 1$.

In the case of the most slowly-decaying PDF of seed handling times, $\beta = 3$, the SDK derived from the method of steepest descents (2.17) can be written as:

$$K(x) \sim \frac{\sqrt{a}}{b\sqrt{6D}} e^{-\left(\int_0^{t_0} h(\tau)d\tau + \frac{x^{\frac{4}{3}}\left(4aD-x^2\right)^{\frac{1}{3}}}{4bD} + \frac{1}{6}\ln(x) + \frac{1}{6}\ln\left(4aD-x^2\right)\right)}, \tag{2.28}$$

where $h(\tau)$ is given in equation (2.13). Note here that branch cuts have not been chosen for the various complex functions in the exponent so we are at liberty to choose branches to keep results on the real axis. Since $\int_0^{t_0} h(\tau)d\tau$ is finite, the dominant term in the exponent of (2.28) is

$$\frac{x^{\frac{4}{3}}\left(4aD-x^2\right)^{\frac{1}{3}}}{4bD} \sim \frac{-x^2}{4bD} \tag{2.29}$$

and therefore

$$\log(|K(x)|) \sim -\left|\frac{-x^2}{4bD}\right|. \tag{2.30}$$

The exponents of Gaussian kernel and Laplace kernels are

$$\log(G(x)) \sim \frac{-x^2}{2^{\frac{7}{3}}bD}, \tag{2.31}$$

and

$$\log(L(x)) \sim \frac{-x}{\sqrt{2^{\frac{2}{3}}bD}}. \tag{2.32}$$

Observing

$$\frac{-x^2}{2^{\frac{7}{3}}bD} < -\left|\frac{-x^2}{4bD}\right| \ll \frac{-x}{\sqrt{2^{\frac{2}{3}}bD}},$$

we conclude that the tail of Gaussian kernel decays to zero most rapidly while the tail of Laplace kernel is the slowest. The tail of the SDK is intermediate between the other two.

2.3.3 Relationship between invasion rate and mean digestion time

We have not chosen scales for generation time, population density and space yet. To compare the speeds of invasion from the population IDE (2.18), we may therefore, without loss of generality, choose mortality $\omega = 0.2$, the reproductive rate $R_0 = 3$ and the diffusion *D=1*. We fix the seed settling parameters $\alpha = 1$ and $\beta = 3$ for the longest tail in $h(t)$. Using these values, we estimate the speeds of invasion corresponding to the SDK, $K(x)$, the Gaussian kernel, $G(x)$, and the Laplace kernel, $L(x)$. Speeds of invasion are compared in figure 2.6 as a function of the mean digestion time scaling parameter b.

There is a strong relationship between the characteristic handling time, *b*, and invasion speed, *c*. The longer it takes to digest a seed, the faster forest migration. For small *b*, the SDK invasion speed is higher than the speeds corresponding to the Gaussian and Laplace kernels. On the other hand, for bigger *b* values, the speed of invasion with the Laplace kernel is fastest, the speed with a Gaussian kernel is slowest and the speed corresponding to the SDK stays between the other two, as might be expected from comparing tails.

As $b \to 0$, not only does the SDK give faster rates of invasion, but also speeds associated with the Gaussian and Laplace kernels decrease to zero whereas speeds corresponding to the SDK are still positive. This happens because both Gaussian and Laplace kernels approach the delta function, $\delta(x)$, as $b \to 0$, meaning that seeds do not disperse. However, the seed digestion kernel has finite support as $b \to 0$ (because $h(t) \sim t^{\alpha-\beta}$ as $b \to 0$). Since mean digestion time is non-zero, the SDK allows for seed dispersal even as *b* tends to zero.

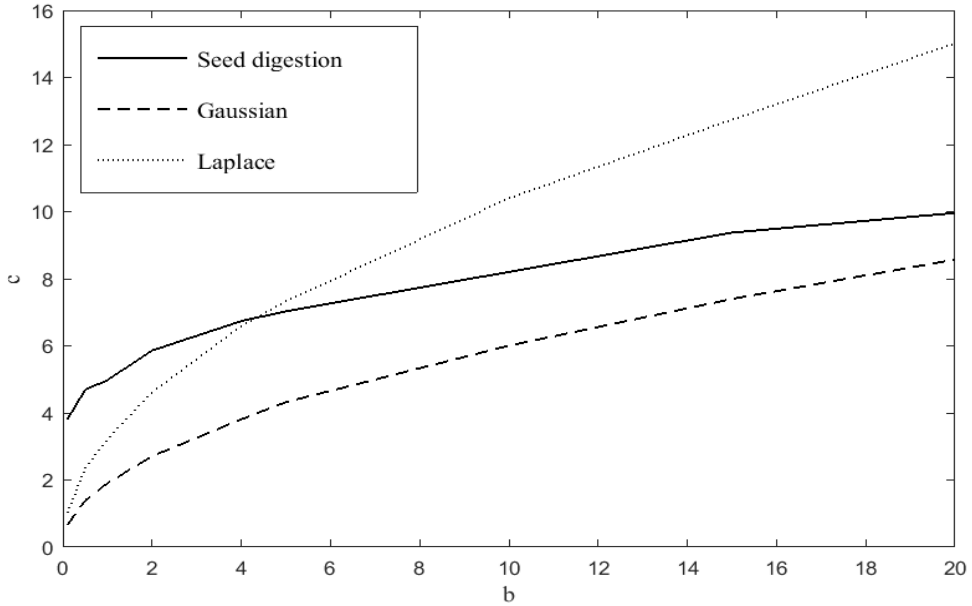

Figure 2.6 Speeds of invasion calculated for the seed digestion kernel, the Gaussian kernel and the Laplace kernel. The solid line indicates the speed with seed digestion kernel, the dashed line indicates the speed with Gaussian kernel and the dotted line is the speed with Laplace kernel. The figure shows that the invasion speed produced from all three kernels always increasing in different rates as the increase of mean digestion time scaling parameter.

2.4 Migration Potential of Pinyon and Juniper

To quantify invasion speeds in terms of yearly distance covered for both pinyon and juniper, we need specific data such as the mean generation time *(G)*, mean dispersal space step (λ), mean dispersal time step (τ), mortality rate (ω) and the characteristic handling time (b) for each species. We also need to estimate the reproductive rate (R_0) and the diffusion rate (D). We are fortunate to have a paired growth rate study on pinyon-juniper in central Utah (Tausch and West 1988) , in which population growth of both species was tracked dendrochronologically from survivors of a fire in the mid-nineteenth century. This allows us to calculate

$$R_0 = \sqrt[G]{\frac{N}{n}}, \tag{2.33}$$

where G is the generation time (duration from seedling to getting matured tree for producing seeds), n is the initial number of trees and N is the total number of trees at the end of the study. To estimate the diffusion rate D for birds, we use

$$D = \frac{\lambda^2}{4\tau}, \tag{2.34}$$

where λ is the root mean square displacement in a time step of the underlying random walk and τ is the mean time between steps in the walk (Turchin 1998). A summary of parameters used for the two species, and supporting references, appears in Table 2.1.

Table 2.1 Parameters used to estimate seed dispersal kernels and migration rates of juniper and pinyon in Utah. References for parameter values are provided.

Parameter	Juniper	Reference	Pinyon	Reference
Generation time (G)	50 yrs	Li et al., (2011)	20 yrs	Suzan-Azpiri et al., (2002)
Mean dispersal space step (λ)	55 m	Chavez-Ramirez and Slack (1994)	4500 m	Vander Wall and Balda, (1977)
Mean dispersal time step (τ)	4 min	Chavez-Ramirez and Slack (1994)	22.5 min	Vander Wall and Balda, (1977)
Diffusion (D)	189.1 m^2/min	Calculated	225,000 m^2 /min	Calculated
Mean handling time (b)	14.9 min	Holthuijzen and Adkisson (1984)	52.5 min	Vander Wall and Balda, (1977)
Reproductive Rate (R_0)	1.17 /gen	Tausch and West (1988)	2.04 /gen	Tausch and West (1988)
Mortality(ω)	0.0004	Shaw et al., (2005)	0.00155	Shaw et al., (2005)

In order to calculate yearly invasion speed, c, we need to rescale both space and time, since we fixed D = 1 (equivalent to nondimensionalized space) in the numerical calculations. Additionally, each step in our IDE is a generation, which must be scaled back to years for comparison purposes. Assuming the dimensional diffusion rate, D, is in m^2

per minute and the mean handling time $\tilde{b}$ is in minutes, the only available space scale in the seed dispersal model (2.1) and (2.2) is $\alpha = \sqrt{D\tilde{b}}$.

Now, if $\tilde{c}$ is the speed of invasion associated with the nondimensional dispersal model ($D = 1$) then yearly migration rates can be calculated:

$$c = \underbrace{\tilde{c}}_{\frac{\text{nondimensional steps}}{\text{generation}}} \times \underbrace{\alpha}_{\frac{\text{meters}}{\text{nondimensional steps}}} \times \underbrace{\frac{1}{\frac{G}{\frac{\text{generation}}{\text{years}}}}}. \qquad (2.35)$$

Now we turn to specific parameter values for pinyon and juniper.

For pinyon we use a generation time $G \sim 20$ years from Suzan-Azpiri et al., 2002. To estimate R_0 we refer to Tausch and West (1988), who determined that only 6 pinyon survived the nineteenth-century fire on their site. The number of pinyon pines increased to 1051 over the next 145 years giving $R_0 = 2.04/\text{generation}$ for pinyon from equation (2.33). Vanderwall and Balda (1977) observed that Clark's Nutcracker fly from 4000 to 5000 meters while caching seeds, taking 15-30 minutes. We therefore take $\lambda = 4500$ meters and use $\tau = 22.5$ minutes, giving $D = 2.25 \times \frac{10^5 \text{m}^2}{\text{min}}$. They further observed seed handling in three phases. Nutcrackers spend 45minutes collecting seeds to fill their pouch, 15-30 minutes to travel to the caching area and 5-10 minutes to cache all seeds carried in their pouch. Averaging and summing, we estimate seed mean handling time to be $\tilde{b} = 52.5$ minutes. This gives a dispersal scale $\alpha = \sqrt{D\tilde{b}} = 3436.93$ m. Shaw et al., 2005 estimate annual mortality at 0.08-0.23% for common pinyon. Taking the mean and converting to a rate per generation gives $\omega = 0.00155$. Taken together, these parameters give a minimum speed of 518.97 m/year and a maximum of 946.1 m/year for pinyon, with an average of 773.31 m/year.

On the other hand, for juniper we use a generation time $G \sim 50$ years from Li et al., 2011. To estimate R_0 we follow Tausch and West (1988), who observed that only 109 junipers survived the nineteenth-century fire on their site. The number increased to 172 over the next 145 years giving $R_0 = 1.17$/generation for juniper from equation (2.33). Chavez-Ramirez and Slack (1994) observed that American robins forage in the range of 10-100 meters with mean 55 meters and average 4 minutes between trees. We therefore take $\lambda = 55$ meters and time step $\tau = 4$ minutes, giving $D = 189.1\ \mathrm{m}^2/\mathrm{min}$. Holthuijzen and Adkisson (1984) report that the cedar waxwing takes between 7.35 and 22.45 minutes to digest red cedar (*Juniperus virginiana)* seeds; we therefore use a handling time $\tilde{b} = 14.9$ min. These estimates give a dispersal scale $\alpha = \sqrt{D\tilde{b}} = 53.1$ m. Shaw et al., 2005 estimate annual mortality at 0.01-0.07% for Utah juniper (*Juniperus osteosperma*). Taking the mean and converting to a rate per generation gives $\omega = 0.0004$. Using these parameter ranges we find that juniper spreads with minimum speed 0.42 m/year and maximum speed 7.3 m/year with an average of 3.3 m/year, two orders of magnitude more slowly than pinyon.

These results match up well with what is known about these two species and their relative movements during the Holocene. Juniper seems to have been present in the Great Basin area for at least 30,000 years, based on evidence from fossilized packrat middens (Nowak et al., 1994). While its range contracted due to climatic shifts there were no significant expansions. By contrast, pinyon pine was limited to Arizona and New Mexico up to 9000 years ago, but migrated up the Wasatch front to the northeastern corner of Utah in the next 1000 - 1500 years (Lanner and Devender 1998), which would have required speeds in excess of 500 m/year.

2.5 Conclusion

Mechanisms of plant migration vary based on the source plant and the dispersal process delivering seeds to new locations for germination. Juniper berries mainly disperse after being eaten by vertebrates who deposit seeds after digestion. Birds, particularly robins, may be the biggest dispersers. Seeds of pinyon trees, on the other hand, are commonly spread while animals cache, and corvids (jays and nutrcrackers), which cache at large distances, are the largest contributors. In this paper, we introduced a PDF of seed-handling to reflect the effects of digestion/caching on dispersal of pinyon and juniper seeds. We connected this distribution to hazard functions or failure rates in an existing random-walk dispersal model to determine a seed digestion kernel modeling the probable location of seeds after active dispersal. As expected, if birds or animals take more time to handle seeds, those seeds are dispersed further away from the source tree. While no closed-form solution for the SDK is available, it is easy to calculate numerically (and would only have to be calculated once, in advance, for implementation in an IDE model for population invasion).

To evaluate migration potential for pinyon and juniper we introduced an IDE model with competition among seedlings, which is appropriate for desert-adapted trees in the xeric environment of the American Southwest. The SDK was compared with well-known Laplace and Gaussian kernels *(L(x)* and *G(x)).* After standardizing the associated PDFs for handling time, the speed of invasion for the SDK was the fastest for shorter handling times (rapidly digesting seeds). As handling times increased, however, the speeds for the SDK fell between the Laplace kernels (faster; based on an assumption of constant seed

deposition) and the Gaussian kernels (slower; based on the assumption of instantaneous seed deposition), as would be expected from the relative behavior of the tails.

Using the SDK and median parameter values estimated from the literature it turned out that pinyon has migration potential at least two orders of magnitude larger than juniper due to avian dispersal. Along with changing temperatures and diminishing moisture levels the favorable environment for P-J is moving northwards through Utah. Over time, these trees will not be able to survive in the southern limits of their current habitat. The large migration potential of pinyon means that it is most likely to occupy new habitats opening to the north.

Of course, juniper already occupies much of the available northern habitat, and with longer generation times and much stronger adaptation to variable moisture regimes juniper can be expected to flourish in northern Utah for the foreseeable future. Moreover, juniper may have much higher migration potential than our analysis indicates. For the slower juniper we can probably not ignore mammalian dispersers (Vander Wall 1997) and passive dispersal agents (such as runoff and streams for dispersing juniper berries, see Chambers et al., 1999). The two main avian juniper dispersers, American robins and cedar waxwings, both forage and defecate locally and therefore do not seem to make a large contribution to juniper spread. However, mammals such as foxes, bears and coyotes may disperse juniper seeds long distances since they have much longer gut-retention times and can travel more than 10 kilometer per day (Willson 1993). Since juniper seeds persist through winter, dispersal by spring runoff can also contribute substantially. Nevertheless, dispersers like pinyon jay and Clark's nutcracker likely give pinyon the dispersal advantage over juniper.

The largest factor ignored in our study is spatial variability. As Powell and Zimmermann (2004) point out, vertebrate dispersers move rapidly through some habitat and linger in others, and western landscapes are comprised of highly variable habitat, particularly at the leading edge of invasions. One would expect step sizes in the random walks that dispersers follow, and therefore their diffusions rates, to vary strongly with habitat type. Recent advances in the use of homogenization (Garlick et al., 2010) make integration of reaction-diffusion models with highly variable constants surprisingly easy, so building SDKs with variable diffusion and applying asymptotic techniques like homogenization will be our future concentration of research.

REFERENCES

Allen, C.D and Breshears, D.D. (1998) Drought-induced shift of a forest-woodland ecotone: Rapid landscape response to climate variation. *Ecology* 95:14839-14842.

Ascher, U.M. and Greif, C. (2011) *A First Course in Numerical Methods*. SIAM, Philadelphia.

Balda, R.P. and Bateman, G.C. (1971) Flocking and annual cycle of pinon jay, *Gymnorhinus cyanocephalus. Cooper Ornithological Society* 73:287-302.

Bradley, B.A. and Fleishman, E (2008) Relationships between expanding pinyon-juniper cover and topography in the central Great Basin, Nevada. *Journal of Biogeography* 35:951-964.

Breshears, D.D., Cobb, N.S., Rich, P.M., Price, K.P., Allen, C.D., Balice, R.G., Romme, W.H., Kastens, J.H., Floyd, L.M., Belnap, J., Anderson, J.J., Myers, O.B. and Meyer, C.W. (2005) Regional vegetation die-off in response to global-change-type drought. *Proceedings of the National Academy of Sciences* 102:15144-15148.

Breshears, D.D., Myers, O.B., Johnson, S.R., Meyer, C.W. and Martens, S.N. (1997) Differential use of spatially heterogeneous soil moisture by two semiarid woody species: *Pinus edulis* and *Juniperus monosperma*. *Journal of Ecology* 85:289-299.

Chambers, J.C., Vander Wall, S.B. and Schupp, E.W. (1999) Seed and seedling ecology of pinyon and juniper species in the pygmy woodland of western North America. *Botanical review* 65:1-38.

Chavez-Ramirez, F. and Slack, R.D. (1994) Effects of avian foraging and post-foraging behavior on seed dispersal patterns of Ashe juniper. *Oikos* 71:40-46.

Clark, C.J., Poulsen, J.R. and Parker, V.T. (2001) The role of arboreal seed dispersal groups on the seed rain of a lowland tropical forest. *Biotropica* 33:606-620.

Corlett, R.T. (1998) Furgivory and seed dispersal by vertebrates in the Oriental (Indomalayan) Region. *Cambridge Philosophical Society* 73:413-448.

Garlick, M.J., Powell, J.A., Hooten, M.B. and MacFarlane, L.R. (2010) Homogenization of large-scale movement methods in ecology. *Bull. Math Biol.* 73:2088-2108.

Gray, S.T., Betancourt, J.L., Jackson, S.T. and Eddy, R.G. (2006) Role of multidecadal climate variability in a range extension of Pinyon Pine. *Ecology* 87:1124-1130.

Herrera, C.M. (1995) Plant-vertebrate seed dispersal systems in the mediterranean: ecological evolutionary and historical determinants. *Annual Review of Ecology and Systematics* 26:705-727.

Holthuijzen, A.M.A. and Adkisson. C.S. (1984) Passage rate, energetics, and utilization efficiency of the Cedar Waxwing. *The Wilson Bulletin* 96:680-684.

Kot, M., Lewis, M.A. and van den Driessche, P. (1996) Dispersal data and spread of invading organisms. *Ecology* 77:2027-2042.

Lanner, R.M. and Van Devender, T.R. (1998) The recent history of pinyon pines in the American Southwest. *Ecology and Biogeography of Pinus* 171-182.

Li, Z., Zou, J., Mao, K., Lin, K., Li, H., Liu, J,. Kallman, T. and Lascoux, M. (2011) Population genetic evidence for complex evolutionary histories of four high altitude juniper species in the Qinghai-Tibetan plateau. *Evolution* 66(3):831-845.

Marsden, J.E. and Hoffman, M.J. (1987) *Basic Complex Analysis.* W.H. Freeman and Company, New York.

Miller, R.F. and P.E. Wigand, P.E. (1994) Holocene changes in semiarid pinyon-juniper woodlands. *BioScience* 44:465-474.

Miller, R.E. and Rose, J.A. (1995) Historic expansion of *Juniperus occidentalis* (Western Juniper) in southeastern Oregon. *Great Basin Naturalist* 55:37-45.

Mueller, R.C., Scudder, C.M., Porter, M.E., Trotter III, T.R., Gehring, C.A. and Whitham, T.G. (2005) Differential tree mortality in response to severe drought: evidence for ling-term vegetation shifts. *Journal of Ecology* 93:1085-1093.

Nelson, K.P. (1987) On the interface between current ecological studies and the paleobotany of pinyon-juniper woodlands. In: Everett RL(ed) Proceedings of the Pinyon-Juniper Conference. General technical report INT-215. US Department of Agriculture, Forest Service, Intermountain Research Station, Reno, Nev., 93-98.

Neubert, M.G., Kot, M. and Lewis, M.A. (1995) Dispersal and pattern formation in a discrete-time predator-prey model. *Theoretical Population Biology* 48:7-43.

Nowak, C.L., Nowak, R.S., Tausch, R.J. and Wigand, P.E. (1994) Tree and shrub dynamics in northwestern Great Basin woodland and shrub steppe during the late Pleistocene and Holocene. *American Journal of Botany* 265-277.

Powell, J.A. and Zimmermann, N.E. (2004) Multiscale analysis of active seed dispersal contributes to resolving Reid's paradox. *Ecology* 85:490-506.

Shaw, J.D., Steed, B.E. and DeBlander, L.T. (2005) Forest Inventory and Analysis (FIA) annual inventory answers the question: What is happening to pinyon-juniper woodlands?. *Journal of Forestry* 280-285.

Suzan-Azpiri, H., Sanchez-Ramos, G., Martinez-Avalos, J.G., Villa-Melgarejo, S. and Franco, M. (2002) Population structure of *Pinus nelson* shaw, an endemic pinyon pine in Tamaulipas, Mexico. *Forest Ecology of Management* 165:193-203.

Tausch, R.J. and West, N.E. (1988) Differential establishment of pinyon and juniper following fire. *American Midland Naturalist* 119:174-184.

Turchin, P. (1998) *Quantitative Analysis of Movement: Measuring and Modeling Population Redistribution on Animals and Plants.* Sinauer Associates Inc., Sunderland, MA.

Vander Wall, S.B. and Balda, R.P. (1997) Dispersal of singleleaf pinyon pine (*Pinus monophylla*) by seed-caching rodents. *Journal of Mammalogy* 78:181-191.

Vander Wall, S.B. and Balda, R.P. (1977) Coadaptations of the Clark's Nutcracker and the pinon pine for efficient seed harvest and dispersal. *Ecology* 47:89-111.

Weisberg, P.J., Lingua, E. and Pillai, R.B. (2007) Spatial patterns of pinyon-juniper woodland expansion in central Nevada. *Rangeland Ecology & Management* 60:115-124.

Wenny, D.G. (2001) Advantage of seed dispersal: A re-evaluation of directed dispersal. *Evolutionary Ecology Research* 3:51-74.

Willson, M.F. (1993) Mammals as seed-dispersal mutualists in North America. *Oikos* 67(1): 159-176.

CHAPTER 3

INVASION SPEEDS WITH ACTIVE DISPERSERS IN HIGHLY VARIABLE LANDSCAPES: MULTIPLE SCALES, HOMOGENIZATION, AND THE MIGRATION OF TREES

Abstract

The distribution of many tree species is strongly determined by the behavior and range of vertebrate dispersers, particularly birds. Many models for seed dispersal exist, and are built around the assumption that seeds undergo a random walk while they are being carried by vertebrates, either in the digestive tract or during the process of seed storage (caching). We use a PDF of seed handling (caching and digesting) times to model non-constant seed settling during dispersal, and model the random component of seed movement using ecological diffusion, in which animals make movement choices based purely on local habitat type instead of population gradients. Spatial variability in habitat directly affects the movement of dispersers and leads to anisotropic dispersal kernels. For birds, which can easily move many kilometers, habitat changes on the scale of tens of meters can viewed as rapidly varying. We introduce multiple scales and apply the method of homogenization to determine leading order solutions for the seed digestion kernel (SDK). Using an integrodifference equation (IDE) model for adult trees, we investigate the rate of forest migration. The existing theory for predicting spread rates in IDE does not apply when dispersal kernels are anisotropic. However, the homogenized SDK is isotropic on large scales and depends only on harmonically averaged motilities and modal rates of

digestion. We show that speeds calculated using the harmonic average motility accurately predict rates of invasion for the spatially variable system.

3.1 Introduction

The diffusion equation represents a fundamental framework for determining the spatial spread of organisms (Hengeveld 1988, Okubo and Levin 1989, Shigesada et al., 1995, Skalski and Gilliam 2003, Morales and Carlo 2006). Fisher (1937) studied asymptotic rates of invasion of mutant genes and his ideas were extended by Skellam (1951) to ecological problems (the spread of animal and plant populations on landscape scales). Later on, diffusion equations were used to describe the spread of the cereal leaf beetle, muskrat, small cabbage white butterfly (Andow et al., 1990) and dispersal of cholla (Allen, 1991).

Diffusion models usually assume that animal movement properties are constant in space and time, but in fact animals move differently in different habitats. Movement occurs while animals search for food, water, breeding sites, mates and shelter. Each of these activities is conditioned by habitat type; deer do not linger to forage on barren slick rock, and birds eating juniper berries spend a great deal of time foraging on juniper trees but very little time in the sagebrush steppe separating stands of juniper. The movement properties of a population are determined by the composition of all landscape elements and the nature of the boundaries between them (Moilanen and Hanski, 1998, Haynes and Cronin, 2003, Ovaskainen, 2004).

Spatial variation in landscape structure is one of the components that affects the mobility of active dispersers. Hanski et al., 2004 have observed that increasing environmental heterogeneity increases the variance in mobility of butterflies. Raposo et al., 2011 have shown that heterogeneous landscape enhances diffusivity and foraging behavior of dispersers under the constant density of scarce resources. Habitat fragmentation is a special kind of variability; Dewhirst and Lutscher (2009) have demonstrated that spread rate of populations increases in fragmented habitat in the absence of Allee effect (but decreases when there is an Allee effect).

At population and landscape scales movement is often modeled by Fickian diffusion (Reeve et al., 2008), in which population redistribution is driven by population gradients. This means that the movement of individuals tends from higher concentrations to lower concentrations, and changes in local habitat only alter the movement rate down the gradient (Okubo and Levin 2001). However, animal responses to spatial heterogeneity are not likely to be Fickian. When deer bed down at or inside a treeline they do not randomly diffuse past the forest edge, and when American robins forage for juniper berries they exhibit high fidelity to the location of the trees and simply avoid the surrounding steppe, unless they are choosing to move between patches of juniper. In both of these cases the animals are making movement choices based on the patch of habitat in which they currently reside, not perceptions of population gradients. A more appropriate way to describe animal movement in which organisms make random steps based on current habitat types is “ecological diffusion” (Turchin 1998). In this approach differences in population dispersion are driven by residence times in differing habitat types. Where residence times

are high (in juniper for robins) populations accumulate, and where residence times are low (in sagebrush) the population density is low. An ecological diffusion model supports discontinuous solutions at boundaries, consequently, deer can accumulate inside of a forest patch without diffusing out into the adjacent meadow against their will. Turchin (1998) observed that residence time and motility (the analog of diffusivity) are inversely proportional. Thus, if the motility is low in a patch (residence time is high) then individuals don't choose to leave the patch very frequently and the population density increases.

Seed transport during vertebrate movement happens mainly in two ways. Dispersal agents either hide seeds at some distance from the fruiting tree for future use or these agents eat seeds and defecate seeds at some new location. When animal motility is independent in space, Neubert et al., 1995 have discussed two limiting cases of seed spread. If every dispersal agent requires exactly the same amount of time to handle individual seeds, seed dispersal on the landscape is Gaussian. On the other hand, if these agents drop seeds at a constant rate in both time and space, seed spread in a Laplace distribution. Both extremes, however, are unlikely in real life scenarios. Neupane and Powell (2015) hypothesized that handling time is sampled from a distribution after seeds are picked. Using a time-dependent seed handling function they calculated seed digestion kernels (SDK). Neupane and Powell showed that the SDK accurately described seed dispersal for pinyon pine and Utah juniper, as reflected in the historical migration rate of these species.

Dispersal kernels in spatially variable landscapes have not received much attention. Simple analytic solutions don't exist for arbitrarily structured spatial landscapes. Numerical approaches are possible, but would require the user to solve the diffusion/settling equations

separately for each generation with different initial conditions for each generations' new location of seed sources. The computational cost of this operation would increase geometrically with landscape complexity. If spatial discretization is chosen small enough to resolve the smallest landscape features, a general rule to maintain numerical stability is that time steps must scale with the square of the size of spatial discretization ($\Delta t \leq C \Delta x^2$, Ascher and Greif 2011). Thus the number of computations tends to follow the cube of the spatial discretization, becoming unattractive for large, complex landscapes.

However, if the scale of spatial variability is very short as compared with the movement capacity of individuals, as occurs with vertebrate dispersers of tree seeds and berries, it is possible to solve Neubert's system analytically using the method of homogenization (Powell and Zimmermann 2004, Garlick et al., 2010). In this multi-scale procedure, slow and fast dispersal scales are introduced, linked by an asymptotically small order parameter. Solutions are then described by a regular perturbation series, leading to a large-scale solvability condition (the "homogenized equation") which determines large-scale solution behavior (Holmes 1995). Powell and Zimmermann (2004) used the homogenization technique to analyze active seed dispersal and forest migration in a heterogeneous landscape, but these authors were working in a Fickian diffusion framework and used constant settling rates instead of sampling the variability in seed handling times. On the other hand, Garlick et al., 2013 used homogenization in an ecological diffusion model to investigate the spread of chronic wasting disease in mule deer, but again the contact rates were assumed to be constant instead of modal.

In this paper we adapt a dispersal model from Neubert et al., 1995 by introducing ecological diffusion with highly variable motility and a modal distribution of seed handling times. We assume that motility varies on short scales and use multiple scales in space and time to apply the method of homogenization for solving the model. Using a solvability condition, we derive a simple constant diffusion equation on large scales and approximate the SDK. This kernel depends on the harmonic average of the motility. We then embed the kernel into an integrodifference equation (IDE) population model for adult plants. The large scale diffusion equation depends on small-scale variability only through the harmonically averaged motility, which inflicts a large-scale isotropic structure on the dispersal kernel. We hypothesize that the harmonic average motility therefore predicts the invasion speed in spatially complex environments. Analytic and numerical simulation methods are used to compare predicted and observed migration speeds. We conclude that observed speed converges asymptotically to the predicted constant speed.

3.2 Methods

3.2.1 Dispersal model on a variable landscape

We introduce a modified version of the Neubert et al., 1995 seed dispersal model to accommodate ecological diffusion and a distribution of seed handling times for vertebrate dispersers of tree seeds. We assume that motility depends only on space, while the distribution of seed handling times depends only on time (that is, time required for digestion is intrinsic to the dispersers, not the habitat). Thus

$$\partial_t(P) = \partial_x^2(D(x)P) - h(t)P, \;\; P(x, t = 0) = \delta(x - x'), \qquad (3.1)$$

$$\partial_t(S) = h(t)P, \;\; S(x, t = 0) = 0, \tag{3.2}$$

where $P(x,t)$ represents the density of seeds during dispersal by frugivorous birds and animals moving in the variable landscape, $D(x)$ is the seed motility rate while being carried by dispersers and $h(t)$ is the hazard function or rate of seed settling. To model real-world variability in the amount of time that seeds spend being carried by dispersers (i.e. distribution of times at which seeds are digested and defecated or carried and cached) we take $h(t)$ to be a probability density function (PDF) in time (Neupane and Powell 2015). Finally, $S(x,t)$ is the seed density on the landscape at time t. The Dirac delta function, $\delta(x - x')$, gives initial seed position at x' and $S(x, t = 0) = 0$ because there are no seeds dispersed at time $t = 0$. The long-time limit of this process will generate a seed digestion kernel (SDK), which is the probability of a seed moving from the starting location, *x'*, to a final location on the landscape, *x*. The term $(D(x)P)_{xx}$ was used by Turchin (1998) to describe "ecological diffusion" for bird or animal movement based on local habitat. We restrict ourselves to one dimension to analyze rates of spread perpendicular to a wave of invasion.

Following Neupane and Powell (2015), we assume that the PDF of seed handling times (digestion or caching) by birds and animals is represented by the distribution

$$h(t) = \frac{a\, t^{\alpha}}{b^{\beta} + t^{\beta}}, \quad \beta > \alpha + 1 > 0. \tag{3.3}$$

Here b scales the mean seed handling time and a is a normalization constant. Notice that $h(t) \sim t^{\alpha}$ as $t \longrightarrow 0$ while $h(t) \sim t^{\alpha-\beta}$ as $t \longrightarrow \infty$.

To find the seed distribution on the landscape associated with the hazard function defined in equation (3.3), we need to solve the model (3.1) and (3.2). First, define $f(t)$ as

$$f(t) = \int_0^t \frac{a\,\tau^{\alpha}}{b^{\beta}+\tau^{\beta}}\,d\tau, \tag{3.4}$$

so $f'(t) = h(t)$. Then, equation (3.1) becomes

$$\partial_t(P) = \partial_x^2(DP) - f'(t)P. \tag{3.5}$$

Multiplying on both sides of the equation by the integrating factor, $e^{f(t)}$, and rearranging terms, we arrive at the equation

$$\frac{\partial}{\partial t}\left(P\,e^{f(t)}\right) = \partial_x^2(DP\,e^{f(t)})\,. \tag{3.6}$$

If

$$u = Pe^{f(t)}, \tag{3.7}$$

equation (3.6) becomes

$$\partial_t(u) = \partial_x^2(D(x)u)\,. \tag{3.8}$$

3.2.2 Introduction of multiple scales for highly variable landscapes

We introduce multiple scales to model highly variable habitat motility in equation (3.8). Let y, the small scale, be $y = \frac{x-x'}{\varepsilon}$ for some order parameter $0 < \varepsilon \ll 1$. The order parameter captures the difference in scale between the patchiness of the landscape and the larger scale at which vertebrate dispersers can move. For example, landcover mapping via geographic information systems is generally framed on 30 meter pixels because habitat varies on scales of tens of meters. On the other hand, birds typically fly distances which are measured in terms of kilometers, so we would take $\varepsilon = \frac{10\text{ meters}}{1\text{ km}} = 0.01$. We assume motility varies on both scales, so that $D = D(x, y = \frac{x-x'}{\varepsilon})$. With the new scales, spatial derivatives are rewritten as

$$\partial_x \longrightarrow \frac{1}{\varepsilon}\partial_y + \partial_x \,,$$

$$\partial_x^2 \longrightarrow \frac{1}{\varepsilon^2}\partial_y^2 + \frac{1}{\varepsilon}2\partial_x\partial_y + \partial_x^2 \,.$$

We must also choose a fast time scale to balance the short space scale. Taking $\tau = \frac{t}{\varepsilon^2}$. the time derivative transforms into

$$\partial_t \longrightarrow \frac{1}{\varepsilon^2}\partial_\tau + \partial_t \,.$$

Applying these transformations to equation (3.8) gives

$$\left(\frac{1}{\varepsilon^2}\partial_\tau + \partial_t\right)u = \left(\frac{1}{\varepsilon}\partial_y + \partial_x\right)^2 \left[D\left(x, y\right)u\right]. \tag{3.9}$$

Assume that the solution can be expanded as a regular asymptotic series,

$$u = u_0 + \varepsilon u_1 + \varepsilon^2 u_2 + O(\varepsilon^3). \tag{3.10}$$

Multiplying by ε^2, equation (3.9) becomes

$$(\partial_\tau + \varepsilon^2\partial_t)(u_0 + \varepsilon u_1 + \cdots) = \left(\partial_y + \varepsilon\partial_x\right)^2\left[D\left(x, y\right)(u_0 + \varepsilon u_1 + \cdots)\right],$$

which can be expanded

$$\partial_\tau u_0 + \varepsilon\partial_\tau u_1 + \varepsilon^2[\partial_t u_0 + \partial_\tau u_2] + \cdots = \partial_y^2(Du_0) + \varepsilon\left[\partial_y^2(Du_1) + 2\partial_x\partial_y(Du_0)\right] + [\partial_y^2(Du_2) + 2\partial_x\partial_y(Du_1) + \partial_x^2(Du_0)] + \cdots . \tag{3.11}$$

3.2.3 Homogenization technique applied to rescaled seed dispersal model

3.2.3.1 Solution at $O(1)$

The method of homogenization is essentially to solve the multi-scale expansion (3.11) at successive orders of ε, being alert for a solvability condition which will reconcile the solution across scales. Equating terms at leading order in (3.11) gives

$$\partial_\tau u_0 = \partial_y^2(D(x, y)u_0). \tag{3.12}$$

This is a parabolic equation and its solution relaxes exponentially to the steady state on the fast time scale. Since we are seeking the long-time limit of the process, we can ignore transients, giving

$$\partial_y^2(D(x,y)u_0) = 0. \tag{3.13}$$

The solution of this equation is

$$u_0 = \frac{C_0(x,t)}{D(x,y)} + \frac{C_1(x,t)}{D(x,y)}y.$$

Recall that the small scale and dispersal are related as $y = \frac{x-x'}{\varepsilon}$. In order to have bounded solutions as $\varepsilon \to 0$ (that is, $|y| \to \infty$), we require

$$u_0 = \frac{C_0(x,t)}{D(x,y)}. \tag{3.14}$$

3.2.3.2 Solution at $O(\varepsilon)$

Equating the terms at order ε from the expanded form of equation (3.11) gives

$$\partial_\tau u_1 = \partial_y^2(D(x,y)u_1) + 2\partial_x\partial_y(Du_0). \tag{3.15}$$

Using u_0 from (3.14) gives

$$2\partial_x\partial_y(Du_0) = 2\partial_x\partial_y(c_0(x,t)) = 0.$$

Then equation (3.15) gives

$$\partial_\tau u_1 = \partial_y^2(D(x,y)u_1).$$

This is again parabolic with exponentially decaying transients on fast time scales. Thus,

$$\partial_y^2(D(x,y)u_1) = 0,$$

which has solution

$$u_1 = \frac{d_1(x,t)}{D(x,y)} + \frac{d_2(x,t)}{D(x,y)}y.$$

Once again, for the solution to be bounded as $\varepsilon \longrightarrow 0$,

$$u_1 = \frac{d_1(x,t)}{D(x,y)}\,. \tag{16}$$

3.2.3.3 Solvability condition at $O(\varepsilon^2)$

Equating terms with ε^2 from the expanded form of equation (3.11) gives

$$\partial_\tau u_2 + \partial_t u_0 = \partial_y^2(Du_2) + \partial_x^2(Du_0) + 2\partial_x\partial_y(Du_1). \tag{3.17}$$

From equation (3.16), $\partial_x\partial_y(Du_1) = \partial_x\partial_y(d_1(x,t)) = 0$, and using the fact that $\partial_\tau u_2 \to 0$ in long time, equation (3.17) gives

$$\partial_t\left(\frac{c_0}{D}\right) = \partial_y^2(Du_2) + \partial_x^2(c_0). \tag{3.18}$$

Rearranging terms in equation (3.18) gives

$$\partial_y^2(Du_2) = \partial_x^2(c_0) - \partial_t\left(\frac{c_0}{D}\right).$$

Integrating this equation with respect to y from $-l$ to l,

$$\partial_y(Du_2)\big|_{y=-l}^{y=l} = \partial_x^2(c_0)\int_{-l}^{l} dy - \partial_t(c_0)\int_{-l}^{l}\frac{1}{D}dy. \tag{3.19}$$

As Holmes (1995) points out, the right hand side of this equation grows in proportion to l for arbitrary c_0 and bounded, nonzero motility. However, the left hand side is bounded and remains small. Thus, equation (3.18) becomes unsolvable unless there is something special about c_0. To continue the perturbation approach and generate a bounded solution for u_2, the right hand side must be zero as $l \to \infty$; thus we have a stability condition as $l \longrightarrow \infty$,

$$2l\,\partial_x^2(c_0) - \partial_t(c_0)\int_{-l}^{l}\frac{1}{D}dy = 0. \tag{3.20}$$

Define the average of a function w as

$$\langle w\rangle = \lim_{l\to\infty}\frac{1}{2l}\int_{-l}^{l} w(y)dy.$$

The second term in the solvability condition can be written

$$\langle \partial_t \left(\frac{c_0}{D}\right)\rangle = \langle D^{-1}\rangle \partial_t c_0 \,, \tag{3.21}$$

where $\overline{D} = \frac{1}{\langle D^{-1}\rangle}$, the harmonic average of D and $\langle D^{-1}\rangle$ gives the average of D^{-1}.

From equations (3.18), (3.20) and (3.21) we now have

$$\partial_t c_0 = \overline{D}(x)\partial_x^2 c_0; \;\; c_0(x,x',0) = D(x',0)\,\delta(x-x'), \tag{3.22}$$

where $D(x',0)$ is the motility at the seeds' starting location, x'.

3.2.4 Solving for seed dispersal

We assume $\overline{D}$ is locally constant, so that the solution to (3.22) can be written

$$c_0(x,x',t) = \frac{D(x',0)}{\sqrt{4\pi\overline{D}\,t}} e^{\frac{-(x-x')^2}{4\overline{D}t}} \,. \tag{3.23}$$

From equations (3.10) and (3.14) we have

$$u(x,y,t) \;= \frac{c_0(x,t)}{D(x,y)} + O(\varepsilon) \,. \tag{3.24}$$

Returning to the original dependent variable, equations (3.7), (3.23) and (3.24) give

$$P(x,x',y,t) \cong \frac{c_0(x,t)}{D(x,y)} e^{-f(t)} = \frac{D(x',0)}{D(x,y)\sqrt{4\pi\overline{D}t}} e^{-f(t)} e^{\frac{-(x-x')^2}{4\overline{D}t}} \,, \tag{3.25}$$

and returning to unscaled spatial variables we have

$$P(x,x',t) \cong \frac{c_0(x,t)}{D(x)} e^{-f(t)} = \frac{D(x')}{D(x)\sqrt{4\pi\overline{D}t}} e^{-f(t)} e^{\frac{-(x-x')^2}{4\overline{D}t}}, \tag{3.26}$$

where $D(x) = D(x,0)$ and $D(x') = D(x',0)$.

Integrating equation (3.2) using (3.26),

$$S(x,x',t) \cong \frac{D(x')}{D(x)} \int_0^t \left(\frac{h(t')}{\sqrt{4\pi\overline{D}t'}} e^{-f(t')} e^{\frac{-(x-x')^2}{4\overline{D}t'}} \right) dt'$$

$$= \frac{D(x')}{D(x)} \int_0^t \left(\frac{h(t')}{\sqrt{4\pi \bar{D} t'}} e^{-\int_0^{t'} h(\tau) d\tau} e^{\frac{-(x-x')^2}{4\bar{D}t'}} \right) dt'. \quad (3.27)$$

3.2.5 Homogenized seed dispersal kernel

Equation (3.27) is the homogenized solution of (3.2) in the long time scale t and the seed digestion kernel is the long time limit of this solution. Thus the homogenized seed digestion kernel (HSDK) becomes

$$K(x, x') \cong \lim_{t \to \infty} S(x, x', t) = \frac{D(x')}{D(x)} \int_0^{\infty} \left(\frac{h(t)}{\sqrt{4\pi \bar{D} t}} e^{-\int_0^t h(\tau) d\tau} e^{\frac{-(x-x')^2}{4\bar{D}t}} \right) dt \, . \quad (3.28)$$

The terms $D(x)$ and $D(x')$ denote dispersal motilities at the starting and ending locations, respectively. Note that, while the homogenization approach has made the form of this solution fairly simple, it is not guaranteed to be a PDF in space; normalization is necessary before (3.28) can be used for seed dispersal (as we will discuss below). Consider the effect of the quotient $\frac{D(x')}{D(x)}$ on the shape of the kernel. If $D(x')$ is high, the quotient $\frac{D(x')}{D(x)}$ is relatively large and more seeds will disperse from the starting location. On the other hand, at some target location, *x*, if *D(x)* is large then residence times are very small at *x*; the quotient is correspondingly small and it is difficult for seeds to end up near *x*. The shape of dispersal kernel with variable motility is shown in Figure 3.1. Now we consider two limiting cases which generate closed form HSDK.

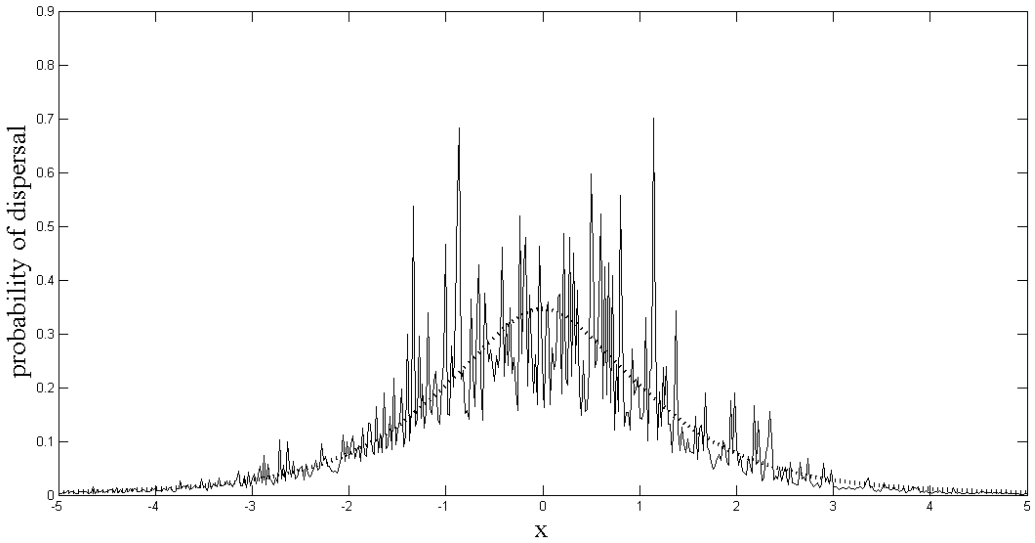

Figure 3.1 This plot gives the shape of seed digestion kernel (dotted line) with constant motility $\overline{D}$ versus the homogenized seed digestion kernel (solid) with variable motility. The jaggedness of the homogenized curve is generated by random variations in motility, $D(x)$, on short spatial scales. We have chosen D from a uniform distribution between $D_{min} = .01$ and $D_{max} = .04$, assumed to be constant for each grid cell (of size $\Delta x = 0.2$). We further have chosen the dispersal starting location $x' = 0$.

3.2.6 Homogenized Gaussian dispersal kernel

Based on Neupane and Powell (2015), when there is no variability in handling times, the function $h(t)$ becomes

$$h(t) = \delta\left(t - \tilde{b}\right). \tag{3.29}$$

Then (3.28) can be integrated directly,

$$G(x,x') = \frac{D(x')}{D(x)} \int_0^\infty \left(\frac{\delta(t-\tilde{b})}{\sqrt{4\pi\overline{D}t}} e^{-\int_0^t \delta(\tau-\tilde{b})d\tau} e^{\frac{-(x-x')^2}{4\overline{D}t}} \right) dt = \frac{D(x')}{D(x)\sqrt{4\pi\overline{D}\tilde{b}}} e^{\frac{-(x-x')^2}{4\overline{D}\tilde{b}}}. \tag{3.30}$$

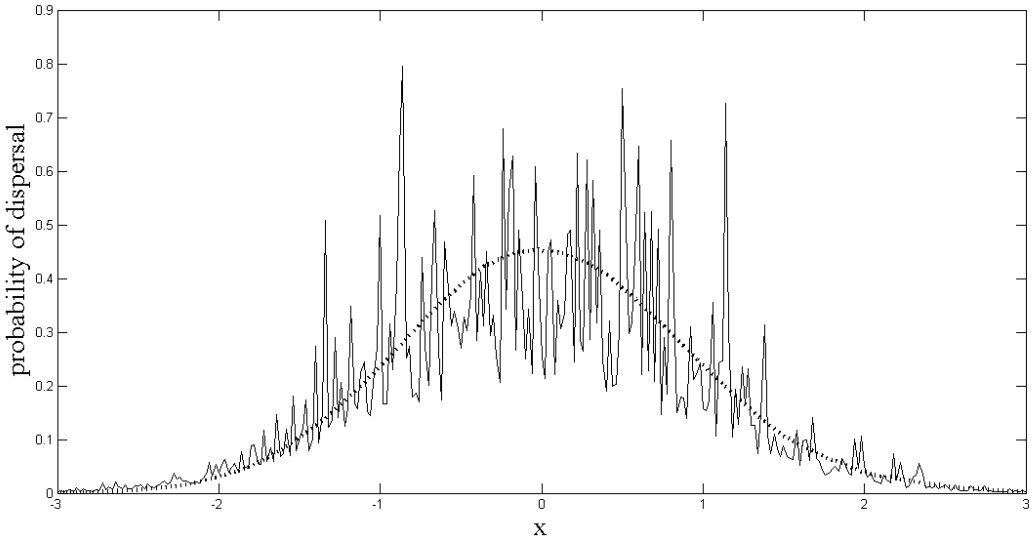

Figure 3.2 This graph shows the Gaussian kernel (dotted line) with constant motility $\overline{D}$ vs the homogenized Gaussian kernel (solid) with variable motility. The jaggedness of the homogenized curve is generated from the smooth Gaussian by random variations in motility, $D(x)$, on short spatial scales. We have chosen D from an uniform distribution between $D_{min} = .01$ and $D_{max} = .04$, assumed to be constant for each grid cell (of size $\Delta x = 0.2$). We have chosen the dispersal starting location $x' = 0$.

This is a homogenized version of the Gaussian kernel, depicted in Figure 3.2. Note that the skeleton of the HDSK is a normal PDF in space with $\sigma^2 = 2\overline{D}\tilde{b}$, modulated up and down by the relative motilities at the starting and ending locations. If motility is constant, *G(x, x')* reduces to the standard Gaussian SDK.

3.2.7 Homogenized Laplace dispersal kernel

Another analytic limit comes from taking the PDF h to be a step function,

$$h(t) = \begin{cases} \dfrac{1}{2\tilde{b}}, & 0 < t \le 2\tilde{b}, \\ 0, & t > 2\tilde{b}. \end{cases} \tag{3.31}$$

where $\tilde{b}$ is the mean handling time; the hazard function is written this way to facilitate comparison with the more general SDK. It was shown in Neupane and Powell (2015) that the solution to model (3.1) and (3.2) with the step function (3.31) can be approximated by

$$\partial_t(P) = \partial_x^2(D(x)P) - \frac{1}{2\tilde{b}}P,\ P(x, t=0) = \delta(x - x'), \tag{3.32}$$

$$\partial_t(S) = \frac{1}{2\tilde{b}}P,\ S(x, t=0) = 0. \tag{3.33}$$

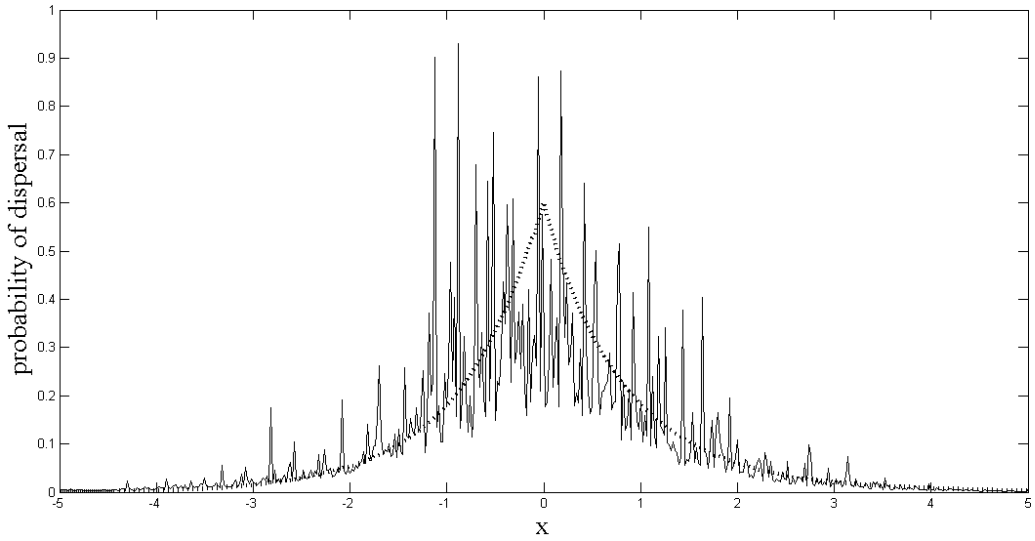

Figure 3.3 This graph shows the Laplace kernel (dotted line) with constant motility $\overline{D}$ vs the homogenized Laplace kernel (solid) with variable motility. The jaggedness of the homogenized curve is generated from the smooth Laplace kernel by random variations in motility, $D(x)$, on short spatial scales. We have chosen D from an uniform distribution between $D_{min} = .01$ and $D_{max} = .04$, assumed to be constant for each grid cell (of size $\Delta x = 0.2$).and The dispersal starting location is $x' = 0$.

Replacing h with the constant $\frac{1}{2\tilde{b}}$ in (3.28),

$$L(x, x') = \frac{D(x')}{D(x)} \int_0^\infty \left(\frac{\frac{1}{2\tilde{b}}}{\sqrt{4\pi\overline{D}t}} e^{-\frac{t}{2\tilde{b}}} e^{\frac{-|x-x'|}{4\overline{D}t}} \right) dt.$$

This latter integral can be evaluated (Neupane and Powell 2015) to give

$$L(x, x') = \frac{D(x')}{D(x) 2\sqrt{2\overline{D}\tilde{b}}} e^{\frac{-|x-x'|}{\sqrt{2\overline{D}\tilde{b}}}}. \tag{3.34}$$

This is a homogenized Laplace kernel, depicted in Figure 3.3. Note that the skeleton of this distribution is a Laplace PDF in space with mean dispersal distance $\sqrt{\bar{D}\tilde{b}}$, modulated up and down by the relative motility at starting and ending locations.

3.2.8 A population model for adult plants

We would like to understand how spatial variability affects the effective migration rates of plants, based on the seed distribution we estimated in equation (3.28). We introduce a simple population model which includes spatially varying dispersal,

$$N_{n+1} = \underbrace{T[K(x,x') * k\ N_n(x)]}_{\text{Newly dispersed survived seeds to germinate}} + \underbrace{(1-\omega)N_n(\mathrm{x})}_{\text{Survived old adults}} \qquad (3.35)$$

where N_n is the population density of adults in generation n, $K(x,x')$ gives the dispersal kernel, k is the number of seeds produced per adult per generation, ω gives the mortality probability of adults per generation, and

$$T = \frac{M\ g\ \sigma\ N_n}{M\ +\ N_n}$$

is the Beverton-Holt model for the number of seedlings surviving in competition with other seedlings after germination. In this model, g is the germination rate, σ is the seed survival rate and M is the maximum density of surviving seeds. The convolution in (3.35) is defined by

$$K(x) * k\ N_n(x) = \int_{-\infty}^{\infty} K(x,x')\ k\ N_n\ (x')dx'. \qquad (3.36)$$

Notice that the dispersal kernel derived in equation (3.28) is anisotropic. Consequently the integrodifference equation (3.35) can not be evaluated rapidly from generation to

generation using Fast Fourier Transforms; as it stands the convolution must be evaluated numerically at every location using direct quadrature.

3.2.9 Invasion speed estimation

We use the population model (3.35) to estimate the speed of invasion in a variable landscape. Since the dispersal kernel is anisotropic we can't evaluate invasion speeds directly by following the method of Kot et al., 1996. However, the homogenized solutions have large scale structure which is isotropic, with spatial parameters determined by the harmonic average ($\overline{D}$) of D. We therefore hypothesize that the speeds can be predicted using the isotropic kernel and the harmonic average motility. That is, for purposes of predicting speeds we will use the isotropic dispersal kernel, $\overline{K}(x-x')$ which provides the skeleton of the HDSK:

$$K(x,x') = \frac{D(x')}{D(x)}\overline{K}(x-x') = \frac{D(x')}{D(x)}\int_0^\infty \left(\frac{h(t)}{\sqrt{4\pi\overline{D}t}} e^{-\int_0^t h(\tau)d\tau} e^{\frac{-(x-x')^2}{4\overline{D}t}}\right) dt \ .$$

Here $\tilde{b}$ is the mode of *h(t)*, which we use to facilitate comparison among the various kernels (see Neupane and Powell 2015 for details).

We outline the method of Kot et al., 1996. Far in advance of the wave of invasion we assume that population density approaches zero as $x \to \infty$,

$$N_n(x) \sim \varepsilon e^{-ux} \ , \tag{3.37}$$

with $\varepsilon \ll 1$ (note this is not the ε from homogenization). At a constant speed of invasion, c, the spreading population can be written as

$$N_{n+1}(x) = N_n(x-c) \ . \tag{3.38}$$

Equations (3.37) and (3.38) give

$$N_{n+1}(x) = \varepsilon e^{-u(x-c)}. \tag{3.39}$$

Putting this all into equation (3.35),

$$\varepsilon e^{-u(x-c)} \sim T[\overline{K}(x-x') * \varepsilon\, k\, e^{-ux}] + \varepsilon(1-\omega)\, e^{-ux}. \tag{3.40}$$

Applying a Taylor expansion for $T(\cdot)$ (and observing *T(0)=0*),

$$e^{-u(x-c)} \sim kT'(0)\overline{K}(x-x') * e^{-ux} + (1-\omega)e^{-ux} + O(\varepsilon). \tag{3.41}$$

Equating leading order terms of equation (3.41) gives

$$e^{-u(x-c)} = R_0\overline{K}(x-x') * e^{-ux} + (1-\omega)e^{-ux}, \tag{3.42}$$

where $R_0 = kT'(0) = kg\sigma$ is the net reproductive rate.

The moment generating function, M, of the skeletal dispersal kernel is defined as

$$M(u) = \int_{-\infty}^{\infty} \overline{K}(v)e^{-uv}\, dv \tag{3.43}$$

and thus we arrive at a dispersion relation relating c and u,

$$e^{cu} = R_0 M(u) + (1-\omega), \tag{3.44}$$

from which

$$c = \frac{R_0 M'(u)}{R_0 M(u) + (1-\omega)}. \tag{3.45}$$

Using (3.44) to eliminate c we get a single equation whose roots determine u,

$$F(u) = u\frac{R_0 M'(u)}{R_0 M(u) + (1-\omega)} - \log[R_0 M(u) + (1-\omega)] = 0. \tag{3.46}$$

The moment generating function and its derivative can be calculated numerically using the trapezoid rule; roots of F are found numerically using fzero in MATLAB. The numerical roots then generate the speed of invasion from equation (3.45).

3.3 Results

For constant motility Neupane and Powell (2015) have already calculated invasion speeds for the Beverton-Holt population model. Speeds of the SDK fall between speeds generated by the Gaussian and Laplace dispersal kernels for large $\tilde{b}$ while for smaller $\tilde{b}$ the fact that $h(t)$ is not compactly supported make the speeds of SDK invasions higher than either Gaussian or Laplace invasions. Here we test whether the speeds predicted using the skeletal kernel, $\overline{K}$, and harmonic motility, $\overline{D}$, accurately predict speeds resulting from simulated invasions with highly variable motility $D(x)$.

3.3.1 Simulating invasions using the homogenized population model

3.3.1.1 Evaluating HSDK numerically

To resolve HSDK numerically, we calculate the integral (3.28) using the trapezoid rule in x at every starting location x' and save these values, giving the kernel at different locations. The kernels calculated in this way are accurate to $O(\varepsilon \approx .01)$ but may not be PDFs because the homogenization procedure does not necessarily preserve the norm. We therefore normalize the kernels numerically. Boundaries must be carefully handled in this calculation. The mean variance of seeds during dispersal is $\sigma = \sqrt{2\overline{D}\tilde{b}}$. For a Gaussian distribution this means that 99.7% of dispersed seeds fall within 3σ of their starting location (Casella and Berger, 2001). Outside this boundary seed dispersal is negligible. For a simulation domain $x \in (-L, L)$ we choose $(-L + 3\sigma, L - 3\sigma)$ as our computational domain. This creates two buffer zones on either end of the simulation domain. Seeds may disperse into the buffer zone, but seeds are not allowed to disperse out of the buffer zone.

Thus dispersal kernels need not be calculated inside the buffer zones, where they can not be normalized. The harmonic average motility,

$$\overline{D} = \frac{1}{2l}\int_{x'-l}^{x'+l} \frac{1}{D(y)}\,dy,$$

is calculated numerically using the trapezoid rule with $l = \min(3\sigma, 10)$.

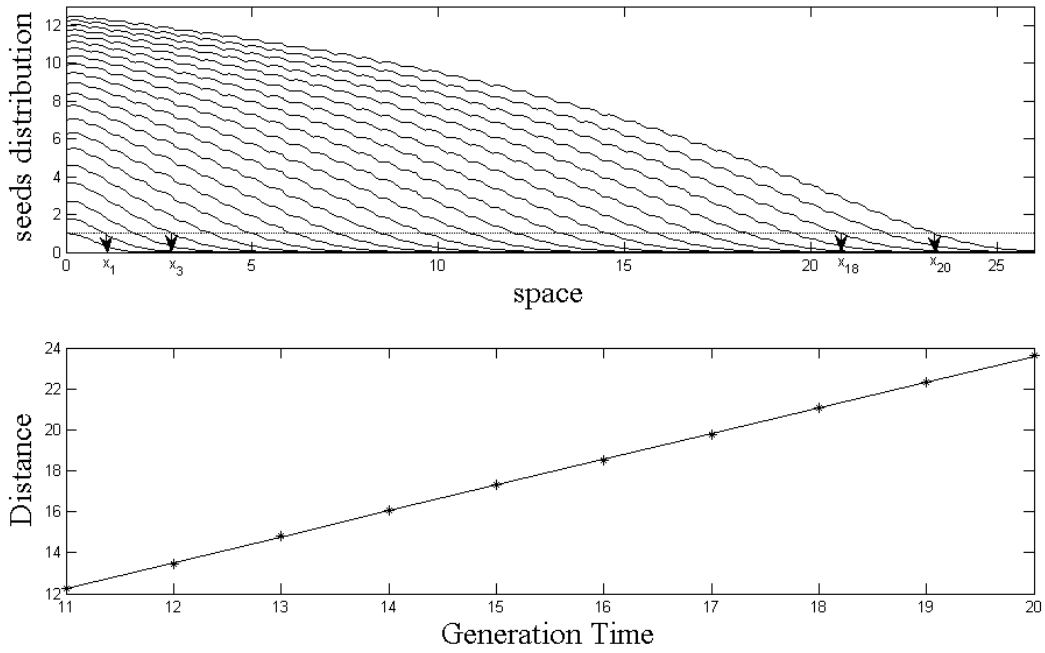

Figure 3.4 The top figure shows the invasion front wave simulated up to 20 generations. The dotted isocline meets with each wave giving a corresponding distance in space. In the bottom figure the last ten distances are fit to a line; the slope of this line gives the observed speed of invasion.

3.3.1.2 Numerical simulation and invasion speed diagnosis

To estimate invasion speed, we run the simulation for 20 generations and then identify the isocline $N_n = 1$, where N_n is the population after n generations (see Figure 3.4, top). In each generation we measure the farthest forward distance along the isocline. The last ten of these distances is fit to a line using regression; the diagnosed wave speed, c_{obs}, is the slope of this line (Figure 3.4, bottom).

3.3.2 Speed comparison

We have chosen $D = .01 + .02 * \left[\left\{\frac{1+\cos\left(\frac{2\pi x}{2}\right)}{8}\right\}\right]^2$ in the simulation so that all simulations have the same motility structure regardless of discretization. For $\tilde{b}$ between 1 and 20 we compare observed speeds computed using the HSDK in (3.35) with predicted speeds using the harmonic average motility, $\overline{D}$. As might be expected on dimensional

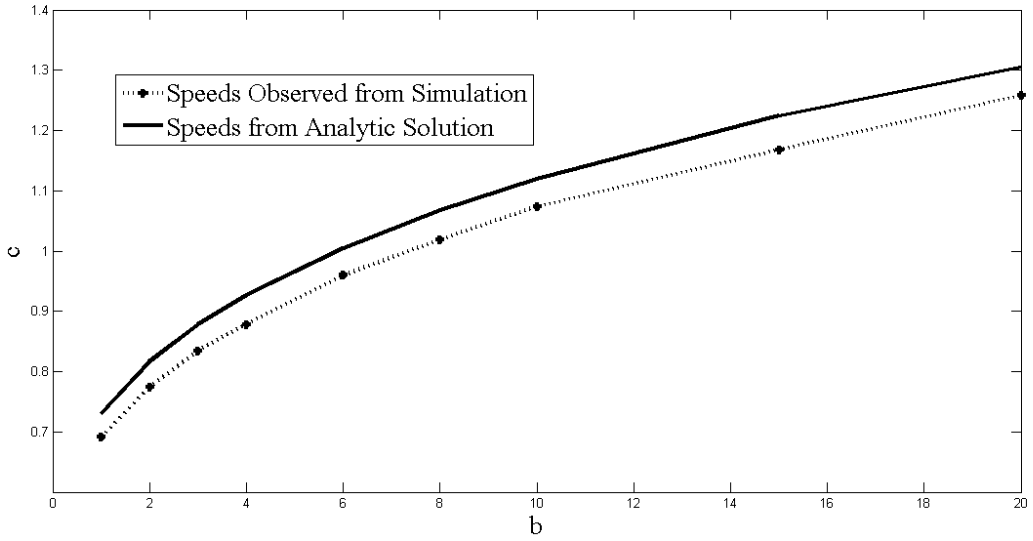

Figure 3.5 The solid line gives the speeds with seed digestion kernel. This kernel is estimated analytically from dispersal model for constant motility rate. The dotted line indicates the speeds with the kernel from numerical simulation using the harmonic average of variable motility rate. The graph shows that both speeds are closely increasing in the same pattern as mean digestion time scaling parameter b increases.

grounds, the predicted speed scales with $\sqrt{\overline{D}\tilde{b}}$. However, in spite of the high variability of $D(x)$, observed invasion speeds conform closely to the predictions using homogenized motility (see Figure 3.5).

While predicted and observed speeds are close, they are not precisely the same. There are two sources of error, one in diagnosing the observed speeds using linear regression (which should be of size $\Delta x = 0.1$ and unbiased) and the other due to

convergence in time. Based on Kot and Neubert (2008), observed speeds should converge from below at a rate like $\frac{1}{n}\log\sqrt{2\pi n c_1}$ (with c_1 a constant, see Kot and Neubert (2008) equation (52)). To test that observed speeds are actually converging to predicted speeds we performed a convergence study at $\widetilde{b}$ = 4, running the same simulation for between 10 and 30 generations (results depicted in Figure 3.6). Results indicate that the observed invasion speeds are converging to predicted speeds as expected.

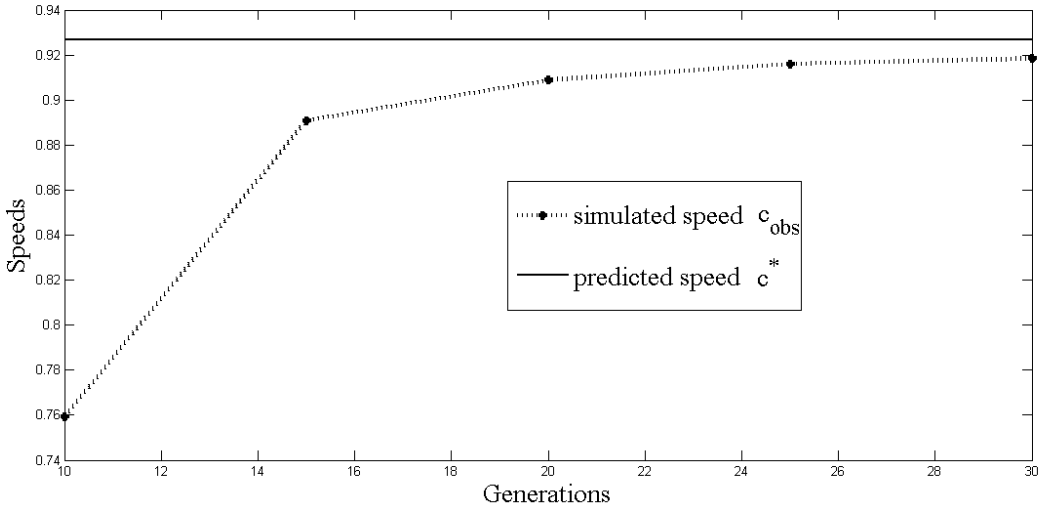

Figure 3.6 The solid (-) horizontal line represents the invasion speed predicted (c^*) from the analytic solution of dispersal model. The dotted line (…) gives the speed estimated (c_{obs}) from numerical simulation. As the number of generations increases, the simulated speed approaches the predicted speed at a rate like *1/n*, per Kot and Nuebert (2008).

3.4 Conclusion

Landscape variability is one of the factors that directly affects the motility of dispersers. Consequently, seed dispersal by active dispersers varies considerably with habitat structure within the landscape. In this paper we have adapted an existing model for active seed dispersal to highly variable landscapes, introducing ecological diffusion (so that disperser motility depends on habitat type alone) and modal seed handling times. We

introduce multiple scales to resolve the effect of rapidly varying habitats and solve the dispersal model using the method of homogenization. The resulting homogenized seed digestion kernel has asymptotically correct large scale isotropic structure conditioned by the harmonic average motility ($\overline{D}$) and appropriate anisotropic small scale variation for seed dispersal reflecting highly variable habitat. This represents a significant advance. Using the formulae derived here analytic predictions for seed dispersal can be generated for arbitrary (but highly variable) landscapes; previously the only available methods would have been tedious and unwieldy numerical computations.

We have also used the homogenized dispersal kernels to calculate rates of invasion in variable landscapes. Using a simple integrodifference equation for adult plants, we include the effects of spatial variability via convolution of the anisotropic dispersal kernels. No general results exist for predicting *a priori* spread rates of adult plants in such circumstances. However, we observe that the homogenized kernels have isotropic large-scale structure, conditioned on the small scale only through the harmonically averaged motility. Using existing theory for predicting spread rates for isotropic dispersal kernels we predict rates of invasion in the IDE model using $\overline{D}$ and compare with simulated invasions for the IDE and spatially complicated dispersal. Our results show that the *a priori* predictions using $\overline{D}$ accurately predict observed invasions, and a convergence study shows that the simulated fronts converge inversely with the number of generations, as predicted by the isotropic theory. This represents a second novel contribution; rates of invasion can now be predicted in arbitrary, rapidly-varying environments.

REFERENCES

Allen, L.J.S., Allen, E.J., Kunst, C.R.G. and Sosebee, R.E., 1991. A diffusion model for dispersal of opuntia (*Cholla*) on rangeland. *Journal of Ecology* 79:1123-1135.

Andow, D.A., Kareiva, P.M., Levin, S.A. and A. Okubo, A., 1990. Spread of invading organisms. *Landscape Ecology* 4:177-188.

Ascher, U.M. and C. Greif, C., 2011. *A First Course in Numerical Methods*. SIAM, Philadelphia, PA, USA.

Casella, G. and Berger, R.L., 2001. *Statistical Inference*. Duxbury Press, Pacific Grove, USA.

Dewhirst, S. and Lutcher, F., 2009. Dispersal in heterogeneous habitats: thresholds, spatial scales, and approximate rates of spread. *Ecology* 90:1338-1345.

Fisher, R.A., 1937. The wave of advance of advantageous genes. *Annals of Eugenics* 7:355-369.

Garlick, M.J., Powell, J.A., Hooten, M.B and MacFarlane, L.R., 2013. Homogenization, sex, and differential motility predict spread of chronic wasting disease in mule deer in southern Utah. *J. Math. Biol.* 69:369-399.

Garlick, M.J., Powell, J.A., Hooten, M.B. and MacFarlane, L.R., 2010. Homogenization of large-scale movement methods in ecology. *Bull. Math Biol.* 73:2088-2108.

Hanski, I., Eralahti, C., Kankare, M., Ovaskainen, O. and Siren, H., 2004. Variation in migration propensity among individuals maintained by landscape structure. *Ecology* 7:958-966.

Haynes, K.J. and Cronin, J.T., 2003. Matrix composition affects the spatial ecology of a prairie planthopper. *Ecology* 84(11):2856-2866.

Hengeveld, R. 1988. Mechanisms of biological invasions. Journal of Biogeography 15:819-828.

Holmes, M.H., 1995. *Introduction to Perturbation Methods.* Sprinter-Verlag, New York, USA.

Kot, M., Lewis, M.A. and van den Driessche, P., 1996. Dispersal data and spread of invading organisms. *Ecology* 77:2027-2042.

Kot, M and Neubert, M.G., 2008. Saddle-point approximations, integrodifference equations and invasions. *Bulletin of Mathematical Biology* 70:1790-1826.

Moilanen, A. and Hanski, I., 1998. Metapopulation dynamics: effects of habitat quality and landscape structure. *Ecology* 79(7):2503-2515.

Morales, J.M. and Carlo, T.A., 2006. The effect of Plant distribution and frugivore density on the scale and shape of dispersal kernels. *Ecology* 87:1489-1496.

Neubert, M.G., Kot, M. and Lewis, M.A., 1995. Dispersal and pattern formation in a discrete-time predator-prey model. *Theoretical Population Biology* 48:7-43.

Neupane, R.C. and Powell, J.A., 2015. Mathematical model of active seed dispersal by frugivorous birds and migration potential of pinyon and juniper in Utah. *Applied Mathematics* 9:1506-1523.

Okubo, A. and Levin, S.A., 2001. *Diffusion and Ecological Problems: Modern perspectives.* Springer-Verlag, New York, Berlin Heidelberg.

Okubo, A. and Levin, S.A., 1989. A theoretical framework for data analysis of wind

dispersal of seeds and pollen. *Ecology* 70:329-338.

Ovaskainen, O., 2004. Habitat-specific movement parameters estimated using mark recapture data and diffusion model. *Ecology* 85(1):242-257.

Powell, J.A. and Zimmermann, N.E., 2004. Multiscale analysis of active seed dispersal contributes to resolving Reid's paradox. *Ecology* 85:490-506.

Raposo, E.P., Bartumeus, F., da Luz, M.G.E., Ribeiro-Neto, P.J., Souza, T.A. and Viswanathan, G.M., 2011. How landscape heterogeneity frames optimal diffusivity in searching process. *PLoS Computational Biology* 7(11):e1002233.

Reeve, J.D., Cronin, J.T. and Haynes, K.J., 2008. Diffusion models for animals in complex landscapes: incorporating heterogeneity among substrates, individuals and edge behaviours. *Journal of Animal Ecology* 77:898-904.

Shigesada, N., Kawasaki, K. and Takeda, Y., 1995. Modeling stratified diffusion in biological invasions. *The American Naturalist* 146:229-251.

Skalski, G.T. and Gilliam, J.F., 2003. A diffusion-based theory of organism dispersal in heterogeneous populations. *The American Naturalist* 161:441-458.

Skellam, J.G., 1951. Random dispersal in theoretical populations. *Biometrika* 38:196-218.

Turchin, P., 1998. *Quantitative Analysis of Movement: Measuring and Modeling Population Redistribution on Animals and Plants.* Sinauer Associates Inc., Sunderland.

CHAPTER 4

CONNECTING REGIONAL-SCALE TREE DISTRIBUTION MODELS WITH SEED DIGESTION KERNELS

Abstract

Regional scale forest distribution models are important tools for biogeography and understanding the structure of forest communities in space. These models take climate and geographic variables as input and are therefore helpful for long-term decision support and climate adaptation planning. Generally local processes of germination and seedling survival are resolved probabilistically with explanatory variables such as elevation, latitude, exposure, soil type, moisture availability, climate and weather inputs and `trained' using landscape and regional presence-absence data. As far as possible without detailed site-level mechanistic processes, these models accurately reflect the fate of seedlings after seeds have arrived at a site. How seeds are distributed in these models, however, is far more problematic since it is difficult to accurately parameterize dispersal models using large-scale presence-absence data, particularly for actively dispersed tree species. The challenge is that variables conditioning vertebrate seed dispersal (motility and probability of utilization or caching in response to cover type) are not represented in large scale distribution models, and in fact vary on scales (10-100 meters) that are much smaller than the smallest pixel size for the distribution model (1-10 kilometers). The homogenized seed dispersal kernel (HSDK) offers a tool to make use of this scale separation. Homogenization naturally links highly variable small-scale processes (like seed foraging and caching by

birds and rodents) with large scale effects (like dispersal of seeds over tens of kilometers). In this paper we develop scenarios for seed dispersal on landscape scales, linking small-scale variables (landscape fraction cover by tree type, residence time spent and cover type utilization by frugivorous birds) with dispersal probabilities on large scales as predicted by HSDKs.

4.1 Introduction

Fleshy fruits are the primary food source for many frugivorous birds, mammals and rodents (Howe 1986). These animals make a major contribution to fruiting tree migration (Howe and Smallwood 1982, Schupp et al., 2010). They either eat fruits and defecate seeds in the landscape or cache fruits at some distance from source trees for future use. In a favorable environment these transported seeds may germinate and grow to adulthood, moving a forest boundary large distances.

There is an interaction between movement of frugivorous birds and fruiting plants and it affects the pattern of dispersal based on available resources and habitat structure. Seed dispersal of fruiting plants is sensitive to existing variable habitat types at many scales. Garcia et al., 2011 observed animal responses toward fruiting tree resource availability and structure of habitats at different spatial scales. They found that seed distribution due to birds was more responsive to habitat features than to resource availability. Seeds mostly end up in the same habitat type as they start due to bird foraging. Carlo et al., 2013 found that the rate of seed dispersal is higher in habitat types occupied with tree cover of fleshy fruits than to the habitat type with other tree cover or to the open pastures. Long distance dispersal is less likely in habitat with many fruiting trees (Herrera

et al., 2011). The nature of dispersal also influences fruit-removal rates and therefore the number of seeds dispersed from the parent plant (Clark et al., 1999). Carlo and Morales (2008) found that higher densities of birds and fruiting plants increase fruit removable rates and decreases dispersal distances. They also observed that there is shorter dispersal distances by birds in heterogeneous landscape compared to homogeneous ones.

Many ecologists have estimated that the shifting of fruiting tree species to new habitats depends on environmental explanatory variables such as temperature, moisture availability and soil properties. To estimate tree shifting over time, different types of data such as geographic information data, soil data, tree mortality data and climate station data are used (Peterman et al., 2012, Coops et al., 2012, Syphard and Franklin 2009, McKenney et al., 2007). To project the future shifting of pinyons and junipers in the Western US, Gibson et al., 2013 used climatic, topographic and presence-absence data existing in big grids (approximately 2400 ha. in area of each grid) for these species. Soil type that is capable of absorbing required water, adaptation to changing climate or drought tolerance explain the successful occurrence of these tree species in the landscape (Mathys et al., 2014).

Edith and Leathwick (2009) have defined species distribution models (SDMs) as "the models that relate species distribution data (occurrence or abundance at known locations) with information on the environmental and/or spatial characteristics of those locations. These models can be used to provide understanding and/or to predict species distribution across a landscape." To project future spread of plants and animals, the use of species distribution models has increased drastically (Guisan and Thuiller 2005, Lobo et

al., 2010). These models mainly depend on species presence/absence data and environmental predictor variables (maximum summer temperature, minimum winter temperature, precipitation, land cover, distance of intermittent water, distance of perennial water, distance of agricultural zone and distance of human modified area). Model prediction accuracy is primarily based on the appropriate choice of variables (Menke et al., 2009, Araujo and Guisan 2006). Many ecologists use climate data, soil type data and landscape use data in species distribution models (Peters et al., 2013, Menke et al., 2009 and Luoto et al., 2007). Araujo and Guisan (2006) demonstrated that climate predictors can be used to project species distribution accurately. Barbet-Massin and Jetz (2014) observed that climate predictors can provide accurate results for bird distributions. However, Austin and Van Niel (2011) concluded that climatic and non-climatic predictors are equally important and need to be tested at high resolution in order to achieve projection accuracy.

There is no consistency in the spatial resolution (from $1\ km^2$ to $2500\ km^2$) used in species distribution models (Gibson et al., 2013, Sanchez-Fernandez et al., 2011, Luoto et al., 2007, Austin and Van Niel 2011). Scales are often chosen due to database management, computational efficiency or data availability constraints as opposed to mechanistic or biological concerns, even though grid size creates uncertainties in the resulting projected distribution. Data with fine resolution may not match with environmental factors appropriately. On the other hand, it is more likely to overestimate while taking the data with broad spatial scale resolution (Wiens et al., 2009). However, almost always the scale of distribution model grids is much larger than the resolution of habitat variability which influences vertebrate motion.

This makes the use of seed dispersal kernels, which describe the probability of seeds moving from one cell to another, very problematic in species distribution models. It is difficult to accurately parameterize dispersal models using large-scale presence-absence data, particularly for actively dispersed tree species. The migration of fruiting trees normally occurs when birds transport seeds from parent plants to new sites (Gosper et al., 2005, Renne et al., 2002, Glyphis et al., 1981). Birds either eat fruits, digest them and defecate seeds somewhere on the ground or cache fruits in the landscape for future use. Seeds settled either way in the landscape might germinate and grow as new trees. Powell and Zimmermann (2004) modelled seed spread controlled by active agents, including the preferential movement of seeds toward caching sites. The scale of habitat patches is tens of meters, but birds can easily fly kilometer every easily. This behavior generates spatial dependence on small scales with modulation on large scales. This multi-scale dependence is perfectly suited to the method of homogenization (Garlick et al., 2010). In principle, dispersal kernels generated via homogenization can accurately represent the large scale modulation of dispersal probabilities while incorporating small-scale habitat features. Neupane and Powell (2015) used homogenization to estimate the shape of transported seeds distribution (the seed digestion kernel, SDK) by frugivorous birds in a variable landscape. However, the technique was applied in only one dimension and dispersal was assumed to be continuous on the large scale. To connect homogenized SDK with the need to describe dispersal discretely on very large grids we need to explicitly homogenize the underlying ecological diffusion model for seed transport in two dimensions with large grids in mind.

In this paper we modify the existing seed dispersal model to reflect animals' utilization of landscape and their space-dependent motility, using an ecological diffusion and variable seed handling time model. The homogenization technique will be used to solve this model assuming that habitat variability is reflected on 30m scales but dispersal is to be resolved on kilometer-scale grids. This generates a simple diffusion equation on large scales which describes large scale modulation of dispersal probabilities, depending on parameters that are defined only on the large grid. The solution is a dispersal kernel including both small scale variability with motility and utilization. We connect this kernel to discrete large-scale dispersal by integrating over large cells, estimating dispersal probabilities that depend on summed landscape cover fractions residence time spent in different cover types, and cover type utilization by frugivorous. Finally, explicit solutions in the constant and uniform handling time limits are derived and solution behavior explored on randomly generated landscapes.

4.2 Methods

4.2.1 Seed Dispersal Model

We have adapted the dispersal model of Neubert et al., 1995 to the case of ecological diffusion, variable utilization of space and a distribution of handling times. The model is expressed as

$$P_t = \nabla^2(D(\boldsymbol{x})P) - U(\boldsymbol{x})h(t)P, \;\; P(\boldsymbol{x}, t=0) = \delta(\boldsymbol{x}-\boldsymbol{x}'), \tag{4.1}$$

$$S_t = U(\boldsymbol{x})h(t)P, \;\; S(\boldsymbol{x}, t=0) = 0, \tag{4.2}$$

where $P(\boldsymbol{x}, t)$ (function of a spatial vector $\boldsymbol{x} = (x_1, x_2)$ and time t) is the density of seeds during dispersal by birds and animals moving in the landscape, $\nabla^2 = \frac{\partial^2}{\partial x_1^2} + \frac{\partial^2}{\partial x_2^2}$ is the Laplacian differential operator, $U(\boldsymbol{x})$ is the utilization function (one if dispersers use the habitat at $\boldsymbol{x}$ for seed storage/defecation, otherwise zero), $D(\boldsymbol{x})$ is the seed motility rate, and $S(\boldsymbol{x}, t)$ gives the seed density on the landscape at time t. The Dirac delta function, $\delta(\boldsymbol{x} - \boldsymbol{x}')$, gives an initial seed position at $\boldsymbol{x}'$, while $S(\boldsymbol{x}, t = 0) = 0$ because no seeds are dispersed initially. The hazard function $h(t)$ represents failure rate of seeds (i.e. distribution of times at which seeds are digested and defecated or carried and cached). The term $\nabla^2(D(\boldsymbol{x})P)$ was used by Turchin (1998) to describe "ecological diffusion", random walk movement in which movement choices are make solely on the basis of current habitat, as is appropriate for birds or animals foraging for fruits and nuts. Turchin (1998) pointed out that animal motility and residence time per area are inversely related, so frugivorous birds have long residence time in habitats with fruits available, leading to small motility, $D(\boldsymbol{x})$.

Dispersers spread seeds either by caching seeds or defecation on the ground; both activities have require some handling time sampled from a modal distribution. To model this temporal variability, Neupane and Powell (2015) defined a probability density function (PDF), $h(t)$, as

$$h(t) = \frac{a\, t^{\alpha}}{b^{\beta} + t^{\beta}}, \quad \beta > \alpha + 1 > 0,$$

where b is the seed handling time scaling parameter and a is a normalization constant.

4.2.2 Solving the seed dispersal model

To solve the model (4.1) and (4.2), we introduce multiple scales and use the homogenization technique (Holmes 1995, Garlick et al., 2010). Let

$$\lambda(\boldsymbol{x}, t) = U(\boldsymbol{x})h(t), \tag{4.3}$$

then the model (4.1) and (4.2) becomes

$$P_t = \nabla^2(D(\boldsymbol{x})P) - \lambda(\boldsymbol{x}, t)P, \;\; P(\boldsymbol{x}, t = 0) = \delta(\boldsymbol{x} - \boldsymbol{x}'), \tag{4.4}$$

$$S_t = \lambda(\boldsymbol{x}, t)P, \;\; S(\boldsymbol{x}, t = 0) = 0. \tag{4.5}$$

Species distribution models operate on scales of kilometers, and we define the smallest pixel of such a model as a "big" grid cell. Landscape classification, on the other hand, commonly occur on 30×30 meter blocks. On these short scales we assume habitat types are homogeneous and consequently bird foraging parameters are constant. Based on this hypothesis we introduce an order parameter, $\varepsilon = \frac{30\text{ m}}{1000\text{ m}} = \frac{\text{short scale}}{\text{long scale}}$, the ratio of spatial scales. Let $\boldsymbol{y} = \frac{\boldsymbol{x}-\boldsymbol{x}'}{\varepsilon}$ be the small scale spatial variable, $\boldsymbol{x}$ is the large scale space variable. The motility $D = D(\boldsymbol{x}, \boldsymbol{y} = \frac{\boldsymbol{x}-\boldsymbol{x}'}{\varepsilon})$ becomes a function of both small and large scale space variable, since motility changes with habitat type (small scales) as well as landscape properties (long scale). Then spatial derivatives transform,

$$\nabla_x \longrightarrow \nabla_x + \frac{1}{\varepsilon}\nabla_y,$$

$$\nabla_x^2 \longrightarrow \frac{1}{\varepsilon^2}\nabla_y^2 + \frac{1}{\varepsilon}\, 2\, \nabla_x.\nabla_y + \nabla_x^2.$$

We also introduce a short time scale, $\tau = \frac{t}{\varepsilon^2}$ to match the small spatial scale. Then time derivatives transform,

$$\partial_t \longrightarrow \frac{1}{\varepsilon^2}\partial_\tau + \partial_t \ .$$

Applying these transformations in equation (4.4) gives

$$(\partial_\tau + \varepsilon^2 \partial_{t)} P = (\nabla_y + \varepsilon \nabla_x).\left[(\nabla_y + \varepsilon \nabla_x) D(x,y) P\right] - \varepsilon^2 \lambda P. \tag{4.6}$$

Assuming the solution for P may be expanded as a regular asymptotic series,

$$P = P_0 + \varepsilon P_1 + \varepsilon^2 P_2 + O(\varepsilon^3), \tag{4.7}$$

equations (4.6) and (4.7) give

$$\partial_\tau P_0 + \varepsilon \partial_\tau P_1 + \varepsilon^2 [\partial_t P_0 + \partial_\tau P_2] + \cdots = \nabla_y^2 (DP_0) + \varepsilon\left[\nabla_y^2 (DP_1) + \right.$$

$$\left. 2\ \nabla_x . \nabla_y (DP_0)\right] + \varepsilon^2\left[\nabla_y^2 (DP_2) + \ 2\ \nabla_x . \nabla_y (DP_1) + \nabla_x^2 (DP_0) - \lambda P_0\right] + \cdots . \tag{4.8}$$

We assume that D is quasi-periodic on small scales, that is, there exists a vector $\boldsymbol{p}(\boldsymbol{x}) = (p_1, p_2)$, such that

$$D(\boldsymbol{x}, \boldsymbol{y} + \boldsymbol{p}(\boldsymbol{x})) = D(\boldsymbol{x}, \boldsymbol{y})$$

This seems strange, since natural landscape is not obviously periodic. However, Garlick et al., 2010 observed that landscapes are often quasi-periodic in the small scale. In the landscape, there are repeating elements such as pinyon-juniper woodland, open meadow and grassland, not to mention the 30 m classification itself, both of which cause a specific peak on the power spectrum of D at $\frac{2\pi}{\|\boldsymbol{p}\|}$, leading to quasi-periodicity.

The equation at $O(1)$ becomes

$$\partial_\tau P_0 = \nabla_y^2 (DP_0) \tag{4.9}$$

This equation is parabolic and its solution relaxes exponentially to the steady state on fast time scales. We therefore have

$$\nabla_y^2 (DP_0) = 0.$$

The solution of this equation becomes

$$DP_0 = c_0(\boldsymbol{x}, t) + c_1(\boldsymbol{x}, t)y_1 + c_2(\boldsymbol{x}, t)y_1,$$

which is a linear equation. To satisfy the assumption of quasi-periodicity, the constants c_1 and c_2 have to be zero. Thus, the solution becomes

$$P_0 = \frac{C_0(\boldsymbol{x},t)}{D(\boldsymbol{x},\boldsymbol{y})}, \tag{4.10}$$

where the constant c_0 does not depend on the small scale $\boldsymbol{y}$.

At $O(\varepsilon)$ equation (4.8) becomes

$$\partial_\tau P_1 = \nabla_y^2(DP_1) + 2\,\nabla_x.\nabla_y(DP_0). \tag{4.11}$$

the last term of equation (4.11) vanishes using equation (4.10) and the fact that $c_0(\boldsymbol{x}, t)$ is independent of $\boldsymbol{y}$ **.** Thus,

$$\partial_\tau P_1 = \nabla_y^2(DP_1). \tag{4.12}$$

This is again parabolic with exponentially decaying transients on short time scales.

$$\nabla_y^2(DP_1) = 0. \tag{4.13}$$

Using quasi-periodicity on small scales as to receive equation (4.10), we find

$$P_1 = \frac{d_1(\boldsymbol{x},t)}{D(\boldsymbol{x},\boldsymbol{y})}. \tag{4.14}$$

At $O(\varepsilon^2)$ equation (4.8) becomes

$$\partial_t P_0 + \partial_\tau P_2 = \nabla_y^2(DP_2) + \nabla_x^2(DP_0) + \lambda P_0 + 2\,\nabla_x.\nabla_y(DP_1). \tag{4.15}$$

Plugging equation (4.14) in (4.15), the last term vanishes and in the steady state we have $\partial_\tau P_2 = 0$. Then equation (4.15) becomes

$$\partial_t P_0 = \nabla_y^2(DP_2) + \nabla_x^2(DP_0) - \lambda P_0. \tag{4.16}$$

From equation (4.10) and (4.16) we have

$$\nabla_y^2(DP_2) = \partial_t\left(\frac{C_0}{D}\right) + \nabla_x^2(c_0) - \lambda\left(\frac{C_0}{D}\right). \tag{4.17}$$

We take an average of each term of this equation over the small scale. Let us assume $l_1 = n_1 p_1$ and $l_2 = n_2 p_2$ are the dimensions of each block of a big grid cell so that the area $\Omega = l_1 \times l_2$. Then the average of a function $w(\boldsymbol{y})$ over each block is defined as

$$\langle w\rangle = \frac{1}{\Omega}\int_0^{l_1}\int_0^{l_2} w(\boldsymbol{y})\, d\boldsymbol{y}. \tag{4.18}$$

Using the Divergence Theorem, the average of LHS of equation (4.17) gives

$$\langle\nabla_y^2(DP_2)\rangle = \frac{1}{\Omega}\int\limits_{\Omega_0} \boldsymbol{n}\,.\nabla_y(DP_2)\, dS_y = 0, \tag{4.19}$$

where $\boldsymbol{n}$ is the unit normal vector to the boundary Ω_0 which integrates to zero because the flux of moving dispersers entering a block is equal to the number leaving from a block due to periodicity. From equation (4.17) and (4.19) we now have

$$\langle\partial_t\left(\frac{C_0}{D}\right)\rangle = \langle\nabla_x^2(c_0)\rangle - \langle\lambda\left(\frac{C_0}{D}\right)\rangle, \tag{4.20}$$

and simplifying,

$$\langle D^{-1}\rangle\partial_t c_0 = \nabla_x^2(c_0) + \langle\lambda/D\rangle c_0.$$

In terms of averaged quantities we write

$$\partial_t c_0 = \overline{D}(\boldsymbol{x})\partial_x^2 c_0 - \bar{\lambda}c_0, \quad c_0(\boldsymbol{x},\boldsymbol{x}',0) = D(\boldsymbol{x}',0)\,\delta(\boldsymbol{x}-\boldsymbol{x}'), \tag{4.21}$$

where $\overline{D} = \frac{1}{\langle D^{-1}\rangle}$,the harmonic average of *D*, and

$$\bar{\lambda}(\boldsymbol{x},t) = \overline{D}\langle\lambda/D\rangle = \overline{D}\langle U(\boldsymbol{x})h(t)/D(\boldsymbol{x})\rangle = \overline{D}\; h(t)\langle U/D\rangle.$$

Assuming $\overline{D}$ is approximately constant, the solution of equation (4.21) is

$$c_0(\boldsymbol{x},\boldsymbol{x}',t) = \frac{D(\boldsymbol{x}')}{4\pi\overline{D}t}\; e^{\frac{-\|\boldsymbol{x}-\boldsymbol{x}'\|^2}{4\overline{D}t} - \int_0^t\bar{\lambda}(\boldsymbol{x},\tau)d\tau} = \frac{D(\boldsymbol{x}')}{4\pi\overline{D}t}\; e^{\frac{-\|\boldsymbol{x}-\boldsymbol{x}'\|^2}{4\overline{D}t} - \overline{D}\,\langle U/D\rangle\int_0^t h(\tau)d\tau}. \tag{4.22}$$

From equation (4.10) and (4.22) we get

$$P(\boldsymbol{x},\boldsymbol{x}',t) \cong \frac{D(\boldsymbol{x}')}{D(\boldsymbol{x})\,4\pi\bar{D}t}\; e^{\frac{-\|x-x'\|^2}{4\bar{D}t}-\bar{D}\,\langle U/D\rangle\int_0^t h(\tau)d\tau}, \tag{4.23}$$

using this in (4.5) and integrating gives an approximate solution for S,

$$S(\boldsymbol{x},\boldsymbol{x}',t) \cong \frac{D(\boldsymbol{x}')}{D(\boldsymbol{x})\,\bar{D}}\,\langle U(\boldsymbol{x})\rangle\int_0^t\left(\frac{h(t')}{4\pi t'}e^{\frac{-\|x-x'\|^2}{4\bar{D}t'}}\,e^{-\bar{D}\,\langle U(\boldsymbol{x})/D(\boldsymbol{x})\rangle\int_0^{t'}h(\tau)d\tau}\right)dt'. \tag{4.24}$$

4.2.3 Homogenized solution for SDK

The seed dispersal kernel is the long time limit of seed settling, which can be written

$$K_0(\boldsymbol{x},\boldsymbol{x}') \cong \lim_{t\to\infty} S(\boldsymbol{x},\boldsymbol{x}',t)$$

$$= \frac{D(\boldsymbol{x}')}{D(\boldsymbol{x})\,\bar{D}}\,\langle U(\boldsymbol{x})\rangle\int_0^{\infty}\left(\frac{h(t')}{4\pi t'}e^{\frac{-\|x-x'\|^2}{4\bar{D}t'}}\,e^{-\bar{D}\,\langle U(\boldsymbol{x})/D(\boldsymbol{x})\rangle\int_0^{t'}h(\tau)d\tau}\right)dt'.$$

Let $\langle U(\boldsymbol{x})\rangle = \bar{U}$ (average utilization in a cell) and $\langle U(\boldsymbol{x})/D(\boldsymbol{x})\rangle = \hat{\tau}$ (mean residence time in utilized habitat in a cell), then this equation becomes

$$K_0(\boldsymbol{x},\boldsymbol{x}') \cong \frac{D(\boldsymbol{x}')}{D(\boldsymbol{x})}\frac{\bar{U}}{\bar{D}}\int_0^{\infty}\left(\frac{h(t')}{4\pi t'}e^{\frac{-\|x-x'\|^2}{4\bar{D}t'}}\,e^{-\bar{D}\hat{\tau}\int_0^{t'}h(\tau)d\tau}\right)dt'. \tag{4.25}$$

Further, extracting the temporal integral,

$$I(\boldsymbol{x},\boldsymbol{x}') = \int_0^{\infty}\left(\frac{h(t')}{4\pi t'}e^{\frac{-\|x-x'\|^2}{4\bar{D}t'}}\,e^{-\,\bar{D}\hat{\tau}\int_0^{t'}h(\tau)d\tau}\right)dt', \tag{4.26}$$

equation (4.25) becomes

$$K_0(\boldsymbol{x},\boldsymbol{x}') \cong \frac{D(\boldsymbol{x}')}{D(\boldsymbol{x})}\;\frac{\bar{U}}{\bar{D}}\,I(\boldsymbol{x},\boldsymbol{x}'). \tag{4.27}$$

We note that the kernel is not normalized. However, when we evaluate the seed dispersal probabilities on the big grid, normalization will be made numerically.

4.2.4 Connecting landscape and dispersal variables

To connect the homogenized seed dispersal kernel with a landscape, we define small-grid variables which will be averaged up to inform dispersal probabilities on large types of grid. A classified landscape consist of different types of habitats (tree cover, grassland, barrier areas, cultivated or developed areas) resolved on the scale of the small grid cells (30 m). We denote these habitat types as $H_k, k = 1, 2, 3 \ldots$. The characteristic function $\chi_k(\boldsymbol{x})$ ($k = 1, 2, 3 \ldots$) is defined as having value one if $\boldsymbol{x}$ belongs to the habitat type H_k and it gives zero otherwise. Movement of birds or animals depends on existing habitat types. They forage differently in different areas. The motility in habitat type k is defined as

$$D_k = \frac{1}{\tau_k}, \tag{4.28}$$

where D_k is motility and τ_k is the residence time per area in habitat type H_k. Thus, motility is

$$D(\boldsymbol{x}) = \sum_{k=1}^{K} D_k \chi_k(\boldsymbol{x}), \tag{4.29}$$

where K is the possible number of habitat types in the big-grid cell.

There might be some types of habitat which birds or animals do not use for purposes of seed deposition. We denote a utilization index as U_k, $k = 1, 2, 3 \ldots$, with $U_k = 1$ if dispersers use habitat H_k, and 0 otherwise. Then the utilization function can be expressed as

$$U(\boldsymbol{x}) = \sum_{k=1}^{n} U_k \chi_k, \tag{4.30}$$

A list of variables and parameters with detail description is displayed in Table 4.1.

Table 4.1: Parameters and variables used in this paper.

Notation	Description
$\boldsymbol{x}'$	Starting location of seed dispersal
$\boldsymbol{x}$	Ending location of seed dispersal
$K_0(\boldsymbol{x}', \boldsymbol{x})$	Homogenized seed dispersal kernel, PDF of seed moving $\boldsymbol{x}' \to \boldsymbol{x}$
$G_0(\boldsymbol{x}', \boldsymbol{x})$	Homogenized Gaussian kernel, PDF of seed moving $\boldsymbol{x}' \to \boldsymbol{x}$
$L_0(\boldsymbol{x}', \boldsymbol{x})$	Homogenized Laplace kernel, PDF of seed moving $\boldsymbol{x}' \to \boldsymbol{x}$
$C_{i,j}$	Initial big grid cell with starting location of seed dispersal
$C_{m,n}$	Targeted big grid cell with ending location of seed dispersal
Ω	Area of each block in a big grid cell
Ω_0	Boundary of each block in the targeted big grid
H_k	Habitat types, $k = 1,2,3$ ... up to the number of existing habitats
U_k	Utilization index, $k = 1,2,3$ ... index (0 or 1) of habitat type H_k
χ_k	Characteristic function, $k = 1,2,3$ ... up to the number of existing habitats inside the big grid
D_k	Motility in habitat type H_k, $k = 1,2,3$ ... up to the number of existing habitats
τ_k	Residence time per area in habitat type H_k, $i = 1,2,3$ ... up to the number of habitats used
$F_{i,j}^k$	Fraction cover, $k = 1,2,3$ ... up to the number of existing habitats
$\overline{D}_{i,j}$	Harmonic average of D
$\tilde{b}$	Mean seed digestion scaling parameter
σ	$= \sqrt{2\,\overline{D}\tilde{b}}$, the variance of homogenized dispersal kernel
$\hat{P}_{i,j}(m,n)$	Probability weights of dispersal before normalization
$P_{i,j}(m,n)$	Probability of dispersal from big grid cell i, j to cell m, n

4.3 Dispersal probabilities on the big grid

We use continuous dispersal, represented by as the homogenized SDK (equation 4.27), to resolve discrete probabilities from one big-grid cell to other big-grid cells. Let us assume $C_{m,n}$ denotes the targeted big-grid cell and $C_{i,j}$ denotes the big-grid cell from where dispersal begins. We evaluate all of the averaged quantities on individual grid cells. The homogenized averaged quantities: motility, utilization index and residence time are respectively denoted by $\overline{D}_{m,n}$, $\overline{U}_{m,n}$ and $\hat{\tau}_{m,n}$. These quantities are evaluated in the big-grid cell $C_{n,m}$. The dispersal probability weights from a starting location $\boldsymbol{x}' \in C_{i,j}$ to some ending location $\boldsymbol{x} \in C_{n,m}$ we define as

$$\hat{P}_{i,j}(m,n) = \iint_{C_{m,n}} K_0(\boldsymbol{x}, \boldsymbol{x}')\, d\boldsymbol{x}, \tag{4.31}$$

From equation (4.27) and (4.31) we have

$$\hat{P}_{i,j}(m,n) = \frac{D(\boldsymbol{x}')\,\overline{U}_{m,n}}{\overline{D}_{m,n}} \iint_{C_{m,n}} \left[\frac{1}{D(x)}\, I\left(\boldsymbol{x}' = \boldsymbol{x_{i,j}}, \boldsymbol{x} = \boldsymbol{x_{m,n}}\right)\right] d\boldsymbol{x}, \tag{4.32}$$

Note that the motility $D(\boldsymbol{x})$ and residence time per area $\tau(\boldsymbol{x})$ are inversely related,

$$\tau(\boldsymbol{x}) \approx \frac{1}{D(\boldsymbol{x})}, \tag{4.33}$$

and residence time per area can be written in the form

$$\tau(\boldsymbol{x}) = \sum_{k=1}^{K} \tau_k \chi_k(\boldsymbol{x}), \tag{4.34}$$

where K is the number of existing habitat type. Thus, from equations (4.32), (4.33) and (4.34) gives

$$\hat{P}_{i,j}(m,n) \approx \frac{D(\boldsymbol{x}')\,\bar{U}_{m,n}}{\bar{D}_{m.n}} \iint\limits_{C_{m,n}} \left[\left(\sum_{k=1}^{K} \tau_k \chi_k(x)\right) I\left(\boldsymbol{x}' = \boldsymbol{x_{i,j}}, \boldsymbol{x} = \boldsymbol{x_{m,n}}\right)\right] d\boldsymbol{x}. \quad (4.35)$$

The fraction cover of habitat type k in large grid cell $C_{m,n}$ is defined as

$$F_{m,n}^{k} = \frac{1}{\Omega} \iint\limits_{C_{m,n}} \chi_k(\boldsymbol{x})\, d\boldsymbol{x}, \quad (4.36)$$

Notice that the integrand in $I(\boldsymbol{x}, \boldsymbol{x}')$ depends only on large scale averages. So $I(\boldsymbol{x}, \boldsymbol{x}')$ is approximately constant in small cells. We therefore factor the integral in (4.35) as

$$\hat{P}_{i,j}(m,n) \approx \frac{D(\boldsymbol{x}')\,\bar{U}_{m,n}}{\bar{D}_{m.n}}\, I\left(\boldsymbol{x}' = \boldsymbol{x_{i,j}}, \boldsymbol{x} = \boldsymbol{x_{m,n}}\right)\left[\sum_{k=1}^{p} \Omega\, \tau_k\, F_{m,n}^{k}\right], \quad (4.37)$$

And using $\sum \tau_k F_{m,n}^{k} = \frac{1}{\bar{D}_{m.n}}$ is true, so equation (4.37) becomes

$$\hat{P}_{i,j}(m,n) \approx \frac{D(\boldsymbol{x}')\,\bar{U}_{m,n}}{\bar{D}_{m,n}^{2}}\, I\left(\boldsymbol{x}' = \boldsymbol{x_{i,j}}, \boldsymbol{x} = \boldsymbol{x_{m,n}}\right) \Omega. \quad (4.38)$$

We must now normalize the $\hat{P}_{i,j}(m,n)$ to create dispersal probabilities. The mean variance of seeds during dispersal is $\sigma = \sqrt{2\bar{D}\tilde{b}}$, where $\tilde{b}$ is the modal (peak) handling time. Approximately 99.7% of dispersed seeds fall within 3σ of their starting location for a Gaussian distribution (Casella and Berger, 2001). Outside this boundary seed dispersal is negligible. We therefore calculate the total weights of probabilistic dispersal in a 3σ region

$$\pi_{m,n} = \sum_{\substack{m-\hat{m} \le p \le m+\hat{m} \\ n-\hat{n} < q < n+\hat{n}}} \hat{P}_{i,j}\,(m,n), \quad (4.39)$$

where $\hat{m} = \hat{n} = \lceil 3\sigma \rceil$, the first integer $\geq 3\sigma$. The probability of dispersing seeds from one big grid cell with location (i,j) to the another big grid cell with location (m,n) is then

$$P_{i,j}(m,n) = \frac{1}{\pi_{m,n}}\, \hat{P}_{i,j}(m,n). \quad (4.40)$$

4.4 Examples

There are pre-existing dispersal kernels corresponding to two differing limits of handling time, namely Gaussian and Laplace kernels. We next write homogenized form of each kernel and compare dispersal probabilities.

4.4.1 Dispersal probabilities associated with Gaussian kernel

Seed handling function $h(t)$ when there is no handling time variability can be written (Neupane and Powell, 2015) as

$$h(t) = \delta\big(t - \tilde{b}\,\big), \tag{4.41}$$

where $\tilde{b}$ is a the seed handling time scaling parameter. In this limit equation (4.29) gives

$$G_0(\boldsymbol{x}, \boldsymbol{x}') = \frac{D(\boldsymbol{x}')}{D(\boldsymbol{x})}\frac{\bar{U}}{\bar{D}}\int_0^{\infty}\left(\frac{\delta(t-b)}{4\pi t'}e^{\frac{-\|x-x'\|^2}{4\bar{D}t'}}\,e^{-\bar{D}\hat{\tau}\int_0^{t'}\delta(\tau-\tilde{b})\,d\tau}\right)dt'. \tag{4.42}$$

Integrating,

$$G_0(\boldsymbol{x}, \boldsymbol{x}') = \frac{D(\boldsymbol{x}')}{D(\boldsymbol{x})}\,\frac{\bar{U}}{4\pi\bar{D}\tilde{b}}\,e^{\frac{-\|x-x'\|^2}{4\bar{D}\tilde{b}}}\,e^{-\bar{D}\hat{\tau}}, \tag{4.43}$$

Following the procedure as in equation (4.39), the weighted dispersal probability becomes

$$\hat{P}_{i,j}(m,n) = \frac{D(\boldsymbol{x}')\,\bar{U}_{m,n}}{4\pi\,\bar{D}_{m,n}^2\,\tilde{b}}\,e^{\frac{-\left\|x_{m,n}-x_{i.j}\right\|^2}{4\bar{D}\tilde{b}}-\bar{D}_{m,n}\,\hat{\tau}_{m,n}}\,. \tag{4.44}$$

4.4.2 Dispersal probabilities associated with Laplace kernel

For maximum variability on seed handling time, i.e. a uniform distribution, the function $h(t)$ is taken (Neupane and Powell, 2015) as

$$h(t) = \frac{1}{2\tilde{b}}, \tag{4.45}$$

where $\tilde{b}$ is a the seed handling time scaling parameter. Then equation (4.29) becomes

$$L_0(\boldsymbol{x},\boldsymbol{x}') = \frac{D(\boldsymbol{x}')}{D(\boldsymbol{x})}\frac{\bar{U}}{\bar{D}}\int_0^{\infty}\left(\frac{\frac{1}{2\tilde{b}}}{4\pi t'}e^{\frac{-\|x-x'\|^2}{4\bar{D}t'}}e^{-\bar{D}\hat{\tau}\int_0^{t'}\frac{1}{2\tilde{b}}d\tau}\right)dt'. \tag{4.46}$$

Rearranging terms from this equation gives,

$$L_0(\boldsymbol{x},\boldsymbol{x}') = \frac{D(\boldsymbol{x}')}{D(\boldsymbol{x})}\frac{\bar{U}}{\bar{D}\hat{\tau}}\int_0^{\infty}\left(\frac{\bar{D}\hat{\tau}}{2\tilde{b}}\frac{1}{4\pi\bar{D}t'}e^{\frac{-\|x-x'\|^2}{4\bar{D}t'}}e^{-\bar{D}\hat{\tau}\frac{t'}{2\tilde{b}}}\right)dt',$$

which can be integrated in terms of Bessel function,

$$L_0(\boldsymbol{x},\boldsymbol{x}') = \frac{D(\boldsymbol{x}')}{D(\boldsymbol{x})}\frac{\bar{U}}{\bar{D}\hat{\tau}}\frac{Y_0\left[\frac{\|x-x'\|}{\sqrt{\frac{2\bar{D}\tilde{b}}{\bar{D}\hat{\tau}}}}\right]}{\frac{4\pi\bar{D}\tilde{b}}{\bar{D}\hat{\tau}}},$$

where Y_0 is a modified Bessel's function of the second kind, zeroth order. Simplifying,

$$L_0(\boldsymbol{x},\boldsymbol{x}') = \frac{D(\boldsymbol{x}')}{D(\boldsymbol{x})}\frac{\bar{U}}{4\pi\bar{D}\tilde{b}}\,Y_0\left(\sqrt{\frac{\hat{\tau}}{2\tilde{b}}}\,\|\boldsymbol{x}-\boldsymbol{x}'\|\right). \tag{4.47}$$

Again, following the procedure as in equation (4.39), the weighted dispersal probability becomes

$$\hat{P}_{i,j}(m,n) = \frac{D(\boldsymbol{x}')\,\bar{U}_{m,n}}{4\pi\tilde{b}\,\bar{D}_{m,n}^2}\,Y_0\left(\sqrt{\frac{\hat{\tau}}{2\tilde{b}}}\,\|\boldsymbol{x_{m,n}}-\boldsymbol{x_{i,j}}\|\right) \tag{4.48}$$

4.4.3 Comparing dispersal on artificially structured random landscapes

To compare dispersal probabilities corresponding to three dispersal kernels namely Gaussian, seed digestion and Laplace, we artificially generate three different landscapes. In the simulation, we generate a 512 by 512 random matrix B with numbers between zero and one using a randomly-phased Fourier field with power spectrum decaying as $\|k\|^{-\frac{H+1}{2}}$, where k is the wave number vector. This generates a fractal landscape of dimension *2-H*.

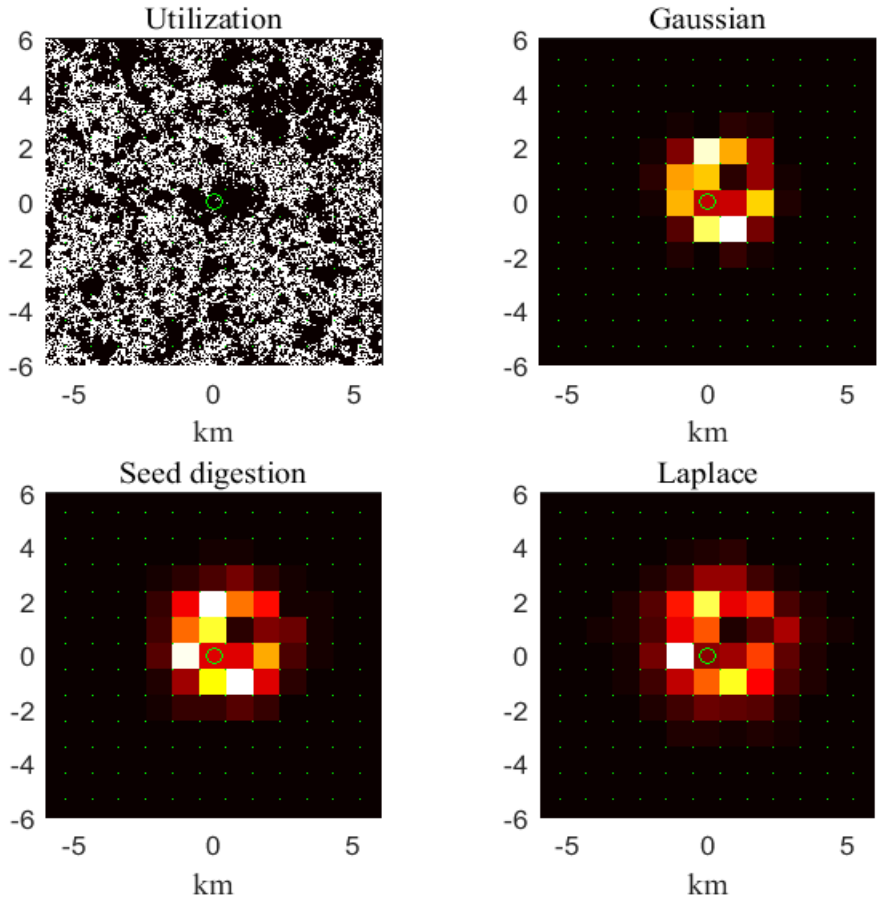

Figure 4.1 Dispersal probabilities in an uncorrelated landscape ($H = 0.25$), using $b = 52.5$ min and $D_{max} = 0.225$ km^2/min to model dispersal of pinyon seeds by jays. Green dots indicate the boundaries of big-grid cells. Each big-grid cell is in sized 0.96 km^2 and it is divided into 1024 small grid cells of size 900 m^2. White portion in the left top square demonstrates possible seeds caching or dropping area. Other three squares show the color maps of probability of dispersal from the central grid cell (indicated by green circle) to surrounding cells corresponding to Gaussian, SDK and Laplace kernels using a 'hot' color map, the brightest color indicates the most seeds dispersed locations.

A matrix of motility values is created using $D = 0.225$ km^2/min $\times B$. A utilization matrix, U, is generated from B by setting $U=1$ where $B< 0.1$. These numbers are chosen to model pinyon jay, which can forage with maximum motility $D = 0.225$ km^2/min and the mode seed handling time $b = 52.5$ min (Neupane and Powell, 2015). Three different landscape structures, using $H = 0.25$ (very uncorrelated, Figure 4.1), $H = 0.5$ (Figure 4.2)

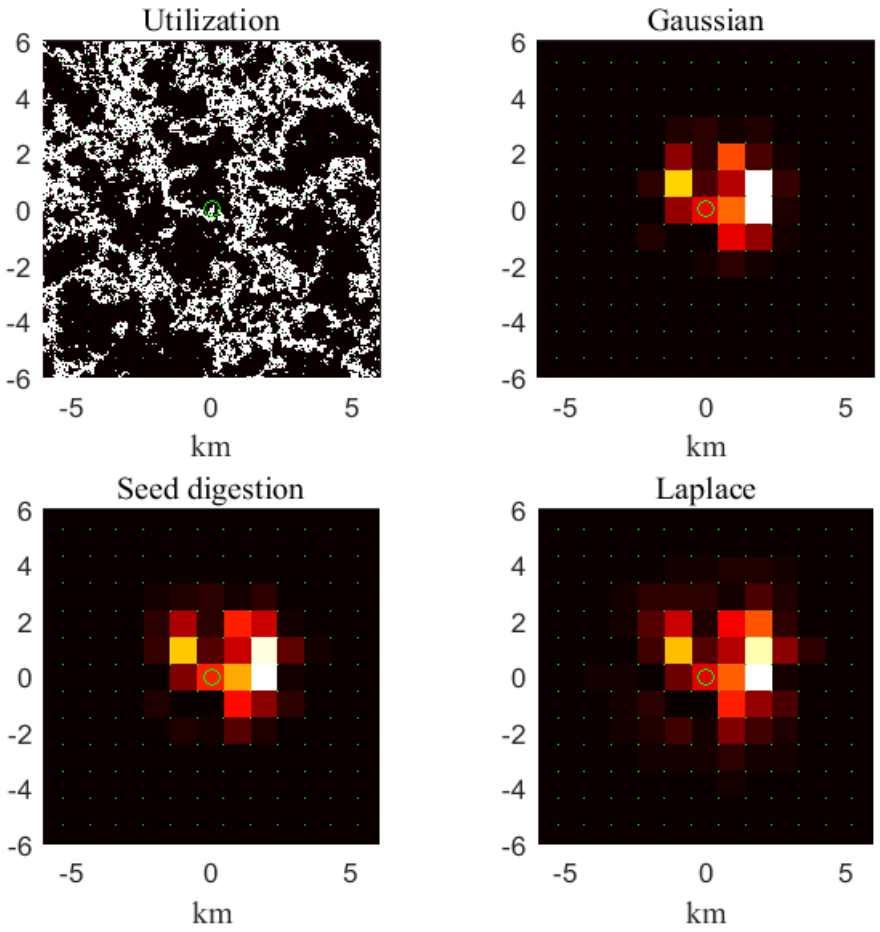

Figure 4.2 Dispersal probabilities in a moderately correlated landscape ($H = 0.5$), using $b = 52.5$ min and $D_{max} = 0.225$ km^2/min to model dispersal of pinyon seeds by jays. Green dots indicate the boundaries of big-grid cells. Each big-grid cell is in sized 0.96 km^2 and it is divided into 1024 small grid cells of size 900 m^2. White portion in the left top square demonstrates possible seeds caching or dropping area. Other three squares show the color maps of probability of dispersal from the central grid cell (indicated by green circle) to surrounding cells corresponding to Gaussian, SDK and Laplace kernels using a 'hot' color map, the brightest color indicates the most seeds dispersed locations.

and $H = 0.75$ (highly correlated, Figure 4.3) are considered. We assume that each big-grid cell is in sized 0.96 km^2 and it is divided into 32×32 small 30 meter grid cells. Dispersal probabilities associated with Gaussian, SDK and Laplace kernels are displayed and compared for each landscape.

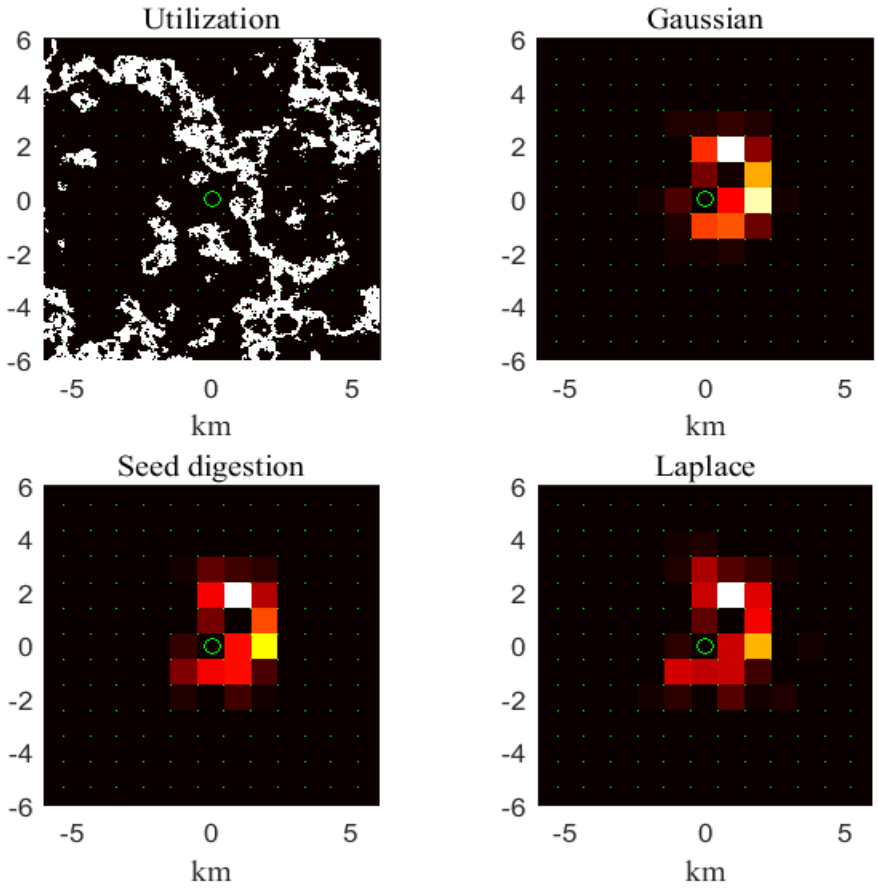

Figure 4.3 Dispersal probabilities in a correlated landscape ($H = 0.75$), using $b = 52.5$ min and $D_{max} = 0.225\ \text{km}^2/\text{min}$ to model dispersal of pinyon seeds by pinyon jays. Green dots indicate the boundaries of big-grid cells. Each big-grid cell is in sized $0.96\ \text{km}^2$ and it is divided into 1024 small grid cells of size $900\ \text{m}^2$. White portion in the left top square demonstrates possible seeds caching or dropping area. Other three squares show the color maps of probability of dispersal from the central grid cell (indicated by green circle) to surrounding cells corresponding to Gaussian, SDK and Laplace kernels using a 'hot' color map, the brightest color indicates the most seeds dispersed locations.

After comparing the dispersal probabilities associated with three kernels in Figure 4.1 Figure 4.2 and Figure 4.3, we found that seeds are dispersed to the furthest for the Laplace, and the least spread for the Gaussian. Seed dispersal with seed digestion kernel is bounded by the other two. The dispersal under seed digestion looks closer to Gaussian than

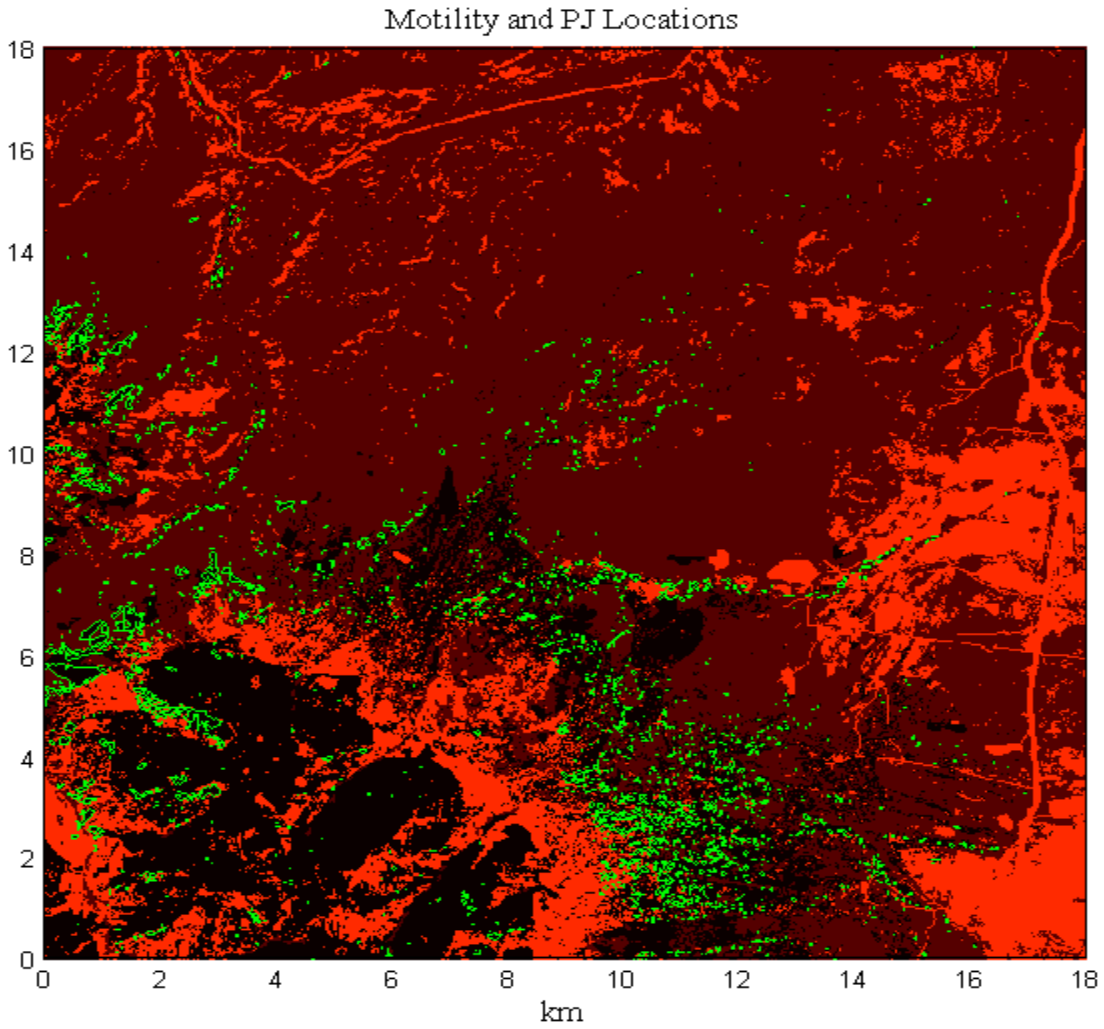

Figure 4.4 The landscape was generated using real data from Colorado Plateau with $b = 52.5$ min and $D_{max} = 0.225$ km^2/min to model dispersal of pinyon seeds by pinyon jays. Both green area (pine cover types) and black area denote the low motility with high utilization locations. Locations with orange color indicate the high motility areas (sand, dirt, farmland urban and water). The dark-brown colored locations are the intermediate motility areas.

the dispersal associated with Laplace. We also found that the high probabilities of dispersal occur when the targeted grid cell has a high fraction of utilization and low $\overline{D}$, which means that birds spend a lot of time there and can find a lot of places to cache seeds, which is reasonable since residence time and motility are inversely related. Furthermore, the kernel realistically 'jumps over' cells with low average utilization, as one would expect in nature.

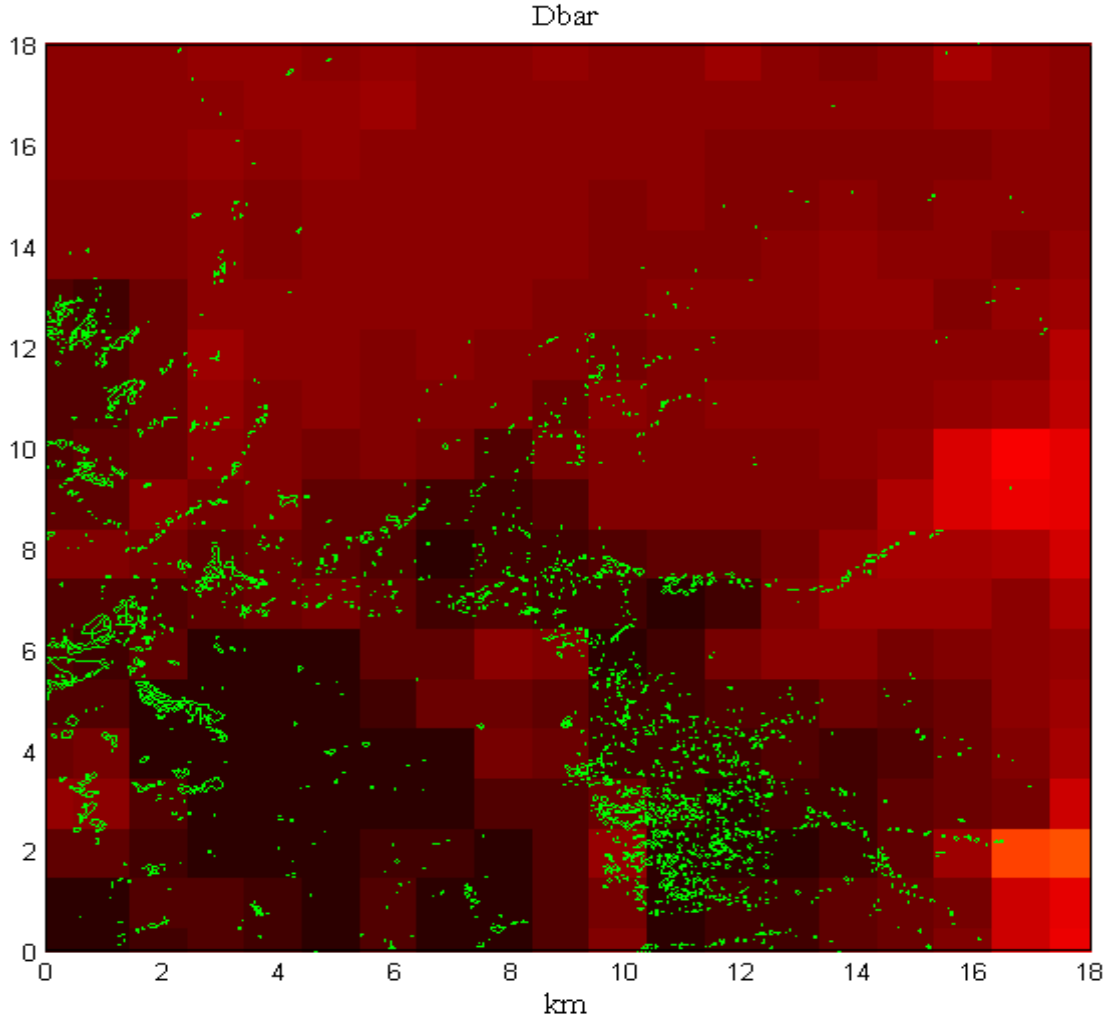

Figure 4.5 The harmonic average motility is received using $D_{max} = 0.225$ km^2/min and $b = 52.5$ min to model dispersal of pinyon seeds by pinyon jays. The green area denotes the pine cover types and the darkest area indicates the lowest motility locations. There is low motility in the locations densely occupied with pine trees. On the other hand, there is high motility to the mid-east and south-east locations with no trees at all.

4.4.4 Pinyon juniper dispersal in real landscape

To estimate the probability of dispersal of pinyon and juniper, we use real landscape data. In the simulation, the matrix of pinyon and juniper landscape class, utilization index for seed caching and motility are generated using real data. Probability of dispersal of pinyon-

juniper is estimated for pinyon jay which can forage with maximum motility $D = 0.225\ \text{km}^2/\text{min}$ and the mode seed handling time $b = 52.5$ min (Neupane and Powell, 2015). We assume that each big-grid cell is in sized $0.99\ \text{km}^2$ and it is divided into 33×33

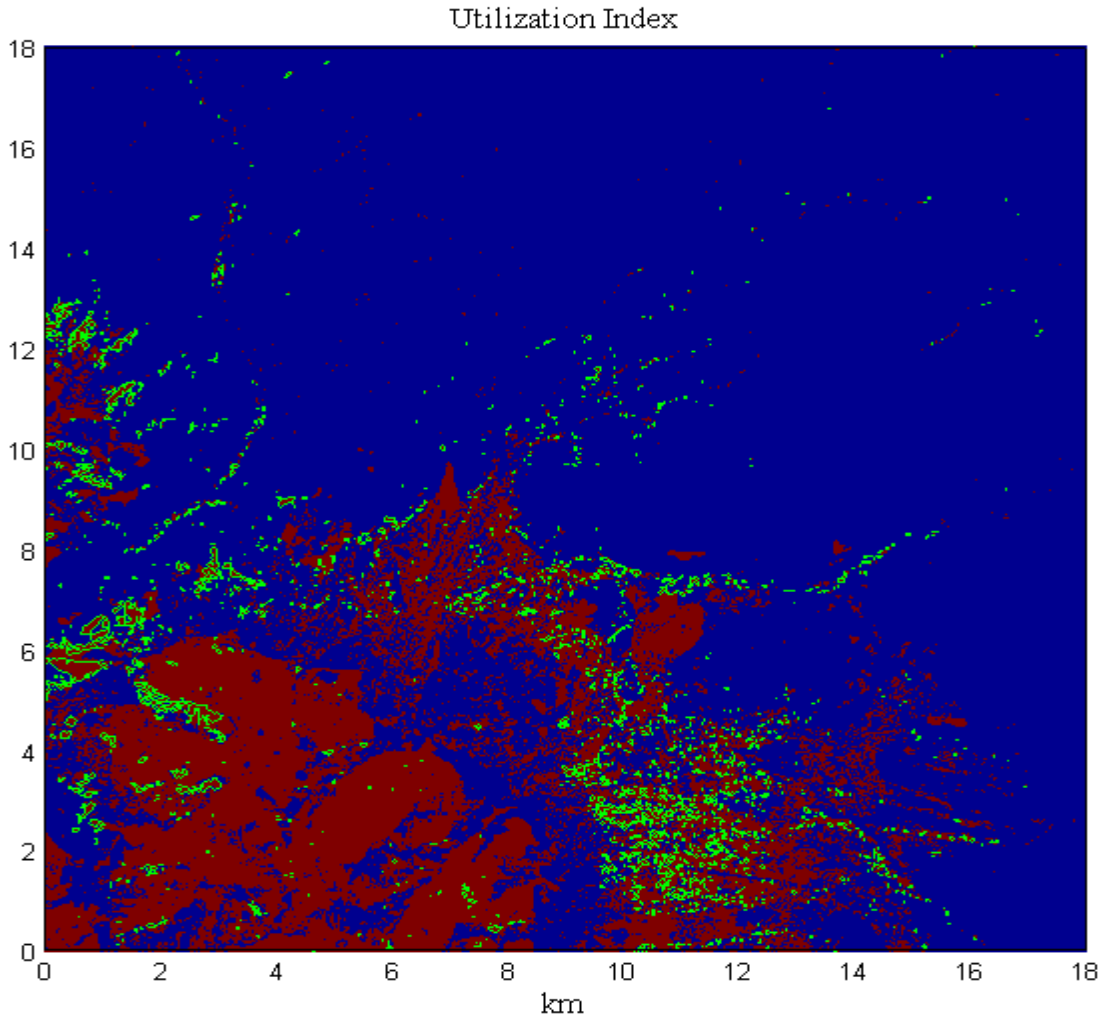

Figure 4.6 The landscape utilization is received using $D_{max} = 0.225\ \text{km}^2/\text{min}$ and $b = 52.5$ min to model dispersal of pinyon seeds by pinyon jays. The green area denotes the pine cover types, the red area indicates the seed caching area ($U = 1$) and the blue area denotes no seed caching area ($U = 0$). The graph shows that seed caching locations are not evenly dispersed and are clumped in the southwest.

small 30 meter grid cells. This landscape was generated by real data from Colorado Plateau displayed in figure 4.4. In this figure, pine cover types are high utilization areas

and low motility locations. The locations covered by sand, dirt, farmland, urban and water are in high motility areas. The harmonic average motility is shown in figure 4.5. It shows that there exists high motility in the dense pine cover types. The potential seed

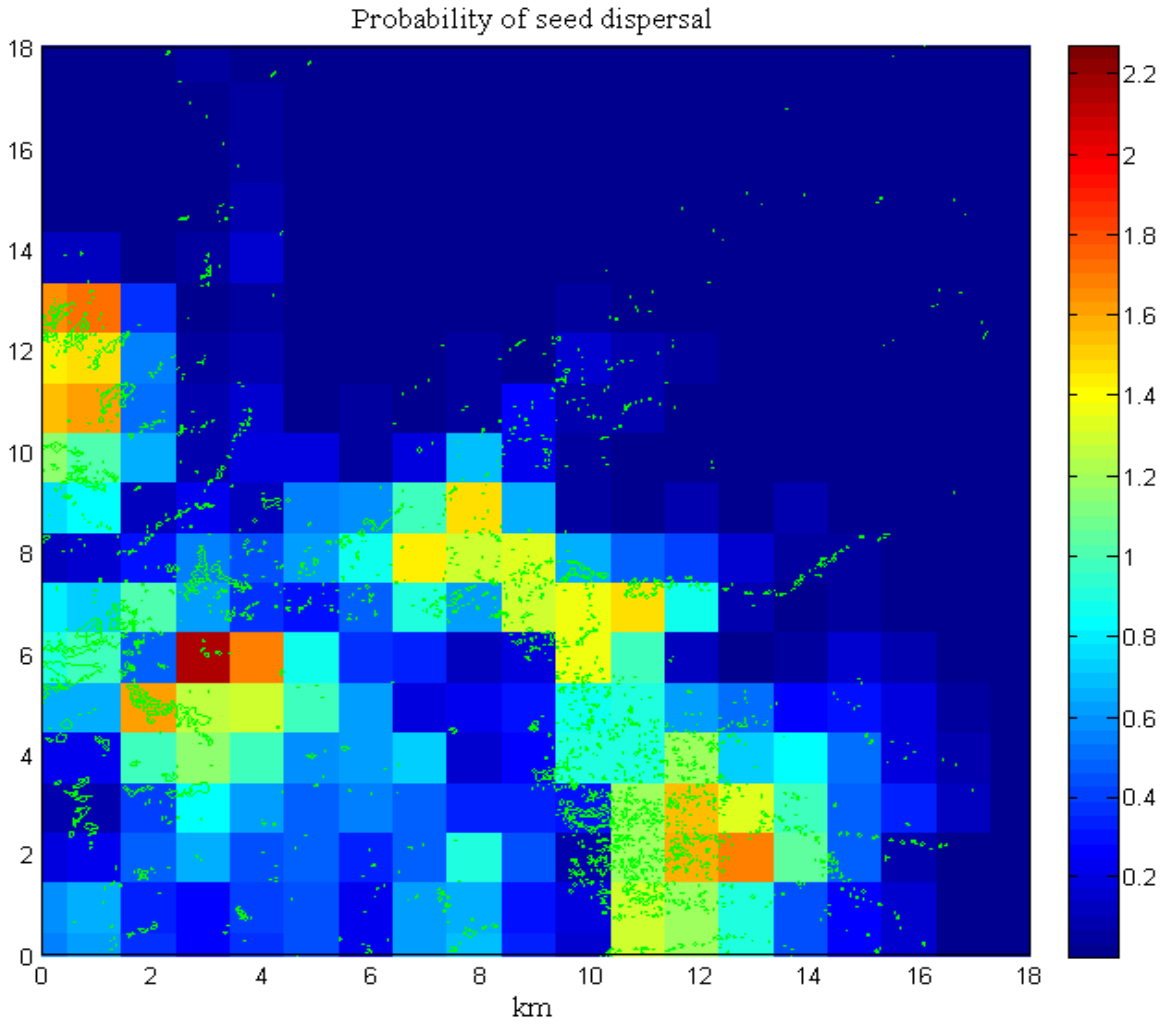

Figure 4.7 Dispersal probabilities are shown using $D_{max} = 0.225$ km^2/min and $b = 52.5$ min to model dispersal of pinyon seeds by pinyon jays. The green area denotes the locations where actual pinyon pines are. The darker the red color, the higher pinyon-juniper dispersal. The location with darkest blue color gives the lowest density of dispersal. The color bar to the right shows label of dispersal density. The high density of dispersal occurs near the pinyon-juniper landscape.

caching areas are displayed in figure 4.6. These areas are not evenly dispersed and are clumped in the southwest locations. Probabilities of dispersal of pinyon-juniper are shown in figure 4.7. We found that high density of dispersal occurs near the pinyon-juniper woodland and there exists some favorable caching area with no densely occupied trees. The motility D varies along with the habitat variation. For instance, it is low in the pinyon-juniper woodland and it is high in sand, dirt, farmland, urban and water. Results from figure 4.7 shows that seed spread originates around the location of adult trees habitat except on the boundaries.

4.5 Conclusion

We modified the pre-exiting seed dispersal model by introducing ecological diffusion, seed handling times, landscape utilization and space-dependent motility associated with frugivorous birds in the model. Method of homogenization was used for solving the model with the assumption that habitats vary in short scales (30 meters) but dispersal is to be resolved on kilometers. The dispersal kernel received from the solution reflects small scale variability and animals' utilization. This dispersal kernel is connected to discrete scale dispersal by integrating over large cells, estimating dispersal probabilities that depend on residence time spent and utilization in different cover types by frugivorous birds. Consequently, homogenized seed dispersal kernel can be applied to estimate fruiting tree distribution from one big-grid cell to the next cell in terms of large-scale variables. Comparing with dispersal probabilities associated with three dispersal kernels: Gaussian, seed digestion and Laplace, we found that seeds are dispersed to the furthest for the Laplace, and the least spread for the Gaussian. Seed dispersal with seed digestion kernel is

bounded by the other two. This result is consistent with the result of seed invasion based on homogenous landscape in chapter 2 and seed invasion in the heterogeneous landscape in chapter 3.

In this chapter we have estimated large scale dispersal probabilities associated with animals' utilization of landscape and their space-dependent motility. The homogenization technique is to be used to solve this model assuming that habitat variability is reflected on 30m scales but dispersal is to be resolved on kilometer-scale grids.

REFERENCES

Araujo, M.B. and Guisan, A., 2006. Five (or so) challenges for species distribution modeling. *Journal of Biogeography* 33:1677-1688.

Austin, M.P. and Van Niel, K.P., 2011. Improving species distribution models for climate change studies: variable selection and scale. *Journal of Biogeography* 38:1-8.

Barbet-Massin, M. and Jetz, W., 2014. A 40-year, continent-wide, multispecies assessment of relevant climate predictors for species distribution modeling. *A Journal of Conservation Biogeography* 20:1285-1295.

Carlo, T.A. and Morales, J.M., 2008. Inequality in fruit-removal and seed dispersal: consequences of bird behavior, neighborhood density and landscape aggregation. *Journal of Ecology* 96:609-618.

Carlo, T.A., Garcia, D., Martinez, D., Gleditsch, J.M. and Morales, J.M., 2013. Where do seeds go when they go far? Distance and directionality of avian seed dispersal in heterogeneous landscapes. *Ecology* 94(2):301-307.

Casella, G. and Berger, R.L., 2001. Statistical Inference. Duxbury Press, Pacific Grove, USA.

Clark, J.A., Silman, M., Kern, R., Macklin, E. and Hillerislambers, J., 1999. Seed dispersal near and far: patterns across temperate and tropical forests. *Ecology* 85(5):1475-1494.

Coops, N.C., Waring, R.H. and Hilker, T., 2012 Prediction of soil properties using a

process-based forest growth model to match satellite-derived estimates of leaf area index. *Remote Sensing Environment* 126:160-173.

Edith, J. and Leathwick, J.R., 2009. Species distribution models: ecological explanation and prediction across space and time. *Annual Review Ecology, Evolution and Systematics* 40:677-697.

Garlick, M.J., Powell, J.A., Hooten, M.B. and MacFarlane, L.R. (2010) Homogenization of large-scale movement methods in ecology. Bull. Math Biol. 73:2088-2108.

Garcia, D., Zamora, R. and Amico, G.C., 2011. The spatial scale of plant-animal interactions: effects of resource availability and habitat structure. *Ecological Monographs* 81(1):103-121.

Gibson, J., Moisen, G., Frescino, T. and Edwards, Jr., T.C., 2013. Using publicly available forest inventory data climate-based models of tree species distribution: examining effects of true versus altered location coordinates. *Ecosystems* 17:43-53.

Glyphis, J.P. Milton, S.J. and Siegfried, 1981. Dispersal of *Acacia cyclops* by birds. *Oecologia* 48(1):138-141.

Gosper, C.R. Stansbury, C.D. and Vivian-Smith, G., 2005. Speed dispersal of fleshy fruited invasive plants by birds: contributing factors and management options. *Diversity and Distributions* 11:549-558.

Guisan, A. and Thuiller, W., 2005. Predicting species distribution: offering more than simple habitat models. *Ecology Letters* 8: 993-1009.

Herrera, J.M., Morales, J.M. and Garcia, D., 2011. Differential effects of fruit availability

and habitat cover for frugivore-mediated seed dispersal in a heterogeneous landscape. *Journal of Ecology* 99:1100-1107.

Holmes, M.H., 1995. Introduction to Perturbation Methods. Sprinter-Verlag, New York, USA.

Howe, H.F. and Smallwood, J., 1982. Ecology of seed dispersal. *Annual Review of Ecology and Systematics* 13:201-228.

Howe, H.F., 1986. *Seed Dispersal by Fruit-eating Birds and Mammals*, edited by Murray, D.R. Academic Press, Sydney, Australia 123-190.

Lobo, J.M., Jimenez-Valverde, A. and Hortal, J., 2010. The uncertain nature of absences and their Their importance in species distribution modeling. *Ecography* 33:103-114.

Luoto, M. Virkkala, R. and Heikkinen, R. K., 2007. The role of land cover in bioclimatic models depends on spatial resolution. *Global Ecology and Biogeography* 16:34-42.

Mathys, A., Coops, N.C. and Waring, R.H., 2014. Soil water availability effects on the distribution of 20 tree species. *Forest Ecology and Management* 313:144-152.

McKenney, D.W., Pedlar, J.H., Lawrence, K., Campbell, K. and Hutchinson, M.F., 2007 Potential impact of climate change on the distribution of North American trees. *BioScience* 57(11):939-948.

Menke, S.B., Holway, D.A., Fisher, R.N. and Jetz, W., 2009. Characterizing and predicting species distributions across environments and scales: argentine ant occurrences in the eye of the beholder. *Global ecology and Biogeography* 18:50-63.

Morales, J.M., Rivarola, M.D., Amico, G. and Carlo, T.A., 2012. Neighborhood effects on seed dispersal by frugivores: testing theory with a mistletoe-marsupial system in Patagonia. *Ecological Society of America* 93(4):741-748.

Neubert, M.G., Kot, M. and Lewis, M.A., 1995. Dispersal and pattern formation in a discrete-time predator-prey model. Theoretical Population Biology 48, 7-43.

Neupane, R.C. and Powell, J.A., 2015. Mathematical model of active seed dispersal by frugivorous birds and migration potential of pinyon and juniper in Utah. *Applied Mathematics* 9:1506-1523.

Neupane, R.C. and Powell, J.A., 2015. Invasion speeds with active dispersers in highly variable landscapes: multiple scales, homogenization, and the migration of trees. *Journal of Theoretical Biology* 387:111-119.

Peterman, W., Waring, R.H., Seager, T. and Polllck, W.L., 2012. Soil properties affect pinyon pine-juniper response to drought. *Ecohydrology* 6:455-463.

Peters, M.P., Iverson, L.R., Prasad, A.M. and Matthews, S.N., 2013. Integrating fine scale soil data into species distribution models: preparing soil survey geographic (SSURGO) data from multiple counties. General technical report NRS-122, US Forest Service, Newtown square PA, http://www.nrs.fs.fed.us/.

Powell, J.A. and Zimmermann, N.E. (2004) Multiscale analysis of active seed dispersal contributes to resolving Reid's paradox. Ecology 85:490-506.

Renne, Jr. I.J., Barrow, W.C., Randall Johnson, L.A. and Bridges, W.C., 2002. Generalized avian dispersal syndrome contributes to Chinese tallow tree (Sapium sebiferum, Euphorbiaceae) invasiveness. *Diversity of Distributions* 8(5):285-295.

Sanchez-Fernandez, D., Lobo, J.M. and Hernandez-Manrique, O.L., 2011. Species distribution models that do not incorporate global data misrepresent potential distributions: a case study using Iberian diving beetles. *Diversity and Distributions* 17:163-171.

Schupp, E.W., Jordano, P. and J. M. Gomez, J.M., 2010. Seed dispersal effectiveness revisited: a conceptual review. *New Phytologist* 188(2):333-353.

Syphard, A.D. and Franklin, J., 2009. Differences in spatial predictions among species distribution modeling methods vary with species traits and environmental predictors. *Ecography* 32:907-918.

Turchin, P., 1998. Quantitative Analysis of Movement: Measuring and Modeling Population Redistribution on Animals and Plants. Sinauer Associates Inc., Sunderland.

Wiens, J.A., Stralberg, D., Jongsomhit, D., Howell, C.A. and Snyder, M.A., 2009. Niches, models, and climate: assessing the assumptions and uncertainties. *Proceedings of the National Academy of Sciences* 106:19729-1976.

CHAPTER 5

CONCLUSION

In this dissertation we consider the active seed dispersal of fruiting trees on homogeneous as well as heterogeneous landscapes. The work is largely inspired by the problem of pinyon and juniper dispersal in the American southwest. Due to concerns about changing climate, we construct mathematical tools to help address the following research questions: (i) Can either pinyon or juniper disperse far enough northward to colonize the new habitat created by climate change? (ii) How rapidly may we expect P-J forest boundaries to move?

We introduced a PDF of seed-handling to reflect the effects of digestion/caching on dispersal of pinyon and juniper seeds. We connected this distribution to hazard functions or failure rates in an existing random-walk dispersal model to determine a seed digestion kernel modeling the probable location of seeds after active dispersal. As expected, if birds or animals take more time to handle seeds, those seeds are dispersed further away from the source tree.

To evaluate migration potential for pinyon and juniper we introduced an IDE model with competition among seedlings, which is appropriate for desert-adapted trees in the xeric environment of the American Southwest. The SDK was compared with well-known Laplace and Gaussian kernels *(L(x)* and *G(x)).* After standardizing the associated PDFs for handling time, the speed of invasion for the SDK was the fastest for shorter handling times (rapidly digesting seeds). As handling times increased, however, the speeds for the SDK fell between the Laplace kernels (faster; based on an assumption of constant seed

deposition) and the Gaussian kernels (slower; based on the assumption of instantaneous seed deposition), as would be expected from the relative behavior of the tails.

Using the SDK and median parameter values estimated from the literature it turned out that pinyon has migration potential at least two orders of magnitude larger than juniper due to avian dispersal. Along with changing temperatures and diminishing moisture levels the favorable environment for P-J is moving northwards through Utah. Over time, these trees will not be able to survive in the southern limits of their current habitat. The large migration potential of pinyon means that it is most likely to occupy new habitats opening to the north.

Introducing ecological diffusion (disperser motility depends on habitat type alone) in the dispersal model is the next step of this dissertation. We use multiple scales approach to resolve the effect of rapidly varying habitats and solve the dispersal model using the method of homogenization. The resulting homogenized seed digestion kernel has asymptotically correct large scale isotropic structure conditioned by the harmonic average motility ($\overline{D}$) and appropriate anisotropic small scale variation for seed dispersal reflecting highly variable habitat.

We have also used the homogenized dispersal kernels to calculate rates of invasion in variable landscapes. No general results exist for predicting *a priori* spread rates of adult plants in such landscape. However, we observe that the homogenized kernels have isotropic large-scale structure, conditioned on the small scale only through the harmonically averaged motility. Using existing theory for predicting spread rates for isotropic dispersal kernels we predict rates of invasion in the IDE model using $\overline{D}$ and

compare with simulated invasions for the IDE and spatially complicated dispersal. Our results show that the *a priori* predictions using $\overline{D}$ accurately predict observed invasions, and a convergence study shows the simulated speed converges from below to the constant predicted speed asymptotically. This represents a second novel contribution; rates of invasion can now be predicted in arbitrary, rapidly-varying environments.

We modified the pre-exiting seed dispersal model by introducing ecological diffusion, seed handling times, landscape utilization and space-dependent motility associated with frugivorous birds in the model. Method of homogenization was used for solving the model with the assumption that habitats vary in short scales (30 meters) but dispersal is to be resolved on kilometers. The dispersal kernel received from the solution reflects small scale variability and animals' utilization. It is possible to express dispersal probabilities using this kernel. These probabilities were factored in terms of pre-defined variables such as fraction covers and other existing variables in the big-grid cell. These variables are determined from regional scale tree distribution models. Consequently, homogenized seed dispersal kernel can be applied to estimate fruiting tree distribution from one big-grid cell to the next cell in terms of large-scale variables.

Comparing with dispersal probabilities associated with the three dispersal kernels: Gaussian, seed digestion and Laplace, we found that seeds are dispersed to the furthest for the Laplace, and the least spread for the Gaussian. Seed dispersal with seed digestion kernel is bounded by the other two. The dispersal under seed digestion looks closer to Gaussian than the dispersal associated with Laplace.

Overall, the most significant aspect of this work is the development of a methodology for active seed dispersal in variable landscapes and implantation of this modeling idea in ecology. Ecologists commonly frame different environmental scenarios within a big (1-10 km) grid in order to estimate future distributions of species. Most plants and animals are migrating at some level; even trees can be found at some locations where they were not found before. In the modern era there is large and growing amount of data (telemetry data, presence absence data) about landscape and animal movement easily available. It is possible to know about what lives in every square kilometer in North America, as well as soil types soil moisture, elevation and aspect. Current distribution models basically determine whether offspring could survive in new habitat, whereas our approach allows researchers to determine if dispersal to new habitat is feasible. In principal, the ingredients for using our model are getting easier and easier to find relative invasion of species.

Our model was developed for seed dispersal by vertebrates. There exists some correlation between animal movement and different habitat types. The lower the habitat utilization, the higher the possible diffusion associated with these animals. This model can also be applied for non-vertebrate dispersal, for instance seed dispersal by wind. Wind is not constant everywhere. In cover with trees and bushes, wind gets stopped and wind blows less rapidly. Consequently, seeds are densely deposited in these locations while seeds move faster in the places where there is dirt, water and open spaces. Additionally, seed deposition varies in space, generally increasing where wind decreases. The diffusion is higher in the place where seed deposition is lower and vice-versa.

The model is not limited to only seed dispersal. There are other direct application areas. In North America, ladybirds beetles (*Coccinellids*) have been used for pest control (Snyder et al., 2004, Koch and Galvan 2007). These beetles disperse, lay eggs and eggs hatch into larvae, which eat pasts. Ladybird beetles do not lay eggs randomly. They lay eggs in places (green crops as opposed to stubble or bare dirt) where there are more likely to be pests. People wonder about where eggs would end up after release by ladybird beetles in some particular location. These scenarios fit perfectly well in our modeling framework.

Both animal movement and habitat variation are sensitive to climate change in some geographical region. Because of the climate change, moisture is changing, some habitats are closing in some places and some habitats are opening up some new locations. The effect of climate change creates a couple of general questions. Can species move through the variable landscapes to get these habitats? Will these species be able to establish there? Will exotic species spread and establish? Even if we were tried to answer these question for particular species like pinyon and juniper, we need to work more broadly in the context of varieties of other species. Our modeling framework applies to many species and we see many possible extensions in the future.

REFERENCES

Koch, R.L. and Galvan, T.L., 2007. Bad side of a good beetle: North American experience with *Harmonia axyridis*. doi: 10.1007/978-1-4020-6939-0_3, *International Organization for Biological and Integrated Control*.

Snyder, W.E., Clevenger, G.M. and Eigenbrode, S.D., 2004. Intraguild and successful invasion by introduced ladybirds beetles. *Population Ecology*, 140:559-565.

APPENDICES

Appendix A: Finite Difference Approximation

We will use two techniques to solve the dispersal model given by equations (2.1) and (2.2) with corresponding seed digestion rate given by the equation (2.3). First, we will solve this PDE numerically using finite difference approximations

$$P_t \approx \frac{P_j^{n+1} - P_j^n}{\Delta t},\ S_t \approx \frac{S_j^{n+1} - S_j^n}{\Delta t} \tag{7.1}$$

where $P_j^n = P(j\Delta x = x, n\Delta t = t)$. We discretize the space derivative with respect to the variable x using a second order centered finite difference,

$$P_{xx} \approx \frac{P_{j+1}^{\ n} - 2P_j^n + P_{j-1}^{\ n}}{\Delta x^2}. \tag{7.2}$$

Using these discretizations and approximating $P(x,t=0) = \delta(x)$ using a standard normal density,

$$P(x,t=0) = \delta(x) \approx \frac{1}{\sqrt{2\pi\sigma^2}} e^{\frac{-x^2}{2\sigma^2}}, \tag{7.3}$$

with variance σ chosen to be very small, the system (2.1) and (2.2) can be solved numerically provided $\Delta t \leq \frac{1}{2} \Delta x^2$ to ensure numerical stability (Ascher and Greif 2011).

Appendix B: Error calculation for seed digestion kernel with step function $h(t)$

The Laplace kernel used for comparison in the main text arises from solving equations (2.1) and (2.2) with a constant hazard function $h(t) = \frac{1}{2\tilde{b}}$. However, since the constant function is not a PDF we must compare the Laplace kernel with the seed digestion kernel with step function *h(t)* defined in equation (2.11), which was standardized for comparison. In this appendix, we analyze the difference between the Laplace kernel, used as the approximation of the systems (2.1) and (2.2) with a step function failure rate $h(t) = \frac{1}{2\tilde{b}}$, and the actual solution.

To calculate the difference between the Laplace and actual kernels, we first find the error in *P* and use it to calculate the error in *S* from the models (2.1) and (2.2). We denote the actual solution for *P* (with stepped hazard function) as P_{act} and the approximate solution (with constant hazard function) for P as P_{appx}. Similarly, the actual and approximate solutions for S are S_{act} and S_{appx} respectively. Notice that both solutions for *P* are equal when $2\tilde{b} < t$ and are different when $t \geq 2\tilde{b}$. Plugging $h(t) = \frac{1}{2\tilde{b}}$ in equation (2.6) we have

$$P(x,t) = \frac{1}{\sqrt{4\pi Dt}} e^{\frac{-x^2}{4Dt} - \frac{t}{2\tilde{b}}} \tag{7.4}$$

The solution for $P(x,t)$ at $t = 2\tilde{b}$ (where $h(t) = 0$) is

$$P\left(x, t = 2\tilde{b}\right) = \frac{1}{\sqrt{8\pi D\tilde{b}}} e^{\frac{-x^2}{8D\tilde{b}} - 1}, \tag{7.5}$$

When $t > 2\tilde{b}$ and $h(t) = 0$, we have

$$P_{act}(x, t > 2\tilde{b}) = \frac{1}{\sqrt{8\pi D\tilde{b}}} e^{\frac{-x^2}{4D(2\tilde{b}+t)}-1} . \tag{7.6}$$

When $t \geq 2\tilde{b}$ and $h(t) = \frac{1}{2\tilde{b}}$, the approximate solution is

$$P_{appx}(x, t \geq 2\tilde{b}) = \frac{1}{\sqrt{4\pi Dt}} e^{\frac{-x^2}{4Dt}-\frac{t}{2\tilde{b}}}, \tag{7.7}$$

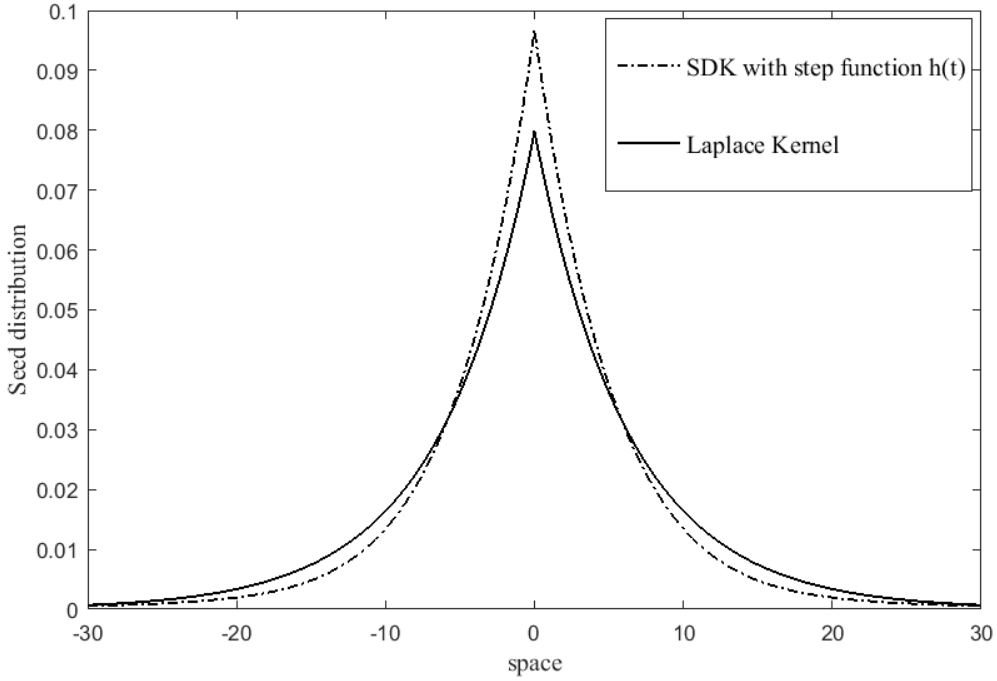

Figure B.1 Comparison of the Laplace kernel (solid line) and seed digestion kernel with step function $h(t)$ (dash-dot line). The error is the difference between the two graphs.

The error in P as $P_{error} = P_{appx} - P_{act}$. From equations (2.42) and (2.2) with $h(t) = \frac{1}{2\tilde{b}}$ we get

$$\frac{\partial}{\partial t}\left(S_{appx}\right)=\frac{1}{2\tilde{b}}P_{appx} \text{ and } \frac{\partial}{\partial t}\left(S_{act}\right)=0 P_{act}=0, \quad t\geq 2\tilde{b}. \tag{7.8}$$

Thus, the error in S is

$$S_{error}(x,t)=S_{appx}(x,t)-S_{act}(x,t)=\frac{1}{2\tilde{b}}\int_{2\tilde{b}}^{t}\left(P_{appx}-0\right)d\tau=\frac{1}{2\tilde{b}}\int_{2\tilde{b}}^{t}P_{appx}d\tau, \tag{7.9}$$

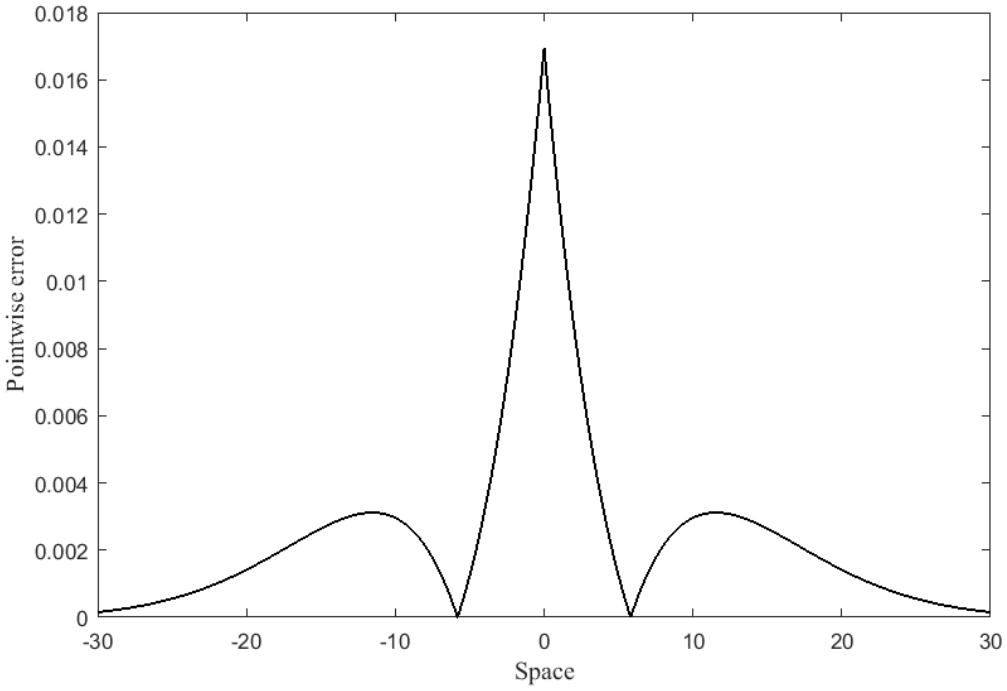

Figure B.2 Calculation of the pointwise error generated using Laplace kernel approximation. The error is high near the center and it is decreasing towards both tails, but is always < 10% of the calculated dispersal kernel.

Finally we must calculate the error in the kernel (K_{error}) which can be obtained by using the limit $t\to\infty$ in equation (7.9). Form equations (7.7) and (7.9) we then have

$$K_{error}=\lim_{t\to\infty}S(x,t)_{error}=\lim_{t\to\infty}\frac{1}{2\tilde{b}}\int_{2\tilde{b}}^{t}\frac{1}{\sqrt{4\pi D\tau}}e^{\frac{-x^2}{4D\tau}-\frac{\tau}{2\tilde{b}}}d\tau. \tag{7.10}$$

We use the trapezoid rule to approximate the integral and note that we have not chosen scalings of time and space, so without loss of generality $D = 1,\ b = 20.$ In a spatial domain *-30 < x <30* the estimated l_1 and l_2 errors are 0.0026 and 0.00052. The two seed dispersal kernels (the Laplace kernel with constant *h(t)* and seed digestion kernel with step function *h(t))* appear in Figure B.1. Pointwise errors are depicted in Figure B.2.

ELSEVIER LICENSE TERMS AND CONDITIONS

Title: Invasion speeds with active dispersers in highly variable landscapes: Multiple scales, homogenization, and the migration of trees

Author: Ram C. Neupane,James A. Powell

Publication: Journal of Theoretical Biology

Publisher: Elsevier

Date: 21 December 2015

Order Completed

Thank you very much for your order.

This is a License Agreement between Ram Neupane ("You") and Elsevier ("Elsevier"). The license consists of your order details, the terms and conditions provided by Elsevier, and the payment terms and conditions.

Get the printable license.

License Number	3780331430848
License date	Jan 01, 2016
Licensed content publisher	Elsevier
Licensed content publication	Journal of Theoretical Biology
Licensed content title	Invasion speeds with active dispersers in highly variable landscapes: Multiple scales, homogenization, and the migration of trees
Licensed content author	Ram C. Neupane,James A. Powell
Licensed content date	21 December 2015
Licensed content volume number	387
Licensed content issue number	n/a
Number of pages	9
Type of Use	reuse in a thesis/dissertation
Portion	full article
Format	both print and electronic
Are you the author of this Elsevier article?	Yes

Will you be translating?	No
Title of your thesis/dissertation	MODELING SEED DISPERSAL AND POPULATION MIGRATION GIVEN A DISTRIBUTION OF SEED HANDLING TIMES AND VARIABLE DISPERSAL MOTILITY: CASE STUDY FOR PINYON AND JUNIPER IN UTAH
Expected completion date	Jan 2016
Estimated size (number of pages)	130
Elsevier VAT number	GB 494 6272 12
Permissions price	0.00 USD
VAT/Local Sales Tax	0.00 USD / 0.00 GBP
Total	0.00 USD

ORDER MORE... CLOSE WINDOW

ELSEVIER LICENSE TERMS AND CONDITIONS

Jan 01, 2016

This is a License Agreement between Ram Neupane ("You") and Elsevier ("Elsevier") provided by Copyright Clearance Center ("CCC"). The license consists of your order details, the terms and conditions provided by Elsevier, and the payment terms and conditions.

All payments must be made in full to CCC. For payment instructions, please see information listed at the bottom of this form.

Supplier	Elsevier Limited The Boulevard, Langford Lane Kidlington,Oxford,OX5 1GB,UK
Registered Company Number	1982084
Customer name	Ram Neupane
Customer address	3 Aggie Village Apt. E LOGAN, UT 84341
License number	3780331430848
License date	Jan 01, 2016
Licensed content publisher	Elsevier
Licensed content publication	Journal of Theoretical Biology
Licensed content title	Invasion speeds with active dispersers in highly variable landscapes: Multiple scales, homogenization, and the migration of trees
Licensed content author	Ram C. Neupane,James A. Powell
Licensed content date	21 December 2015
Licensed content volume number	387
Licensed content issue number	n/a
Number of pages	9
Start Page	111
End Page	119
Type of Use	reuse in a thesis/dissertation
Portion	full article
Format	both print and electronic
Are you the author of this Elsevier article?	Yes

Will you be translating?	No
Title of your thesis/dissertation	MODELING SEED DISPERSAL AND POPULATION MIGRATION GIVEN A DISTRIBUTION OF SEED HANDLING TIMES AND VARIABLE DISPERSAL MOTILITY: CASE STUDY FOR PINYON AND JUNIPER IN UTAH
Expected completion date	Jan 2016
Estimated size (number of pages)	130
Elsevier VAT number	GB 494 6272 12
Permissions price	0.00 USD
VAT/Local Sales Tax	0.00 USD / 0.00 GBP
Total	0.00 USD
Terms and Conditions	

INTRODUCTION

1. The publisher for this copyrighted material is Elsevier. By clicking "accept" in connection with completing this licensing transaction, you agree that the following terms and conditions apply to this transaction (along with the Billing and Payment terms and conditions established by Copyright Clearance Center, Inc. ("CCC"), at the time that you opened your Rightslink account and that are available at any time at http://myaccount.copyright.com).

GENERAL TERMS

2. Elsevier hereby grants you permission to reproduce the aforementioned material subject to the terms and conditions indicated.
3. Acknowledgement: If any part of the material to be used (for example, figures) has appeared in our publication with credit or acknowledgement to another source, permission must also be sought from that source. If such permission is not obtained then that material may not be included in your publication/copies. Suitable acknowledgement to the source must be made, either as a footnote or in a reference list at the end of your publication, as follows:
"Reprinted from Publication title, Vol /edition number, Author(s), Title of article / title of chapter, Pages No., Copyright (Year), with permission from Elsevier [OR APPLICABLE SOCIETY COPYRIGHT OWNER]." Also Lancet special credit - "Reprinted from The Lancet, Vol. number, Author(s), Title of article, Pages No., Copyright (Year), with permission from Elsevier."
4. Reproduction of this material is confined to the purpose and/or media for which permission is hereby given.
5. Altering/Modifying Material: Not Permitted. However figures and illustrations may be altered/adapted minimally to serve your work. Any other abbreviations, additions, deletions and/or any other alterations shall be made only with prior written authorization of Elsevier Ltd. (Please contact Elsevier at permissions@elsevier.com)
6. If the permission fee for the requested use of our material is waived in this instance, please be advised that your future requests for Elsevier materials may attract a fee.
7. Reservation of Rights: Publisher reserves all rights not specifically granted in the combination of (i) the license details provided by you and accepted in the course of this licensing transaction, (ii) these terms and conditions and (iii) CCC's Billing and Payment terms and conditions.

LIMITED LICENSE

The following terms and conditions apply only to specific license types:

15. **Translation**: This permission is granted for non-exclusive world **English** rights only unless your license was granted for translation rights. If you licensed translation rights you may only translate this content into the languages you requested. A professional translator must perform all translations and reproduce the content word for word preserving the integrity of the article.

16. **Posting licensed content on any Website**: The following terms and conditions apply as follows: Licensing material from an Elsevier journal: All content posted to the web site must maintain the copyright information line on the bottom of each image; A hyper-text must be included to the Homepage of the journal from which you are licensing athttp://www.sciencedirect.com/science/journal/xxxxx or the Elsevier homepage for books athttp://www.elsevier.com; Central Storage: This license does not include permission for a scanned version of the material to be stored in a central repository such as that provided by Heron/XanEdu.

Licensing material from an Elsevier book: A hyper-text link must be included to the Elsevier homepage at http://www.elsevier.com . All content posted to the web site must maintain the copyright information line on the bottom of each image.

Posting licensed content on Electronic reserve: In addition to the above the following clauses are applicable: The web site must be password-protected and made available only to bona fide students registered on a relevant course. This permission is granted for 1 year only. You may obtain a new license for future website posting.

17. **For journal authors:** the following clauses are applicable in addition to the above:

Preprints:

A preprint is an author's own write-up of research results and analysis, it has not been peer-reviewed, nor has it had any other value added to it by a publisher (such as formatting, copyright, technical enhancement etc.).

Authors can share their preprints anywhere at any time. Preprints should not be added to or enhanced in any way in order to appear more like, or to substitute for, the final versions of articles however authors can update their preprints on arXiv or RePEc with their Accepted Author Manuscript (see below).

If accepted for publication, we encourage authors to link from the preprint to their formal publication via its DOI. Millions of researchers have access to the formal publications on ScienceDirect, and so links will help users to find, access, cite and use the best available version. Please note that Cell Press, The Lancet and some society-owned have different preprint policies. Information on these policies is available on the journal homepage.

A PERMISSION-TO-REUSE MAMUSCRIPT

Ram Neupane < ram.neupane@aggiemail.usu.edu > Mon, Jan 4, 2016 at 12:31 AM

Dear Jinrong,
I need a permission from Scientific Research Publishing for my published (through SRP) manuscript tilted

"Mathematical Model of Seed Dispersal by Frugivorous Birds and Migration Potential of Pinyon and Juniper in Utah" http://dx.doi.org/10.4236/am.2015.69135

in order to REUSE the manuscript in my Ph.D. Dissertation tilted
"MODELING SEED DISPERSAL AND POPULATION MIGRATION GIVEN A DISTRIBUTION OF SEED HANDLING TIMES
AND VARIABLE DISPERSAL MOTILITY:
CASE STUDY FOR PINYON AND JUNIPER IN UTAH"

Could you please reply this email stated that you are agree and no problem if I use the manuscript given above in my Dissertation.

Sincerely,
Ram Neupane

---

am@scirp.org <am@scirp.org> Mon, Jan 4, 2016 at 1:08 AM

Dear Ram,

You can use the paper in your Ph.D dissertation. Please remember to cite the paper source.

Please feel free to contact me with any problems.
Best Regards,
Jinrong Ge (Sherry)
AM Editorial Office
Scientific Research Publishing
http://www.scirp.org/journal/am
Email: am@scirp.org
Paper Submission Entrance
LinkedIn: www.linkedin.com/in/sherrygejournals
A 2-year Google-based Journal Impact Factor (2-GJIF) is calculated for AM. For this impact factor AM achieved a value of 0.60.
If you have any complaints or suggestions, please contact feedback@scirp.org.

Ram Neupane < ram.neupane@aggiemail.usu.edu > Mon, Jan 4, 2016 at 7:31 AM

Dear Jinrong,

Of Course, I already have cited the paper source in my dissertation. I would also like to let you know that I will attach this e-mail communication to my dissertation at Utah State University (2015).

Thank you for your cooperation.

Sincerely,
Ram Neupane

VITA

Ram C. Neupane
Department of Mathematics & Statistics
3900 Old Main Hill Utah State University,
Logan, UT 84322-3900
E-mail: ram.neupane@aggiemail.usu.edu
Phone (department): 435-797-2809, Fax: 435-797-1822

EDUCATION

Ph.D., Applied Mathematics, Utah State University, Logan, Utah, USA 2015

- Advisor: Dr. James A. Powell
- Dissertation: "Modeling Seed Dispersal and Population Migration Given a Distribution of Seed Handling Times and Variable Dispersal Motility: Case Study for Pinyon and Juniper in Utah"

M.A., Mathematics, University of Louisville, Louisville, Kentucky, USA 2009

- Advisor: Dr. Patricia Cerrito
- Project Report Title: "Data Mining to Investigate the Treatment of Asthma"

M.A., Mathematics, Central Dept. of Math, Tribhuvan University, KTM, Nepal 1999

B.Ed., Mathematics, Saptagandaki Multiple Campus, Bharatpur, Nepal 1996

B.A., Math (Major), Economics (Minor), Birendra M. Campus, Chitwan, Nepal 1994

RESEARCH INTERESTS

Mathematical ecology, mathematical biology and applied mathematics

PUBLICATIONS

Journals

R. C. Neupane and J. A. Powell. Mathematical Model of Active Seed Dispersal by Frugivorous Birds and Migration Potential of Pinyon and Juniper in Utah. *Journal of Applied Mathematics* 6(9): 1506-1523, 2015
http://dx.doi.org/10.4236/am.2015.69135

R. C. Neupane and J. A. Powell. Invasion Speeds with Active Dispersers in Highly Variable Landscapes: Multiple Scales, Homogenization, and the Migration of Trees. *Journal of Theoretical Biology* 387:111-119, 2015
http://dx.doi.org/10.1016/j.jtbi.2015.09.029

Book chapter

Outcomes Research in the Treatment of Asthma, in Cases on Health Outcomes and Clinical Data Mining: Studies and Frameworks, 2010 by Patricia B. Cerrito, Hershey, PA: IGI Publishing

ASSISTANTSHIPS AND AWARDS

- Received Student travel fund ($900.00), Society of Mathematical Biology (SMB) Annual Conference, Atlanta, GA, June 30-July 3, 2015.
- Utah State University Office of Research and Graduate Studies Dissertation Fellowship 2015 (Spring and Summer, $27,386.48)
- Received Student travel fund, MAA Intermountain Meeting March 2014
- Active participation of devoted parents award 2012 - 2013 from Bear River headSTART, Logan Utah
- Graduate Teaching Assistantship, Utah State University, Aug. 2010 to present
- Received Student travel fund ($600.00), SAS Data Mining Conference M2008, Las Vegas, NV, October 2008
- Graduate Teaching Assistantship, University of Louisville Aug. 2007 to May 2009

SKILLS

- Computer skills: MATLAB, Maple, LaTeX, SAS, MS Word, Excel and PowerPoint
- Languages: Fluent in English, Nepali and Hindi